Control of Fuel-Cell Systems in Aircraft

Control of multi-stack air-cooled open-cathode fuel-cell propulsion system for aircraft

Vishwajeetsinh Jadhavrao

TU Delft

DLR

Control of Fuel-Cell Systems in Aircraft

Control of multi-stack air-cooled open-cathode fuel-cell propulsion system for aircraft

Thesis report

by

Vishwajeetsinh Jadhavrao

to obtain the degree of Master of Science in Aerospace Engineering
at the Delft University of Technology
to be defended publicly on May 8, 2026 at 09:00

Thesis committee:

Chair:	Dr. Ewoud J.J. Smeur
TU Delft Supervisors:	Dr. Rene van Paassen
	Dr. Erik-Jan van Kampen
DLR Supervisor:	Ir. Daniel Juschus
External examiner:	Dr. Woutijn J. Baars
Place:	Faculty of Aerospace Engineering, Delft
Project Duration:	September, 2025 - May, 2026
Student number:	5281172

An electronic version of this thesis is available at `http://repository.tudelft.nl/`.

The Imponator was designed and built in the project BETA, funded by the Federal Ministry of Transport and Digital Infrastructure of the Federal Republic of Germany, by DLR and in cooperation with Airbus, ZAL GmbH and the Helmut Schmidt Universität [1], [2], [3], [4], [5]. After the end of the project, the Imponator was lent to DLR by Airbus. We would like to thank all involved partners.

The research activities in the project D-LIGHT+ are carried out within the framework of the German Aerospace Center's core funded research [6]. The cover photo of the D-LIGHT+ aircraft is rendered by DLR (German Aerospace Center).

Faculty of Aerospace Engineering · Delft University of Technology

Preface

Welcome to my thesis report, I am excited to share with you all the findings and all that I've learned during my thesis! My thesis took place at the DLR (German Aerospace Center) at the Aachen-Merzbruck site, which is actually situated in Wurselen, Germany. My thesis took place right after my internship at the DLR, and I enjoyed working in the same field of hydrogen-electric aviation.

A small background about me is that I previously worked as the Technical Manager and Systems Engineer at AeroDelft, a student team that is building a hydrogen fuel-cell powered aircraft. During this time, I also met Daniel Juschus, my internship and now thesis supervisor at DLR who was also working in hydrogen-electric aviation. During my internship I worked on implementing embedded systems in a fuel-cell testrig, combining both my primary areas of expertise, control (from MSc) and fuel cells (from AeroDelft). I wanted to research deeper in this field, and therefore for my thesis I worked on automating the startup and shutdown sequences for a larger multi-stack hydrogen fuel-cell propulsion system for an aircraft. Here I got to implement the control-theory I learned during my Control and Simulation Aerospace Engineering master, in the hydrogen-electric aviation field I'm quite interested in.

I would like to especially thank my DLR supervisor Daniel Juschus, and TU Delft supervisors Rene van Paassen and Erik-Jan van Kampen, for their unwavering support and feedback during the thesis. A special thanks to members at the TT institute who I had meetings with during my thesis, namely Torben, Florian and Christoph. I would also like to thank all members in the D-LIGHT+ team, and also all colleagues at the INK office who supported me during the thesis, namely Simon, Soren, Pranav, Nitheesh.

I would also like to thank my friends who supported me and helped me during my thesis, namely Serban and Enrique. The time we spent was always a joy, whether this is in Germany, Netherlands or the UK. Thanks to Maurits and Timo for visiting me during the Christmas markets, and special thanks to Topias all the way to New Zealand. Notably, I also want to thank Luca, an old friend, somehow we were together for DSE, AeroDelft and also at DLR now, thanks for the tischtennis times.

Lastly, I would like to thank my family for supporting me during this time, it is much appreciated. In general, thank you all, this was a lot of fun!

Vishwajeetsinh Jadhavrao
Aachen, April 2026

Executive Summary

Hydrogen fuel-cell propulsion applications in aviation are growing, and research is being done in DLR to bring this technology into real aircraft. Safe and reliable control of this hydrogen fuel-cell propulsion remains a core challenge in experimental systems such as the Imponator, which is multi-stack air-cooled and open-cathode made by DLR, Airbus and other partners. The system has been lent to DLR by Airbus to carry out further research. This project focuses on developing a method to achieve safe and reliable automation of the startup and shutdown sequences of the Imponator as seen in Research Objective.

Research Objective

To safely and reliably automate the startup and shutdown of a multi-stack air-cooled open-cathode hydrogen fuel-cell propulsion system for aircraft.

This project was approached by first conducting a literature review to achieve this Research Objective, during which a primary research question and 5 sub research questions were developed to break the problem down. Herein, the control safety and reliability requirements were formulated to define the automation based on understanding fuel cell systems including the Imponator specifically. Secondly, relevant control-oriented models and controllers were identified and chosen for the project to answer the remaining parts of the objective. A Multi-level Flow Model was first created to define mass and energy flows, control functions as well as hazards for the Imponator system. This MFM helped in creating specific control requirements, as well as making functional groupings to define the 6 physical subsystems needed.

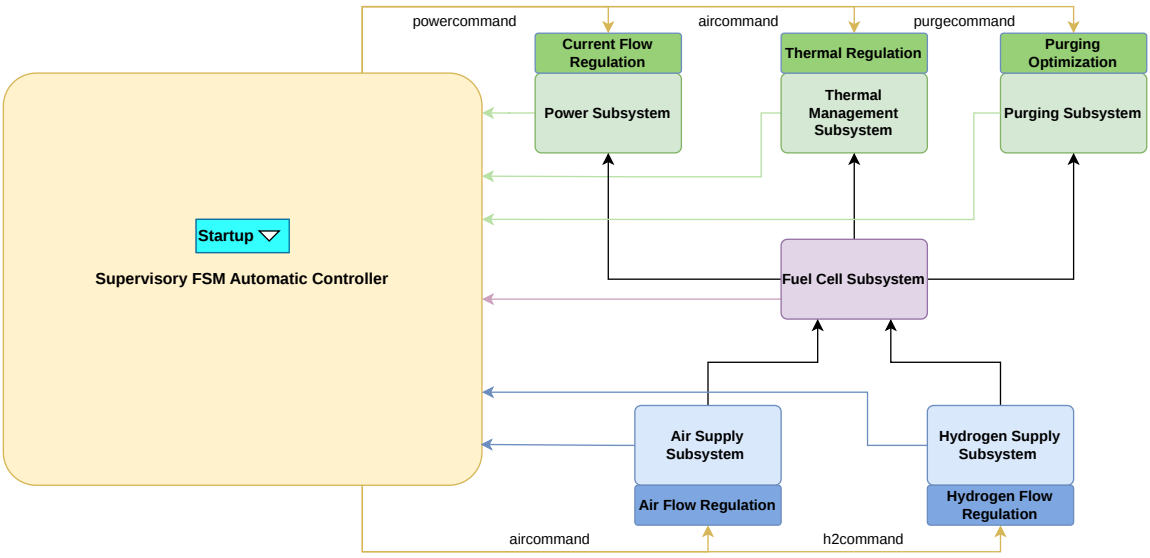

Figure 1: Simulink diagram with FSM and 6 physical subsystems integrated

Then a supervisory FSM automatic controller was designed to define the inputs and outputs needed from the physical subsystems based on the MFM control functions and hazards, and thereafter the physical subsystem models were created as seen in Figure 1. These are Air Supply Subsystem (AS) and Hydrogen Supply Subsystem (HSS) which act as inputs, Fuel-Cell Subsystem (FCS) where the reaction occurs, and Power Subsystem (PWS) , Thermal Management Subsystem (TMS) and Purging

Subsystem (PS) which act as the outputs. Thirdly, with experimental data, parameter estimation was performed on the temperature and voltage models, and validation was subsequently performed on the temperature, voltage and hydrogen pressure models (which test parts of all 6 physical subsystems).

The validation metrics R^2, RMSE and MEBE in Table 1 demonstrate that the voltage model relatively performed the best, with the MBE of the temperature model shows that better experimental temperature data is needed where environmental wind has no influence. Whereas the hydrogen pressure model had a high RMSE, and this is due to the lower mass flow controller (MFC) model fidelity, which can also be improved in future with experimental sensor data from the real mass flow controller. Additionally, the FSM was also verified, by checking that it is able to switch states and sequentially set the different modes for the subsystems. Overall, based on the validation metrics, the model accuracy was deemed acceptable to build subsystem controllers.

Table 1: Model performance metrics comparison

Metric	Temperature	Voltage	H_2 Pressure
$R^2[-]$	0.81	0.93	0.81
RMSE	1.18 °C	1.60 V	62.24 mbar.g
MBE	-0.92 °C	-0.28 V	0.49 mbar.g

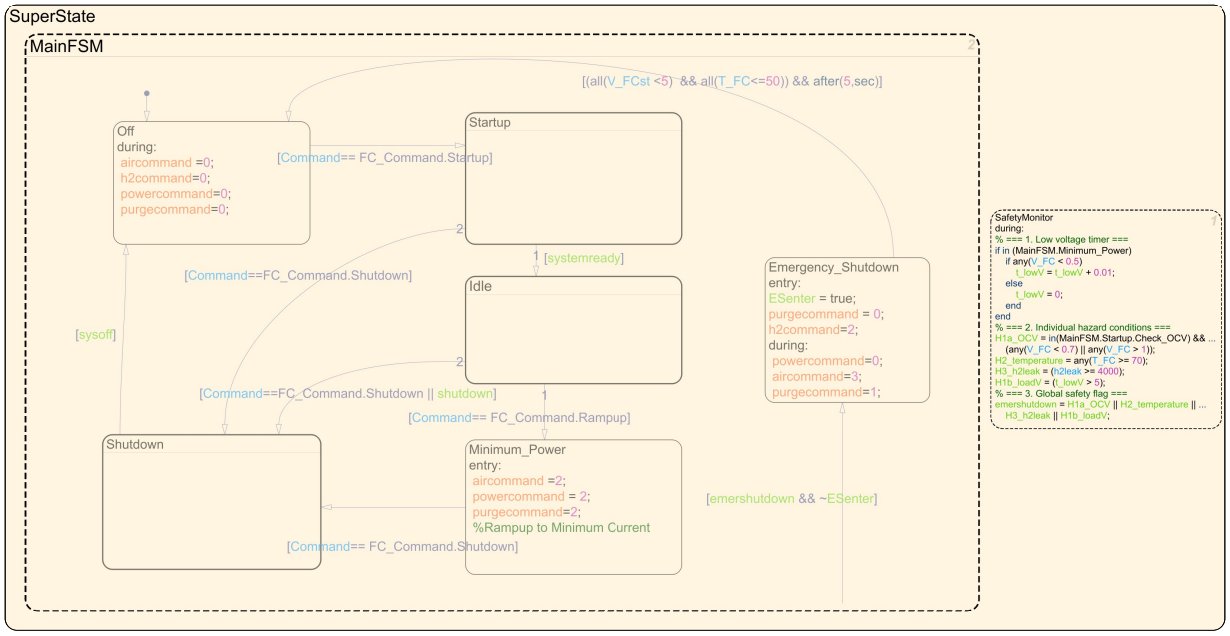

Figure 2: Finite State Machine Chart of the Imponator System

The supervisory FSM automatic controller was being designed in parallel to the physical models, and it defines the required sequence of actions in the startup and shutdown, by switching the modes in the controllable subsystems using aircommand (AS and TMS), h2command (HSS), powercommand (PWS) and purgecommand (PS) as seen in Figure 2. Now the subsystem controllers were responsible for actually carrying out the action after FSM assigns them the operational mode. Therefore fourthly, based on specifically the control reliability requirements, besides turning switches and valves on and off, a temperature PID controller, current Nonlinear Reference Governor, and purging controller (Feedforward Interval Scheduler and Integral Threshold Duration controller) were designed and tuned. The FSM was responsible for meeting the control safety requirements, as it had a Safety Monitor state running in parallel which would detect a hazard, and it would initiate Emergency Shutdown once a hazard is detected. Verification of the FSM meeting the control safety requirements can be seen by the safe and immediate Emergency Shutdown for hydrogen leakage, overheating, OCV under voltage and loaded under voltage in Figure 3, Figure 4, Figure 5 and Figure 6 respectively.

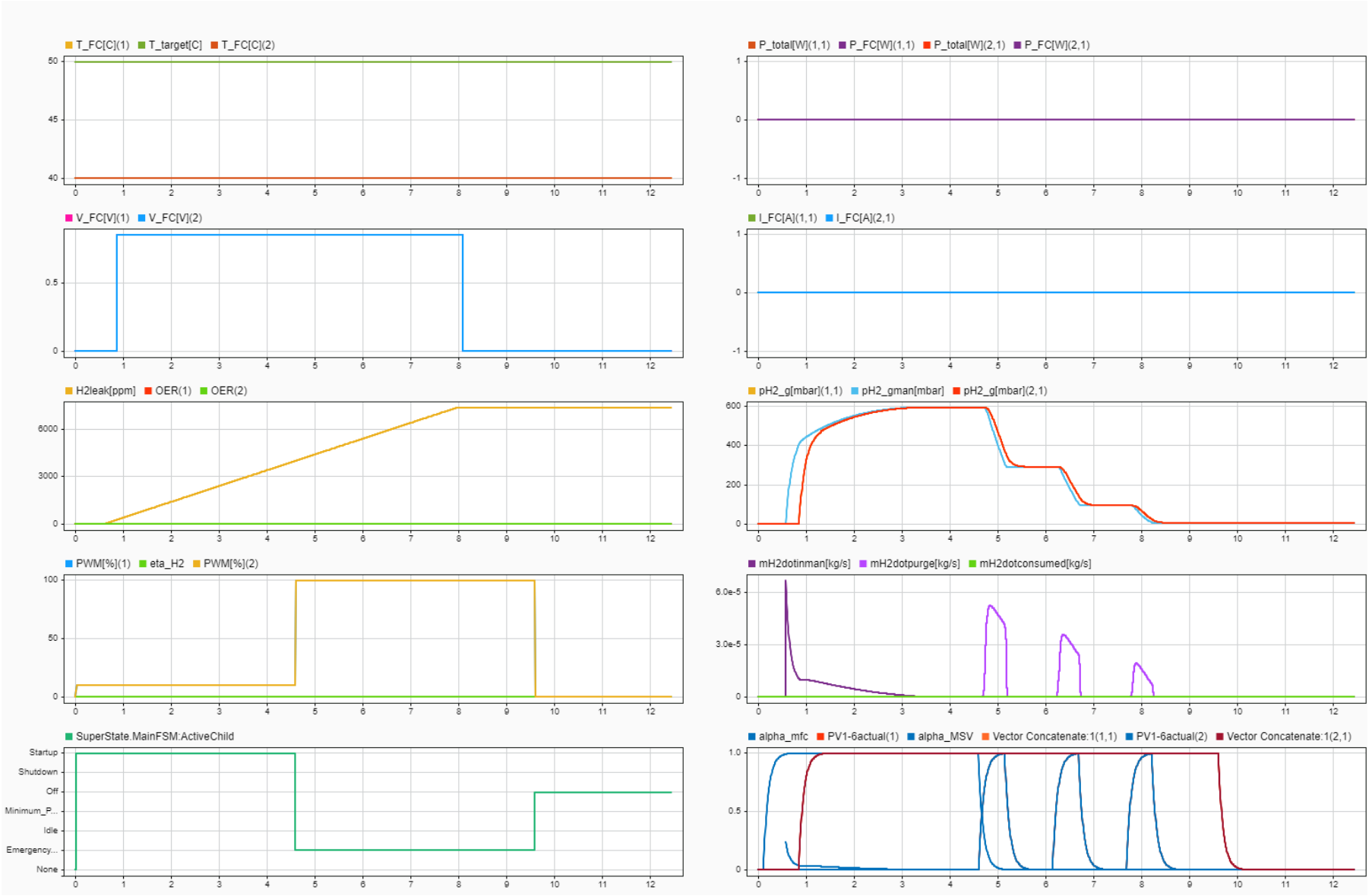

Figure 3: Response to ramping hydrogen leakage of 4000 ppm from model sensor

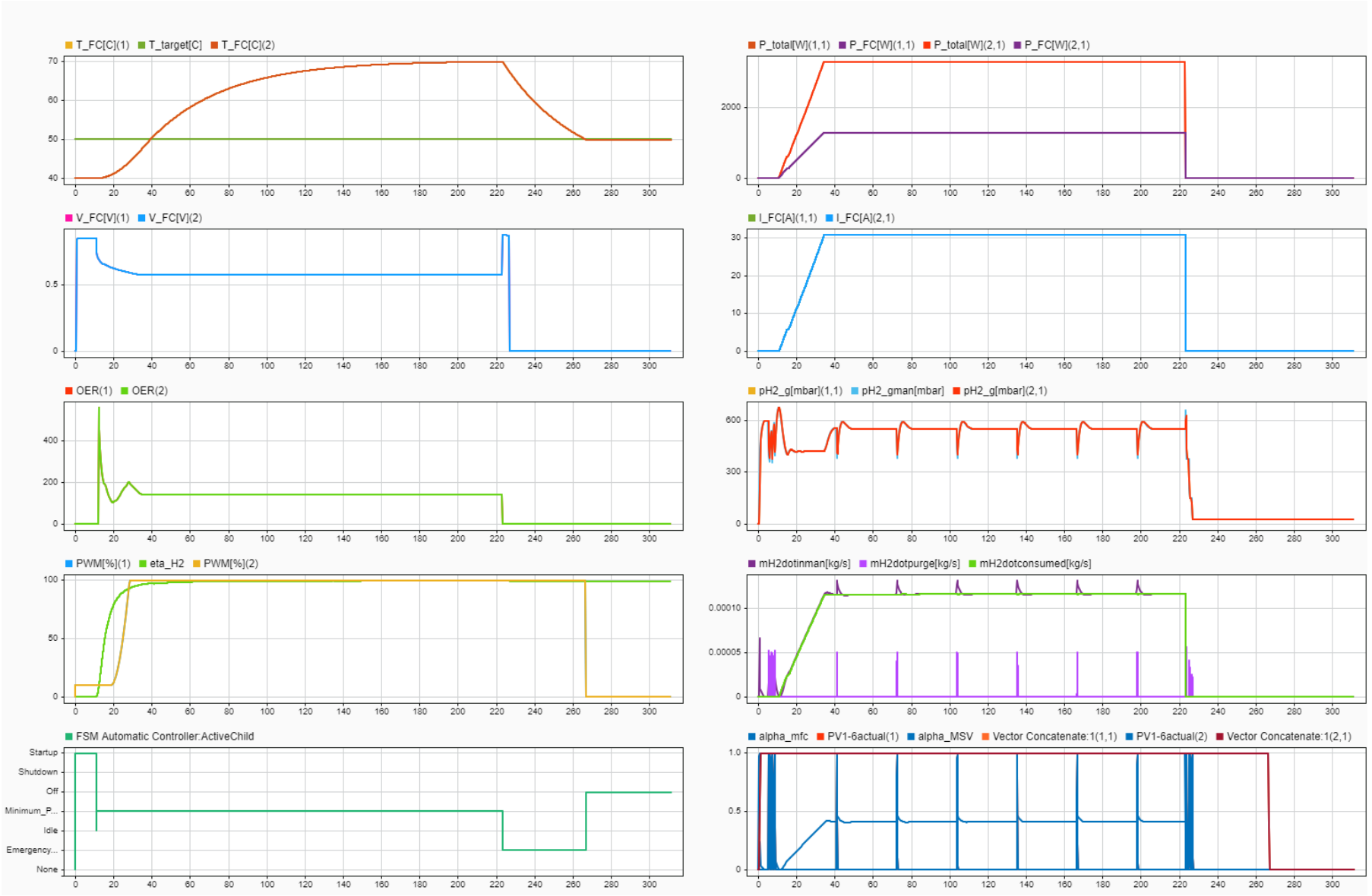

Figure 4: Response to stack temperature overheating to $70°C$

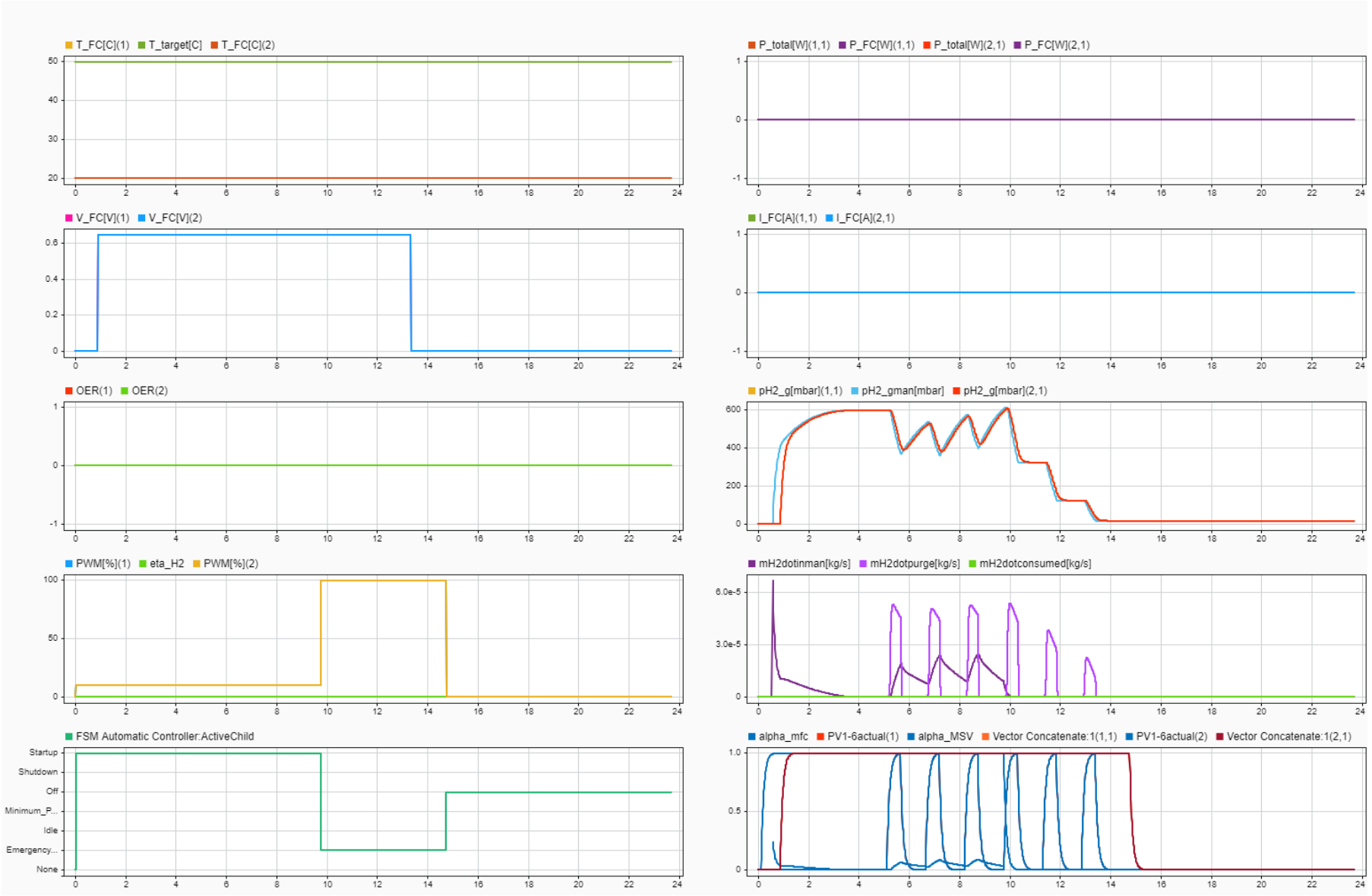

Figure 5: Response to OCV under voltage of 0.65V

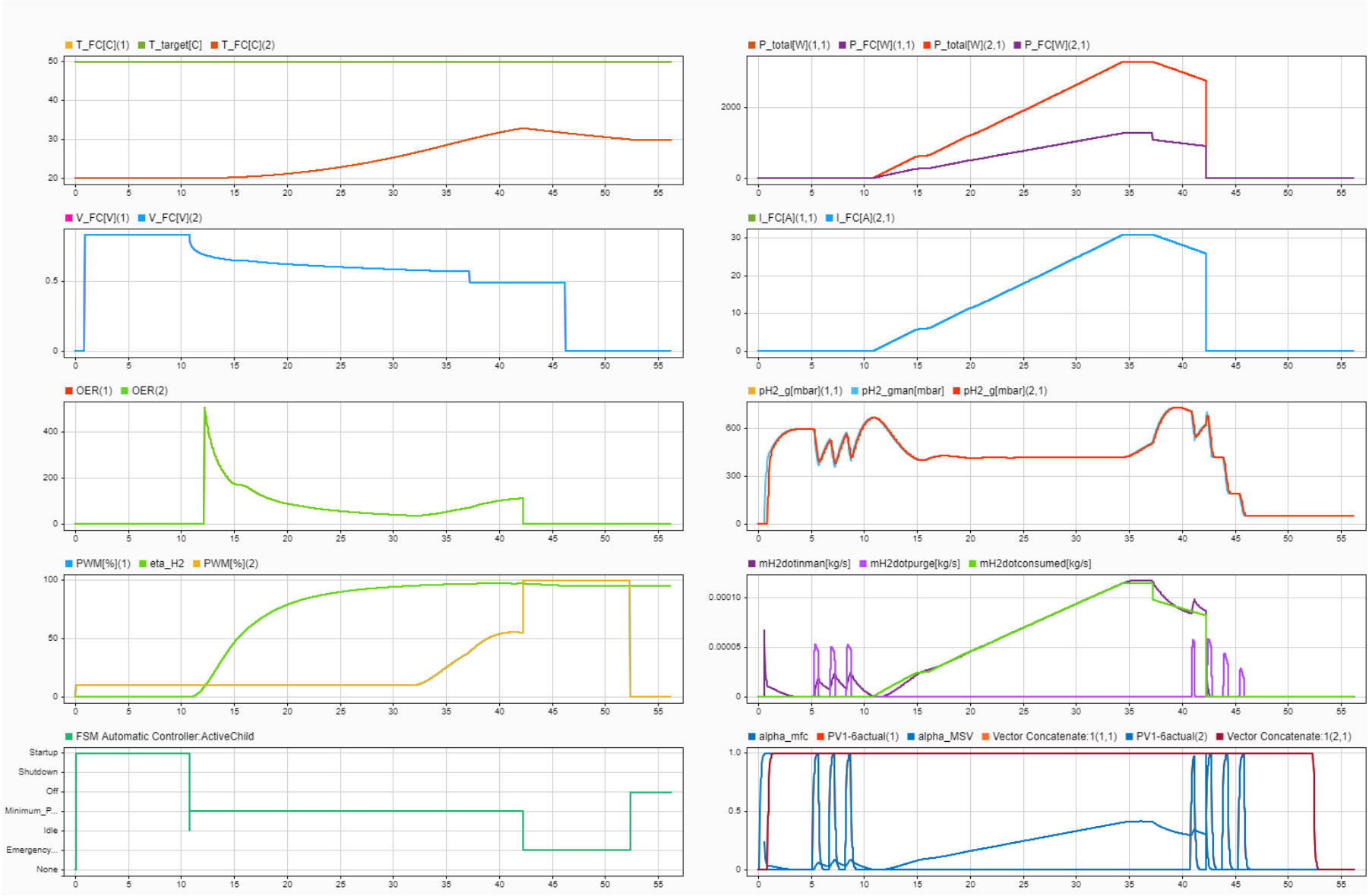

Figure 6: Response to loaded under-voltage of 0.49V for > 5s

The subsystem controllers together with the supervisory FSM automatic controller, achieve the control safety and reliability requirements as seen by the final control-model results in Figure 7 for 4A minimum current and Figure 8 for 31A maximum possible current at $20°C$ ambient. Most interestingly for 31A the controller dynamics are seen most clearly, as the temperature PID controller is continuously working to keep temperature $\leq 50°C$, current NRG ramping by abiding voltage (0.5-0.92V) and hydrogen pressure (400-700 mbar.g) ranges, and purging controller determining the intervals and durations to maximize hydrogen utilization giving 99.4%. Notably, the current ramp times can be made faster by tuning the MFC PID gains to better respond to purging and consumption with a higher fidelity model. Overall, these results demonstrate that this method achieves safe and reliable automation of the startup and shutdown for the Imponator hydrogen-electric propulsion system with a Simulink control-model, which can be implemented within the real system and improvements to the model with further exploration are possible.

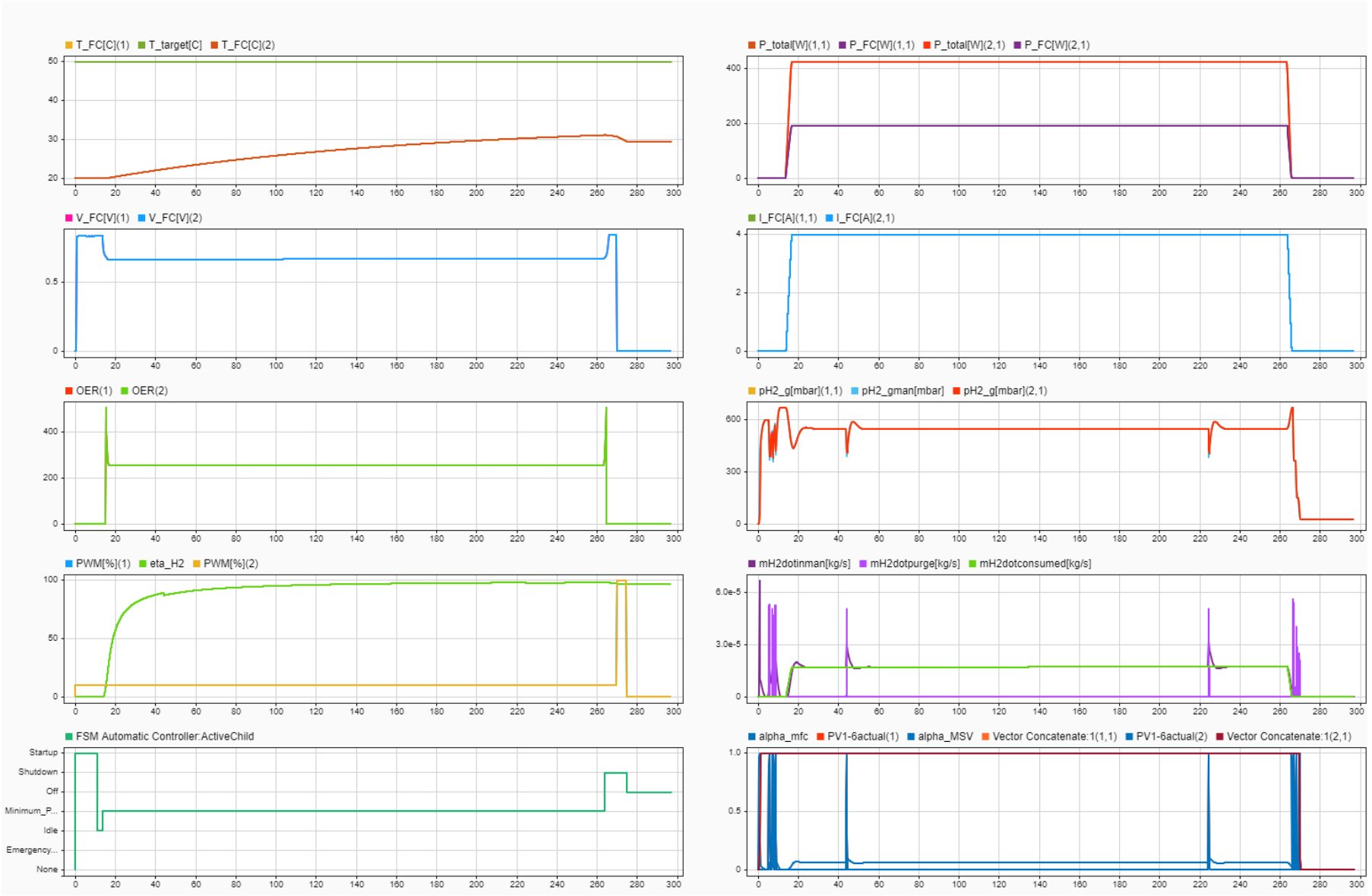

Figure 7: Final Imponator control-model results: 4A minimum current

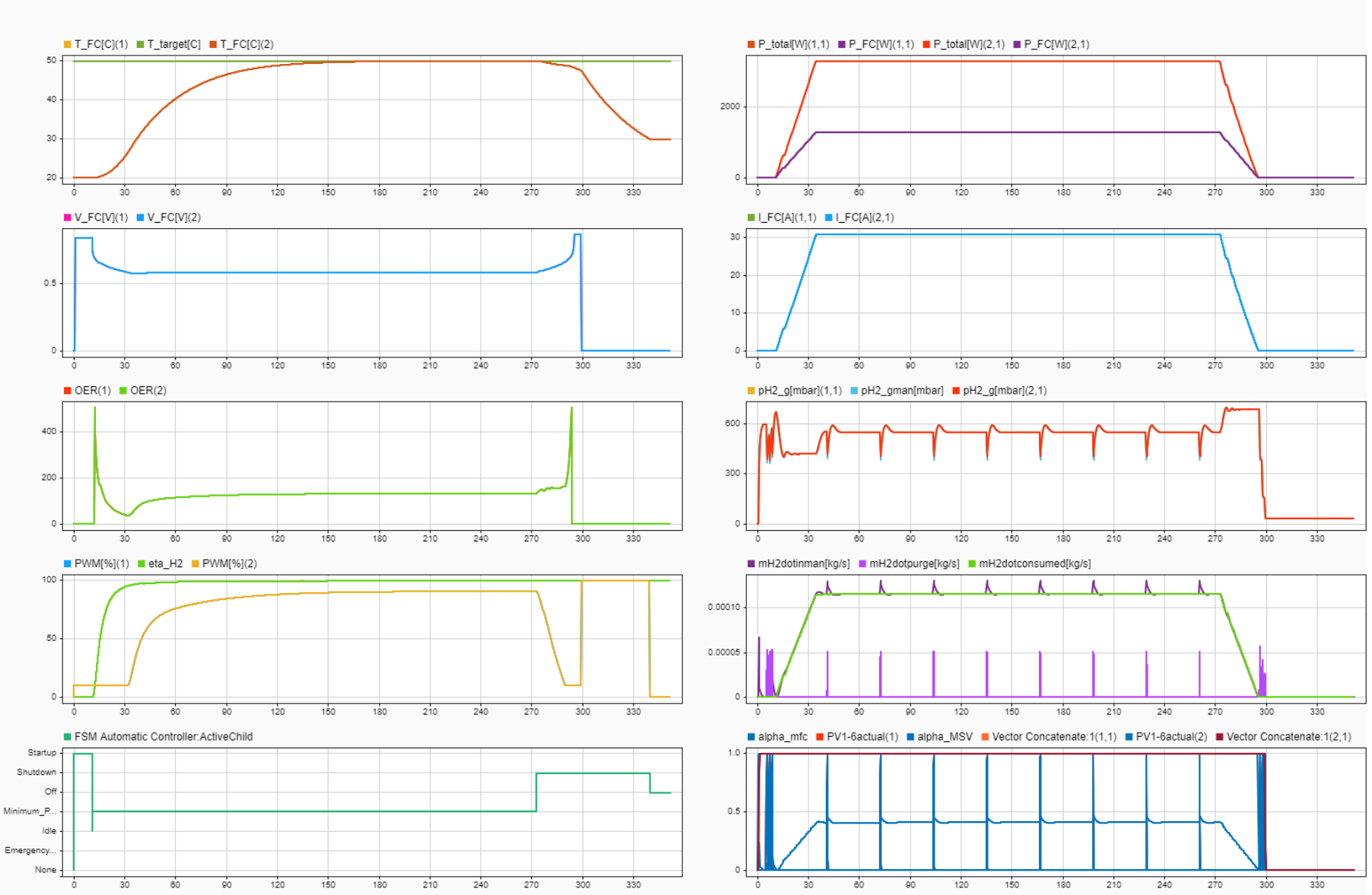

Figure 8: Final Imponator control-model results: 31A maximum possible current (with $T_{amb} = 20°C$)

Contents

Nomenclature

List of Abbreviations

PRQ	Primary Research Question
PEMFC	Proton Exchange Membrane Fuel Cell
SOFC	Solid Oxide Fuel Cell
P&ID	Piping and Instrumentation Diagram
DC	Direct Current
OCV	Open Circuit Voltage
MFM	Multi-level Flow Modelling
PN	Petri Nets model
FSM	Finite State Machine
PID	Proportional Integral Derivative controller
MPC	Model Predictive Control
SMC	Sliding Mode Control
PWM	Pulse Width Modulation
OER	Oxygen Excess Ratio
AS	Air Supply Subsystem
HSS	Hydrogen Supply Subsystem
FCS	Fuel-Cell Subsystem
PS	Purging Subsystem
TMS	Thermal Management Subsystem
PWS	Power Subsystem
EFS	Energy Flow Structure
MFS	Mass Flow Structure
MEFS	Mass & Energy Flow Structure
CFS	Control Flow Structure
RMSE	Root Mean Squared Error
MBE	Mean Bias Error
MFC	Mass Flow Controller

List of Symbols

w	Fan speed [$\frac{rev}{min}$]
u	Fan PWM [%]
Q	Flow rate [$\frac{m^3}{s}$]
ρ_{air}	Air density sea level [$\frac{kg}{m^3}$]
$\dot{m}_{air}$	Air mass flow [$\frac{kg}{s}$]
y_{O2}	Mass fraction of oxygen in air [-]
M_{O2}	Molar mass of oxygen [$\frac{kg}{mol}$]
F	Faraday's constant [$\frac{C}{mol}$]
$\dot{m}_{O2in}$	Incoming oxygen mass flow [$\frac{kg}{s}$]
$\dot{m}_{O2consumed}$	Consumed oxygen mass flow [$\frac{kg}{s}$]
I_{FC}	Stack Current [A]
$\dot{I}_{FC}$	Stack current ramp rate [$\frac{A}{s}$]
p	Anode manifold pressure [Pa]
V_{FC}	Cell voltage [V]
V_{FC}^{st}	Stack voltage [V]
T_{FC}	Stack temperature [K]
N_{FC}	Number of cells in stack [-]
$\dot{m}_{H2in}$	Incoming hydrogen mass flow [$\frac{kg}{s}$]
$\dot{m}_{H2cons}$	Consumed hydrogen mass flow [$\frac{kg}{s}$]
$\dot{m}_{H2purge}$	Purged hydrogen mass flow [$\frac{kg}{s}$]
R_{H2}	Hydrogen gas constant [$\frac{J}{Kmol}$]
T_{amb}	Ambient temperature [K]
V_{total}	Total anode volume [m^3]
α_{MSV}	Main supply valve position [%]
α_{SV}	Stacks' supply valve positions [%]
α_{MFC}	Mass flow controller valve position [%]
V_{oc}	Cell open circuit voltage [V]

V_{act} Cell activation over voltage [V]

V_{ohm} Cell ohmic over voltage [V]

V_{conc} Cell concentration over voltage [V]

E^0 Gibbs free energy change [V]

Δs Entropy change [$\frac{J}{mol \cdot K}$]

T_{FC}^0 Standard fuel cell temperature [K]

p_{pH_2} Partial pressure of hydrogen [-]

p_{pO_2} Partial pressure of oxygen [-]

α Charge transfer coefficient [-]

i_n Exchange current density [$\frac{A}{cm^2}$]

i_o Limiting current density [$\frac{A}{cm^2}$]

R_{ohm} Ohmic resistance [cm^2]

i_{FC} Current density [$\frac{A}{cm^2}$]

n Concentration over voltage constant [$\frac{cm^2}{A}$]

m Concentration over voltage coefficient [V]

PV Purge valve position [%]

K_{vs} Standard water flow coefficient [$\frac{m^3}{h}$]

K_v Flow coefficient [$\frac{m^3}{h}$]

p_{amb} Ambient pressure [bar]

ρ_{H2} Standard hydrogen density [$\frac{kg}{m^3}$]

Q_N Normal flow rate [$\frac{m^3}{h}$]

C_t Thermal capacity [$\frac{J}{K}$]

η_{fan} Fan efficiency [%]

P_{total} Total power [W]

P_{FC} Electrical power [W]

$\dot{Q}_{\text{coolant}}$ Cooling power [W]

c_p Heat capacity of air [$\frac{J}{kgK}$]

$\dot{M}_{H2,used}$ Molar hydrogen consumption rate [$\frac{A \cdot mol}{C}$]

ΔH Enthalpy change [$\frac{J}{mol}$]

$\dot{n}_{reactant}$ Molar reactant flow [$\frac{mol}{s}$]

$\dot{n}_{purge}$ Molar purge flow [$\frac{mol}{s}$]

V_{H2purged} Volume of hydrogen purged [m^3]

C_{st} Stack hydrogen consumption $\frac{g}{kW \cdot s}$

R^2 Coefficient of Determination [-]

K_p Proportional gain [-]

K_i Integral gain [-]

K_d Derivative gain [-]

$I_{FC,req}$ Requested current [A]

$\dot{I}_{FCmaxup}$ Max ramp-up rate [$\frac{A}{s}$]

$\dot{I}_{FCmaxdown}$ Max ramp-down rate [$\frac{A}{s}$]

V_{min} Minimum cell voltage [V]

V_{max} Maximum cell voltage [V]

V_{buffer} Buffer cell voltage [V]

P_{H2min} Minimum anode pressure [mbar.g]

P_{H2max} Maximum anode pressure [mbar.g]

P_{buffer} Buffer pressure [mbar.g]

s_{up}, s_{down} Ramp scale [-]

η_{H2} Hydrogen utilization [%]

T_{ref} Reference purge interval [s]

I_{ref} Reference purge current [A]

T_{min} Minimum purge interval [s]

T_{max} Maximum purge interval [s]

$T_{interval}$ Feedforward purge interval [s]

$Q_{H2purge}$ Volumetric purge mass flow [$\frac{m^3}{s}$]

$V_{H2target}$ Target purge volume [m^3]

V_{stack} Stack anode volume [m^3]

V_{man} Anode manifold volume [m^3]

List of Figures

List of Tables

1

Introduction

1.1. General Introduction

Hydrogen fuel-cell propulsion systems are emerging as a strong solution to achieve net zero-emissions in aviation. The German Aerospace Center (DLR) is conducting research into developing and testing fuel-cell propulsion systems for aircraft in several projects, such as D-LIGHT+. Within the D-LIGHT+ project, a hydrogen-electric aircraft is being designed, and they're interested in exploring the limits and capabilities of a specific type of fuel-cell known as air-cooled open-cathode. This thesis is focused on the control of a multi-stack air-cooled open-cathode fuel-cell system. This system originated from a previous research project which involved DLR, Airbus and other partners. Thereafter, this system was lent to DLR by Airbus, for further research.

Through the development of fuel-cells in aviation, several unique operational challenges arise when considering the safety and reliability of the propulsion system. This is a particular challenge DLR is currently facing, in a specific kind of experimental fuel-cell propulsion system where they require operational automation. This operational automation is desired for the startup and shutdown sequences of a multi-stack experimental fuel-cell system known as the Imponator. Currently the startup and shutdown process requires lots of manual checks giving high workload to the users, and also requires the user to handle safety fully. Automating this would allow a safer and more reliable operation, which helps in testing and in building towards a demonstrator. This directly links to the RO research objective of this thesis, which is to safely and reliably automate the startup and shutdown of a multi-stack air-cooled open-cathode hydrogen fuel-cell propulsion system for aircraft.

The structure of the thesis aims to chronologically answer the primary research question's sub research questions as shown in PRQ. Firstly, this thesis starts by conducting a literature review in Chapter 2 on the background of fuel cells in aircraft propulsion and understanding the experimental Imponator propulsion system. Thereafter, literature is studied for relevant types of models and controllers. Based on this a project plan along with main research activities are defined. Secondly, control-based modelling of the Imponator with FSM and physical models is done in Chapter 3. Thirdly, these physical models are validated and FSM verified in Chapter 4. Fourthly, subsystem controller design on these built-up models is done in Chapter 5, considering both reliability and safety. Fifthly, the final results of the entire thesis are synthesized in Chapter 6. Lastly, the thesis is concluded in Chapter 7, and recommendations to improve the control-model and also integrate it with the physical system are given in Chapter 8.

1.2. Research Formulation

Research Objective

To safely and reliably automate the startup and shutdown of a multi-stack air-cooled open-cathode hydrogen fuel-cell propulsion system for aircraft.

Primary Research Question

How can startup and shutdown of a multi-stack air-cooled open-cathode hydrogen fuel-cell propulsion system for aircraft be automated in a safe and reliable way?
Sub research questions:

1. *How can the control system design requirements be defined to ensure safe and reliable startup and shutdown procedures?*
2. *What are the most relevant control-oriented model types and controllers in automating the startup and shutdown?*
3. *How can the fuel-cell system be modelled, along with its startup and shutdown procedures?*
4. *How can the accuracy of the model to the real system be measured?*
5. *How can relevant model-based control systems be developed to automate the startup and shutdown?*

2

Literature Review

This chapter is a literature review on the topic of control of fuel cell systems. The objective is to develop an understanding, of how can the startup and shutdown of a fuel-cell system be automated as seen in RO. This can be formulated into the primary research question as seen in PRQ, which can be broken down into sub research questions. During this literature review, general answers to these research questions will be sought from literature, which shall help determine the research plan with a set of research activities. With these research activities, the research questions can be answered in more detail. Firstly, background on fuel cells in aircraft propulsion will be covered to introduce relevant terminology in Section 2.1, followed by understanding the Imponator fuel-cell system at hand in Section 2.2. Then literature will be reviewed into types of control-oriented models and relevant control systems in Section 2.3 and Section 2.4 respectively. The literature review will conclude in the research plan with activities outlined for the thesis in Section 2.5.

2.1. Background on Fuel Cells in Aircraft Propulsion

Firstly, it is important to get some background information on the topic of fuel cells in aircraft propulsion, and clarify some of the terms being used with the help of literature. Some general information regarding fuel-cells is given in Section 2.1.1, followed by how fuel-cells are used in aircraft propulsion in Section 2.1.2. Then lastly, some challenges regarding a fuel-cell type is discussed in Section 2.1.3.

2.1.1. Fuel-cells for Aircraft

Hydrogen fuel-cells refer to a device in which the chemical reaction of hydrogen and oxygen combining take place, producing water, electrical and heat energy. The electrical energy produced from this chemical reaction can be used to power electrical components such as motors, which can be used to propel an aircraft. Their key chemical reaction can be visualized in a process that can be seen in Figure 2.1 and Figure 2.2, which are for popular fuel-cell types of Proton Exchange Membrane (PEMFC) and Solid Oxide (SOFC) respectively.

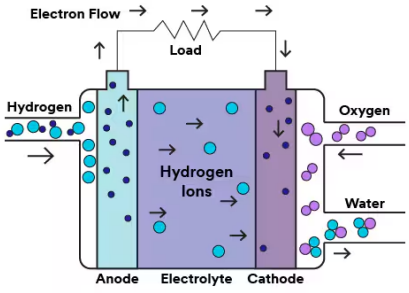

Figure 2.1: PEM fuel cell schematic [7]

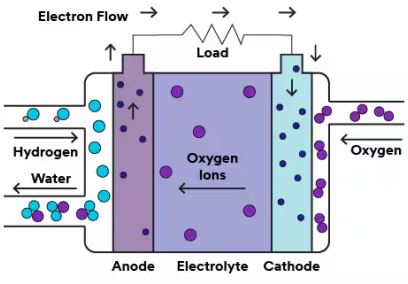

Figure 2.2: SO fuel cell schematic [7]

In the PEMFC, hydrogen is supplied at the anode, and through a catalyst it is oxidized [7]. The positive hydrogen ions (protons) pass through the PEM to reach the cathode, whilst hydrogen electrons reach the cathode through an external load circuit. Oxygen reduces at the cathode (where it is supplied), and combines with the hydrogen ions to form water. The electrons flowing around creates the current, and

this is the power output. Whereas for SOFC, it is the oxygen ions that diffuse through and combine with the hydrogen ions to form water. SOFC have long startup times and high operating temperatures upto 1000°C, and therefore aren't suitable for transportation applications. PEMFC on the other hand, have shorter startup times and lower operating temperatures, and therefore are primarily being developed for transportation, with aerospace applications. Therefore, the focus of this project will be on a system that contains a PEMFC [8].

2.1.2. Types of PEMFC

Within PEMFC, there are also further types of PEMFC. These include low temperature, high temperature, air cooled and liquid cooled PEM fuel cells [9]. The D-LIGHT+ project in DLR is designing a 9-seater hydrogen-electric commuter aircraft, in which they're specifically interested in investigating the air cooled and liquid cooled PEM fuel cells. So it is relevant to introduce these two concepts.

Air-cooled PEMFCs are open-cathode, meaning that the cathode is not in a closed loop. Rather, the cathode side is open, often with a fan, which provides the oxygen as well as the cooling for the stacks. It is quite lightweight and compact due to the absence of a separate liquid cooling loop, however it has lower power density due to the reduced cooling capability, and less precise thermal control [9].

On the other side, there are liquid-cooled PEMFcs which are closed-cathode, meaning that there are several components in the cathode loop, and there is a separate liquid cooling loop. This results in a higher power density and precise thermal management which is scalable for large aircraft, however it has several more balance of plant components like pumps, radiators and coolant. This makes the system heavier and more complex [9].

So there's a tradeoff between the two PEMFC types. Notably, the D-LIGHT+ aircraft is a distributed propulsion aircraft, something that can be powered by several air-cooled fuel cells in parallel, for example. And they are specifically interested in seeing, how far the air-cooled fuel cells can be taken, and whether they can provide sufficient power in a distributed propulsion concept. This comes with facing several challenges, some of them will be relevant for this project.

2.1.3. Challenges in Air-Cooled Open-Cathode PEMFCs

As mentioned before, investigating whether the air-cooled open-cathode PEMFcs can be used in aircraft comes with several challenges. One of the main, is to provide sufficient power, despite having lower cooling capability. It is possible to use many of these stacks in parallel to multiply the power output, however that increases the complexity of operation and control. this means concurrent control of valves for supplying and purging hydrogen.

Secondly, temperature control is less precise, since there is only a fan that has to do the job of cooling as well as ensuring sufficient oxygen is being provided. The control of this, also remains a challenge. Specifically, DLR recognizes that the startup and shutdown of these processes is complicated, and would benefit from automating them in control. Now, it is useful to learn more about the actual system at hand, on which this project will be based on.

2.2. Imponator Fuel-Cell System

Now that some background on fuel-cells was covered, it is useful to find out information about the system at hand. It is useful to understand the Imponator fuel-cell system, such that appropriate research in determining relevant models and control systems can be done. The Imponator is an experimental six-stack air-cooled open-cathode hydrogen fuel-cell system, applied to aircraft. Figure 2.3 shows the physical appearance of the Imponator, currently in an experimental stage. This chapter will dive deeper into this system, firstly by creating a P&ID in Section 2.2.1, making an inventory in Section 2.2.2, outlining the startup and shutdown procedures of general open cathode stacks in Section 2.2.3, and then discussing the reliability and safety considerations in Section 2.2.4 and Section 2.2.5 respectively.

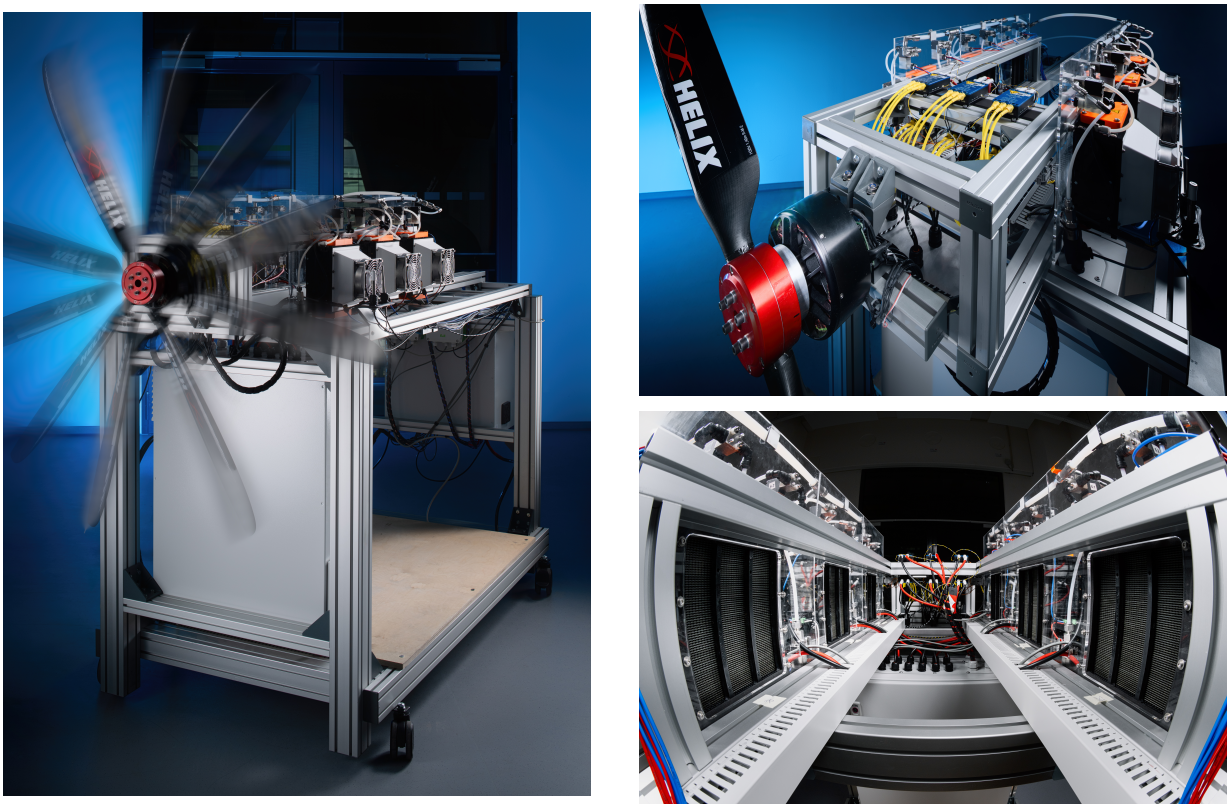

Figure 2.3: [The Imponator fuel-cell propulsion system]. Source: DLR (German Aerospace Center)

2.2.1. System Diagram and P&ID

The P&ID of the Imponator has been made, and it can be seen in Figure 2.4. With respect to this P&ID, the component and color legends can be seen in Table 2.1.

Table 2.1: Imponator P&ID Legends

(a) Component Tag Legend

Tag	Component
MPV	Manual Pressure Valve
MSV	Manual Supply Valve
MM	Mass Flow Controller
SV1–SV7	Supply Valves
PRV	Pressure Relief Valve
PR1–7	Pressure Sensors
PV1-PV6	Purge Valves
RPM1–RPM6	Fan Speed Control
LSW1–LSW6	Load Switches
MCU1–MCU6	Motor Control Units
V, I, P (at MCU)	Voltage, Current, Power Sensors
T1–T7	Temperature Sensors
RH1	Relative humidty ambient sensor

(b) Color Code Legend

Color	Meaning
Red	Anode inlet loop (H_2 supply)
Orange	Anode purge loop (to exhaust)
Green	Cathode air flow loop (fan to stack)
Blue	Stack DC Power Line
	(stacks → MCUs → motor)
Purple	Electrical control and feedback loop

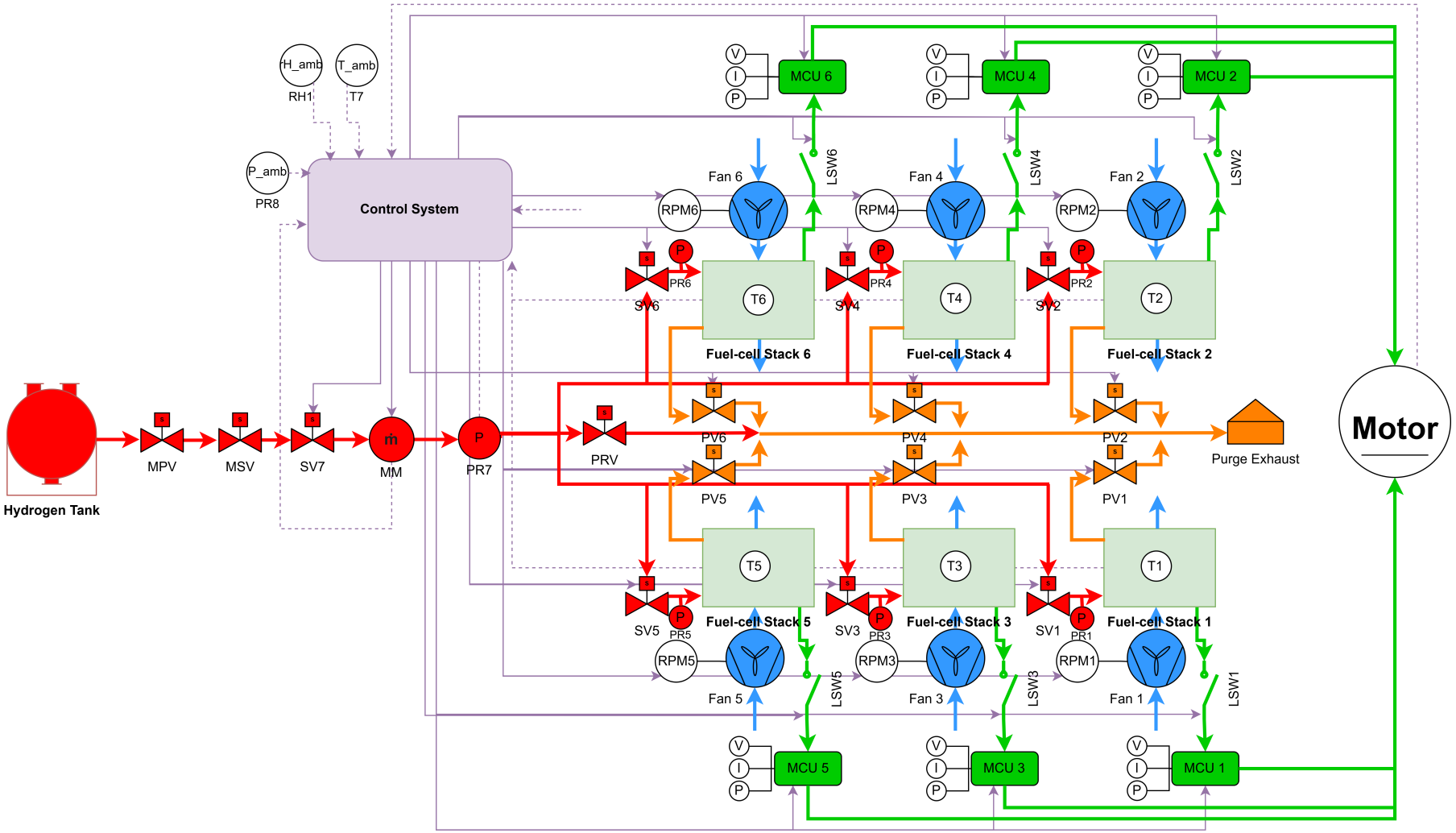

Figure 2.4: P&ID of the Imponator fuel-cell system.

In this diagram in Figure 2.4, all the main components of the Imponator can be visualized with their interconnections. Most importantly, the Imponator can be subdivided into 5 subsystems which are color coded, and can be seen below. For example the fuel cell stacks, MCUs, the motor and all load switches would all be a part of the Power module as seen in green.

1. Anode Hydrogen Supply module (red)
2. Anode Hydrogen Purge module (orange)
3. Cathode Air and Cooling module (blue)
4. Power module (green)
5. Control module (purple)

2.2.2. Inventory

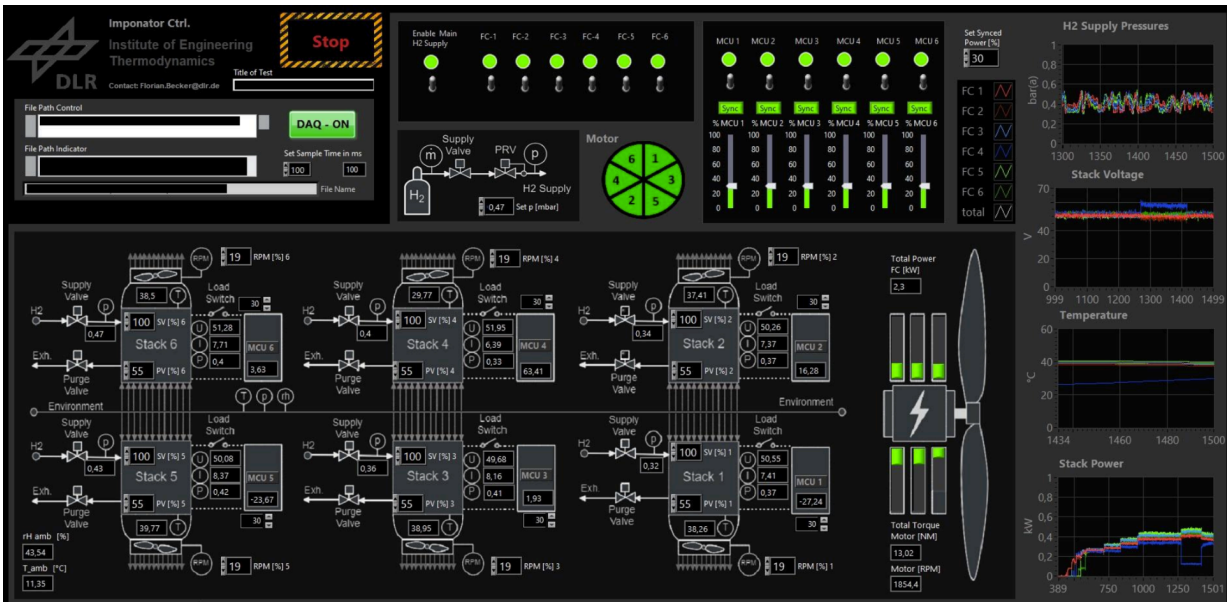

Figure 2.5: Imponator in LabVIEW. Source: DLR (German Aerospace Center)

This section shall summarize the main controllable components involved in the Imponator system. It shall also show the quantities of these different kinds of existing components, including actuators, sensors and control units. The overview of these components can be seen in Table 2.2, and they are interpreted from the LabVIEW controls of the Imponator as seen in Figure 2.5.

Table 2.2: Overview of the main components in the Imponator system.

No.	Component	Description / Notes
1	6× Fuel cell stacks	Primary power sources of the system.
2	6× Fans (cathode side)	Cooling fans located on the cathode side.
3	1× Motor	Main propulsion motor of the system, having 6 MCUs.
4	6× Motor Control Units (MCUs)	Each MCU controls one fuel cell stack. They display voltage, current, and power data. Operation: turn on each MCU, set values (0–100), and press *sync* to run all in unison.
5	1× Propeller	Mechanically driven by the motor for thrust generation, load of the system.
6	6× Hydrogen purge valves	Used to regularly purge excess air and water from the stacks.

Table 2.2: Overview of the main components in the Imponator system (continued).

No.	Component	Description / Notes
7	7× Hydrogen supply valves	Control hydrogen flow to each fuel cell stack.
8	6× Load switches	Used to connect or disconnect electrical loads from each stack.
9	6× Temperature sensors	Measure stack temperatures for monitoring and control.
10	7× Hydrogen pressure sensors	Measure hydrogen pressure at each stack input.
11	1× Ambient sensor module	Measures ambient temperature, pressure, and relative humidity.
12	1× Pressure Relief valve	Allows to set the desired hydrogen pressure in the anode loop after the hydrogen tank.
13	1x Massflow Meter	Measures the hydrogen massflow leaving the hydrogen tank
14	1× CompactRIO	Main control computer running LabVIEW for data acquisition and control.

2.2.3. Startup and Shutdown Procedure

In this section, the startup and shutdown procedure of the Imponator stacks will be documented. These procedures can be implemented in future, in determining a logic flow of components. This shall demonstrate the scope of the startup and shutdown process, helping to later chose the type of relevant models and control systems. Both the startup and shutdown sequences below are recommended by the Intelligent Energy AC64 stack manufacturer, but can be generalized to air-cooled open-cathode fuel-cells.

Startup procedure

It is important to define what the startup entails, which means where it starts and where it ends. Here, it is decided to define startup as going from an off state, to where the system is delivering a certain amount of baseline power. This essentially means that the system ramps up current to a certain baseline power, which is mentioned in step 6. The challenge here is to ramp up the current optimally, so it is fast without dehydrating the membranes (lowering their cell voltage).

1. Switch on fans to minimum set-point at which they move air.
2. Open hydrogen inlet supply valve.
3. Toggle hydrogen outlet valve to displace air and water from the anode. 2-3 purge cycles are recommended.
4. Check open-circuit voltage (OCV) for no load (0A).
   (a) Expected OCV (dry stack) - 0.8V/cell
   (b) Expected OCV (recently operated) 0.92V/cell
5. After confirming OCV is acceptable on all cells, the load should be applied quickly to avoid staying in OCV for too long.
6. Load should be increased slowly to give time for the membranes to hydrate.

Shutdown procedure

The first step in the shutdown procedure will be conducted when a certain load is being pulled from the stack. It is important to note, that this is a normal shutdown procedure, and a faster shutdown may be possible to avoid degradation or to ensure safe system operation.

1. Remove the electronic load from the stack, and return to OCV.
2. Shut off hydrogen supply to the stack.
3. Remove air supply by turning off fans.
4. Stack voltages need to be <5V to be declared off or to carry out any hands-on work. The stack voltage may remain for >30mins after the hydrogen supply has been isolated.

2.2.4. Reliability Considerations

It is important to consider safety and reliability of the startup and shutdown operation. These operations, as indicated by DLR, must be reliable to avoid degradation of the fuel cell stack. Firstly, lets take into account how to ensure the process is reliable, by performing smart control to avoid degradation. From the AC64 manual, degradation of the fuel cells arise from 3 main modes that can be controlled during operation:

1. **Anode starvation:** This degradation mode comes from insufficient purging and hydrogen flow, which can get worse with sudden load increases. Inadequate purging of the nitrogen and excess water in the anode loop can lead to poor cell balance, short term power loss. In the long term, the catalyst can have irreversible damage if the anode is starved of hydrogen [10]. At the same time, too frequent anode purging can lead to wasting hydrogen. This anode starvation can be detected when there are sudden voltage dips, as well anode pressure dips. The purging can be optimized by controlling the purge frequency and duration with the proportional purge valves for each stack [11]. The hydrogen flow can be controlled with the valves and pressure regulator. The manual gives an optimization strategy.
2. **Membrane dehydration:** Membranes can dehydrate if fan airflow too high as humidity is removed, if stack is being overheated which dries membrane, or if current ramp up is too fast. This can be detected with gradual voltage drop, and when the cell voltage decreases lower than the operating limit, that is when degradation starts to occur [12]. This means that the ohmic resistance increases. Goal is to control stack temperature (prevent overheating) and keep the oxygen excess ratio sufficient, by manipulating the fan speed and current ramp rate [13]. The fan here is responsible to keep stack at operating condition of 50°C (cooling), whilst also not drying the membrane (humidity).
3. **High cathode potentials:** Improper startup and shutdown sequencing may lead to hydrogen and air coexisting across membrane. This means, local potentials can spike >1V, platinum oxidizes and dissolves, carbon supports corrode, and local hot spots can cause delamination which is severe [10]. At startup, this can be controlled by purging anode with hydrogen before activating load. This is to avoid oxygen filled anode, which causes high local voltage. Additionally, fuel-cell shouldn't be in OCV for too long as it creates high cathode potentials, and thus load should be applied quickly [14]. In shutdown, load needs to be stopped and then anode needs to be purged to push air out. This is also to avoid air diffusing into anode, to prevent oxygen and hydrogen mixing which reverses potential and leads to corrosion. Potentials can be detected by voltage sensors.

There are more modes of degradation that occur such as ambient contamination or impurities, temperature gradients across stack and long-term catalyst degradation. However, these modes cannot be prevented or avoided using the existing setup and the control tools at hand. There are also strategies of interest such as purging anode loop with nitrogen to do inertization, which are deemed outside of the scope of the control methods at hand. Therefore this project will only try to control the degradation modes mentioned above during the startup and shutdown procedures.

2.2.5. Safety Considerations

Secondly, it is relevant to take into account the safe operation of the system. When it comes to the fuel cell, there are 4 main events that cause for an emergency procedure, derived from an user manual not publicly available:

1. When there is hydrogen leakage in excess. This means, that either hydrogen leakage is taking place in a closed environment. Or it can also mean, that the rate of hydrogen leakage is too large for the ventilation system of the environment. Since there is no hydrogen sensor in the system currently, this will be given as an improvement.
2. When the stack core temperature is $\geq$70°C.
3. When a cell voltage is <0.5V for >5s, whilst a load is applied on the stack.
4. When OCV <0.7V on any cell. This is in the case that no load is being applied.

In the case that any of the above events occur, the shutdown procedure must be immediately engaged. It is still important to ensure that the fans are kept on, such that the stack core temperature(s) return to below 50°C, after which they can be turned off. .

2.3. Types of Control-oriented Models and Supervisory Control

To be able to control a system effectively, a model of that system is needed. Often times, a statistics based model is difficult and expensive to make as informed by DLR, and usually is not directly useful to perform control. Therefore an accurate but simple model of a system is required, which can be used to effectively control a system. Many such models exist, and in this chapter, the most relevant types of models will be studied and reviewed in order to chose which model(s) to implement in the thesis. Firstly the Multi-level Flow Modelling was reviewed in Section 2.3.1, followed by Petrinets modelling in Section 2.3.2, Finite State Machine modelling Section 2.3.3 and some lower-level physics based models in Section 2.3.4.

2.3.1. Multi-level Flow Modelling

As recommended by Dr. Rene van Paassen, Multi-level Flow Modelling (MFM) can be used to create a high-level simple model of the fuel-cell system, which can be directly used by a control system. Therefore, it is useful to learn more about MFM and understand how it can be used in the thesis.

From Morten Lind's book called "Foundations for Functional Modelling of Technical Artefacts", it is found that MFM is a high-level functional modelling method for complex technical systems [15]. Essentially it represents mass, energy and information flows, and links them to functions and goals. MFM models the purpose and dependencies of components in the system, as supposed to modelling equations which is what a physical model does. The "Multi-level" refers to the hierarchy in the model, descending from goals to functions to components, and here is their definition below:

1. **Goals**: Highest level system objectives, describing why the system exists.
2. **Functions**: Description of what must be achieved to fulfill the goals, in terms of mass, energy or information flows. This describes the purpose of the actions, without mentioning hardware.
3. **Components**: The actual hardware that realize the functions, and are responsible for how the hardware implement the functions. They specify how a function is achieved.

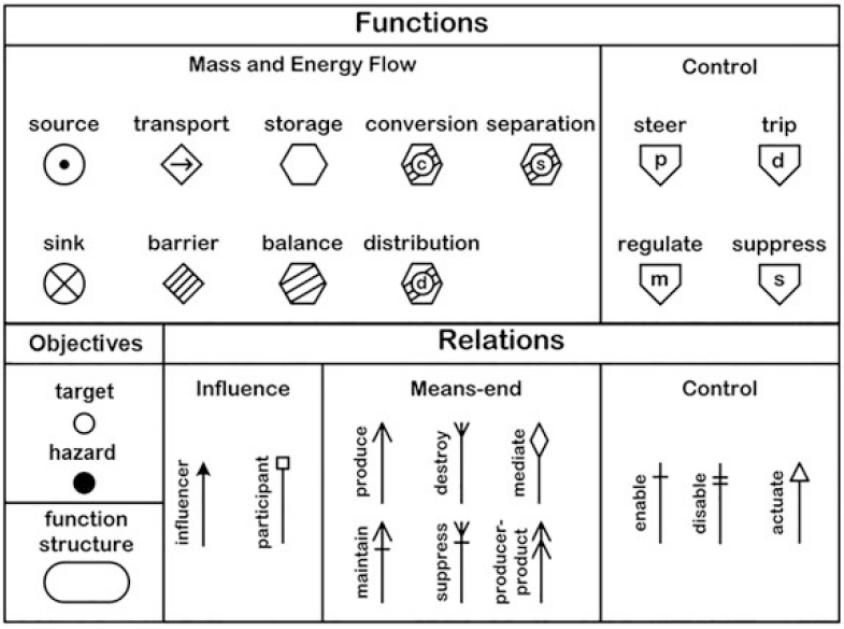

Figure 2.6: Concepts of Multi-level Flow Modelling [15]

The main concepts of MFM can be seen in Figure 2.6, distinguished in terms of objectives, functions and the relations. These are the concepts used in order to make a MFM, which essentially links an objective (goal and hazards) to a function, and that function can be related to the respective component(s). Within functions, there are the mass and energy flow functions, and the control functions. And there are 3

types of relations, influence, means-end and control. These relations connect functions to objectives, to other functions, and to components as well. This leads to a complete model, which has a source and sink, and within the diagram it contains objectives, functions and specific components which can all be related to each other. For example, there could be a **function** of **transport** air which **maintains** the **objective** of **target** airflow. This **function** of **transport** air can be achieved by **actuating** the **component** fan. All of these different kinds of objectives and flows required by the system for a safe operation can be neatly represented in a Multi-level Flow Model, such that all process are acknowledged.

Generally, MFM is mainly useful because it captures the intentions and goals of a system quite well, instead of just physical details. It can link plant functions to control actions, and can explicitly model safety functions and barriers in the operation of the system. These benefits supports the automation of procedures, as MFM can be used to derive action sequences for a startup or shutdown procedure, which is of interest in this project.

2.3.2. Petri nets Modelling

Petri nets (PN) model is a graphical and mathematical representation of discrete distributed systems. It is a modelling language which graphically depicts the structure of a distributed system as a directed bipartite graph decision [16]. It is useful in control because it explicitly models concurrency, when there's multiple components with overlapping sequences like stacks, and act as supervisory control. They also represent resource contention, deadlock analysis and liveness checks.

Its important to cover the core components of a Petri net, which can be seen below [17]:

- **Places**: They represent the system states, conditions, or resources, and are drawn as circles. They can hold 0 or more tokens.
- **Tokens**: These are markers that denote the current state of resources.
- **Transitions**: They represent events or any actions that change the state. When a transition is fired, it consumes tokens from its input places and produces tokens in its output places, which are subjected to rules. They are drawn as bars or boxes.
- **Arcs**: These simply connect places to transitions called input arcs, and transitions to places called output arcs.
- **Firing rules**: A transitions is enabled when all of its input places have the required number of tokens, after which they're fired. Then the transfer of tokens from input places to output places take place.

Here are some of the main symbols used in a Petri net in Figure 2.7, along with their primitives to represent system features as seen in Figure 2.8.

Figure 2.7: Petri net symbols [16]

It is found, that a PN model has been developed for fuel cell systems, as seen in the paper "A Petri net approach for performance modelling of polymer electrolyte membrane fuel cell systems" [18]. In this application of interest, a Petri net is described as a directed, weighted bi-partite graph where the nodes are places (physical resources, conditions or the state of a component/system), and transitions are connected by arcs. This is quite similar to the conventional Petri nets, however they made use of Timed Colored Petri nets, for a better description of complex systems. These token colors contribute to define enabling conditions for the firing of transitions, and additionally different firing modes can be defined for the same transition depending on the token colors.

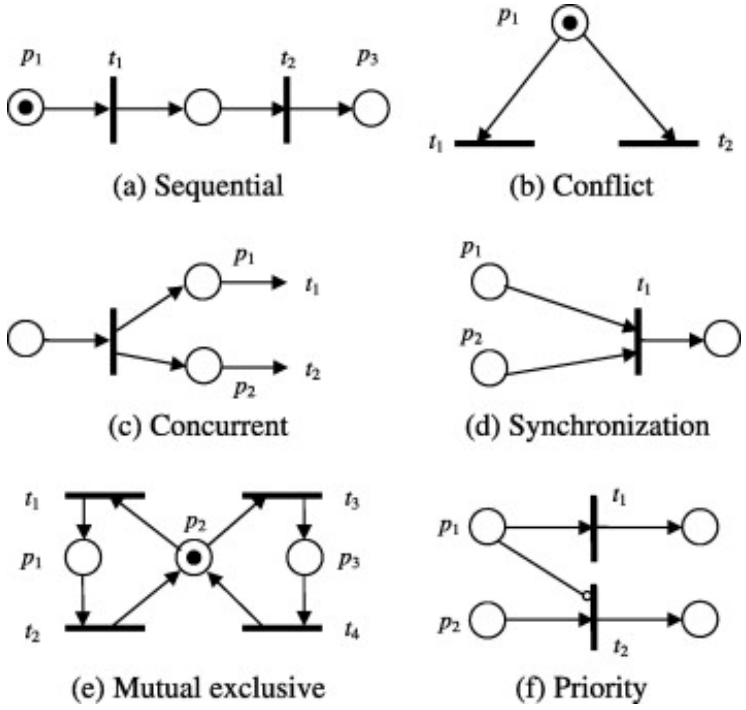

Figure 2.8: Petri net primitives [16]

An example of the Petri nets being applied can be looked at to better understand how it can be modeled. For example, the paper looks at the hydrogen supply system as seen in Figure 2.9, and then models it with Petri nets as seen in Figure 2.10.

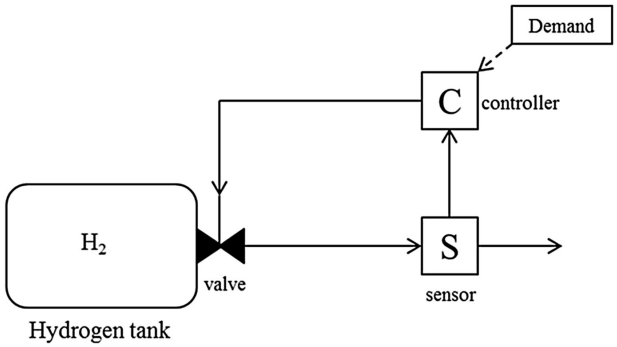

Figure 2.9: Hydrogen supply system [18]

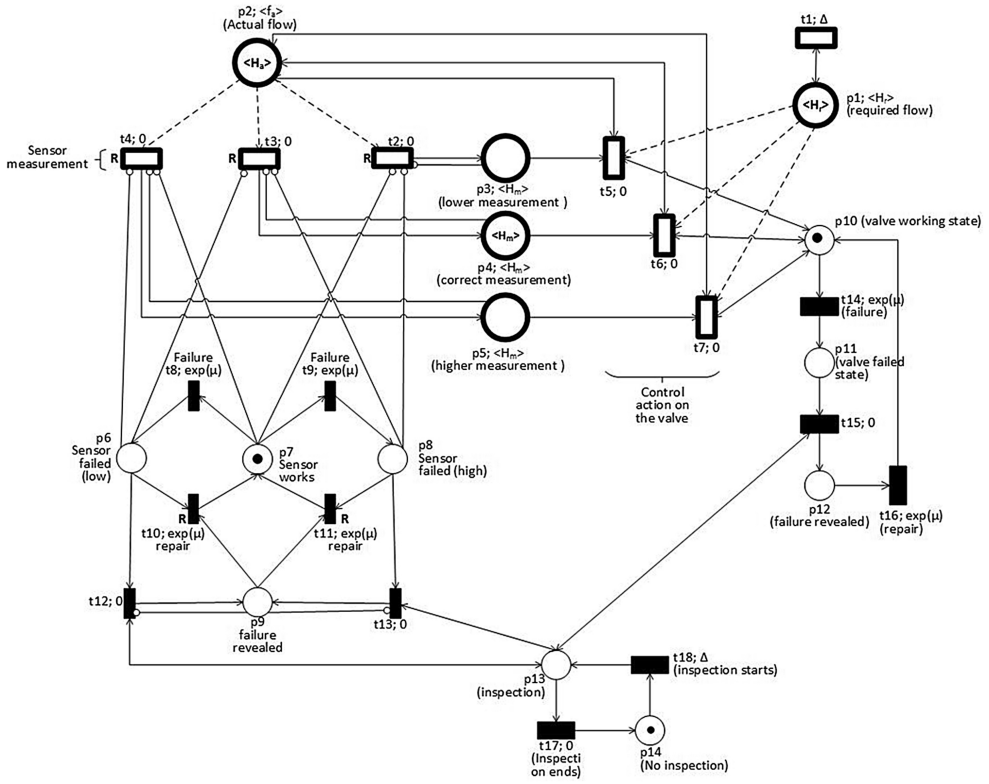

Figure 2.10: Hydrogen supply system modeled with Petri nets [18]

2.3.3. Finite State Machine Model

Finite State Machine (FSM) is a high-level discrete-event logic based model and supervisory controller, which encompasses system behavior. It is a representation of an event-driven system, that transitions between states if the transition conditions are met [19]. It is at the same level as a Petri nets model, however is intuitive and readily available in Simulink. Just like any other high level model, it also always needs lower level physical models to be useful for control. There are 3 main components that are needed when building a state machine:

- **States:** Different steps or modes of operation that distinguish processes occurring in a system
- **Transitions:** Methods of moving from one state to another
- **Actions:** Changes or events that occur whilst executing the state machine. This occurs for example when entering or leaving a state.

Essentially, the FSM is a clear and intuitive model type that can be used to model the startup and shutdown procedure of a fuel cell system. Considering this, a paper was found that implemented FSM on a fuel-cell system model on MATLAB, and developed control strategies to perform startup and shutdown [20]. The paper developed a fuel cell supervisory controller for automotive hybrid fuel cell vehicle, which consists of a State Machine, an Optimal Setpoint Generator (OSG) and a Power Limit Calculator (PLC). The State Machine coordinated the different operational states of the system, including the startup and shutdown processes. The OSG was used to maximize the fuel cell system's efficiency and also minimize its degradation, by solving optimization problems and taking into account manufacturer's requirements. The PLC essentially assessed stack's power output capability, which was used to calculate current setpoints, and this information was used in the power distribution calculations of fuel cells and batteries.

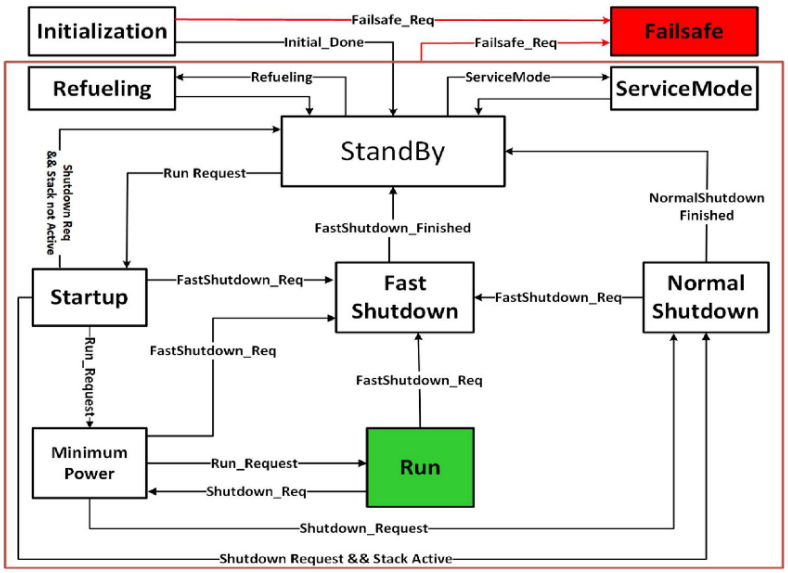

Figure 2.11: State Machine scheme for a fuel-cell system [20]

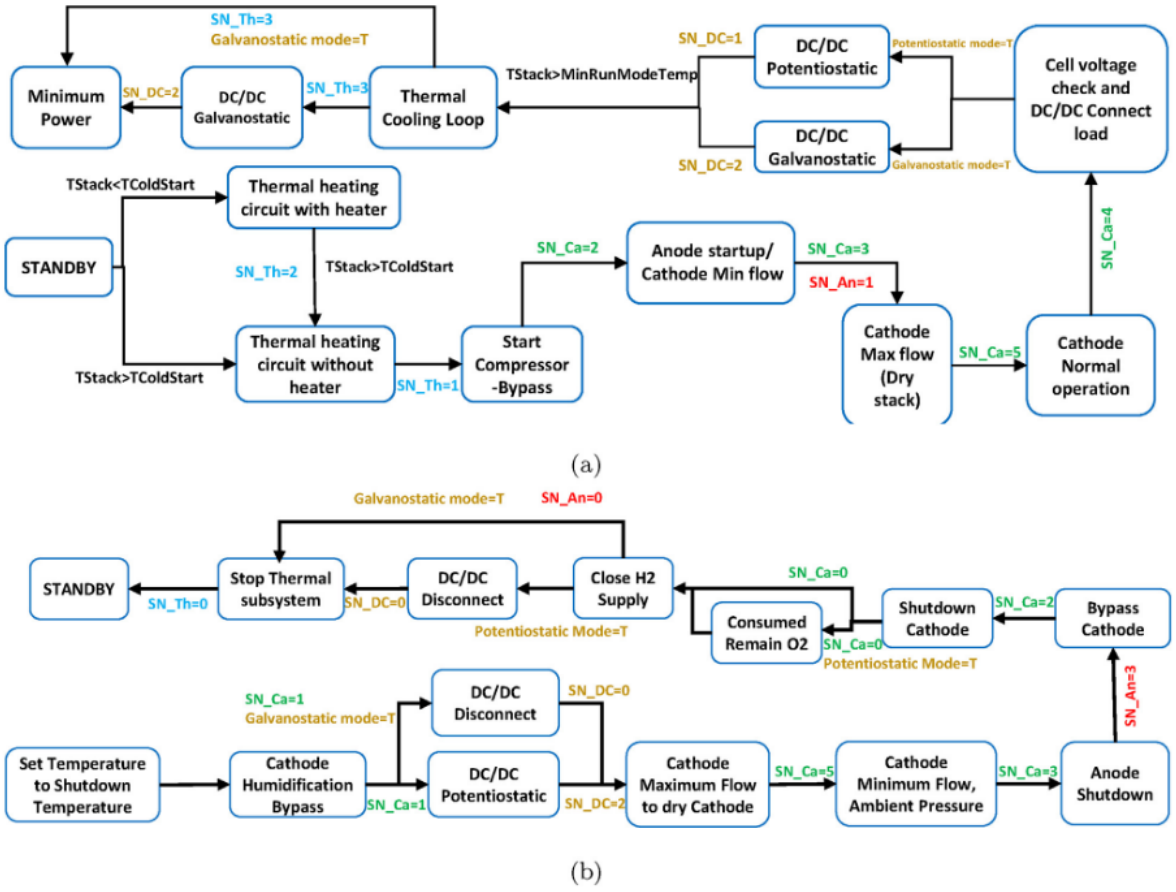

Figure 2.12: Startup and Shutdown sub-State Machines for the automotive fuel-cell system [20]

The overall State Machine scheme developed in the paper can be seen in Figure 2.11, which essentially shows how the transition between states works. The system starts in Initialization, and after the initialization

conditions are done, it can go to StandBy, unless a Failsafe is requested in which case it goes into Failsafe. From StandBy, the paper mentions a VCU which would send a Run Request, after which system will be in Startup. If certain conditions are met, system goes to Minimum Power state and then eventually goes into Run state.

The paper also highlights the sub-State Machines for the fuel cell system's startup and shutdown, which can be seen in Figure 2.12. The paper also defines several subsystems and all their available operating modes, labeled by status numbers (SN) which can be seen in Figure 2.12. These subsystems include cathode, thermal, anode and DC/DC subsystems. All these subsystems are controlled within the startup and shutdown procedure, which is displayed in the sub-State Machine charts. For example, to go from Start Compressor to Cathode Min flow, the Cathode subsystem needs to confirm that $SN - Ca$ of 2 is reached, meaning the compressor started successfully.

2.3.4. Control-based PEMFC Physical Models

To complete the picture, low-level models, usually physical, are often needed together with a high-level model to achieve good control. A paper recognizes that open-cathode fuel cell systems are gaining popularity in low to medium power applications, and want to help bring this technology into practice. They see that to achieve safe operation, increase durability and optimal performance, advanced control algorithms need to be implemented. These advanced control algorithms typically require control-oriented models, and this this paper develops control-oriented non-linear physical models for individual components of air-forced open cathode fuel cell systems [21]. The paper validates the developed model with experimental results, and shows that the models have a good prediction capability, as seen be seen for the voltage and temperature models for the fuel cells Figure 2.13.

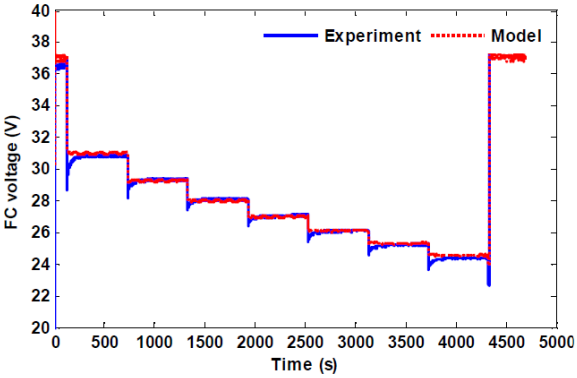

Figure 1. Experimental voltage measurements versus model output.

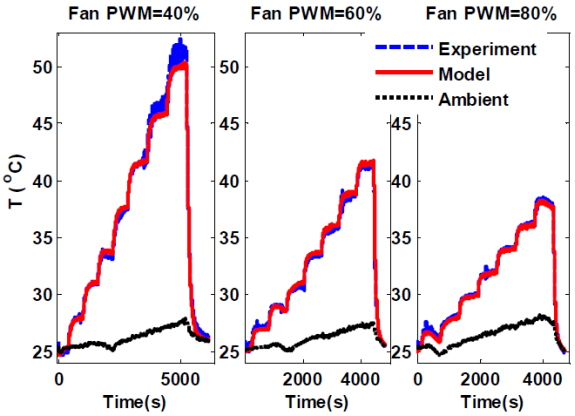

Figure 5. Temperature model validation test results.

Figure 2.13: Fuel cell voltage and temperature model validation [21]

The paper essentially develops low-level component models for fuel cell voltage, cathode, anode and thermal subsystem. These types of models is more relevant for continuous control design, such as fan speed control, stack voltage regulation, and purging effectively and efficiently. These are needed in low-level controllers (inner control loops), and can be used together with a higher-level MFM or Petri nets model.

2.4. Types of Relevant Subsystem Control Systems

In order to determine relevant controllers, it is important to determine which subsystems exist, and which of them are going to be especially modeled with a simplified physics based model. The list of important subsystems that need to be modelled were defined in Section 2.2.1. For each subsystem, the most important parameters to be modelled are control variables (which are values that can be directly tuned and controlled), and what effect this has on physical changes that can be measured (such as pressure,

tempperature, massflow, voltages etc...). Essentially, low level models need to be chosen from literature that describe the behavior of components in the fuel-cell system, due to changing the inputs. In this chapter, several papers are explained which use such models to test and build controllers to carry out control objectives optimally. Firstly, controllers for the cathode air and anode hydrogen supply subsystems are discussed in Section 2.4.1, for the cathode cooling subsystem in Section 2.4.2 and for the anode purge subsystem in Section 2.4.3.

2.4.1. Control of Cathode Air and Anode Hydrogen Supply Subsystems

During operation, ensuring sufficient air and hydrogen is delivered to the system is important for reliable operation, since it prevents degradation from oxygen starvation and anode starvation. A paper was found that made model-based control systems, and tested out several controllers and compared their performances [22]. Firstly, the developed and validated several models such as for the fuel cell stack, air supply (which includes blower motor dynamics, blower map and manifold dynamics), along with a hydrogen valve pressure control model to balance the anode and cathode pressures. All of these models, are relevant to this thesis project.

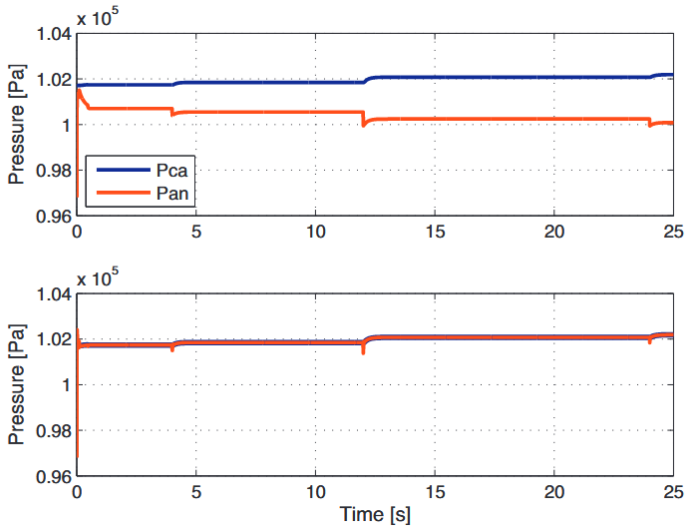

Figure 2.14: P (top) and PI controller (bottom) to match anode and cathode pressures with hydrogen valve [22]

Most notably, the paper shows use of a P and PI controller to control the anode pressure via the hydrogen control valve. They use the cathode pressure as a reference, which means that the control goal is to minimize the pressure difference between the anode and cathode. They recommend the use of a PI controller instead of just a P controller, due to the stationary and integral behavior of the system, and the results are evident as seen in Figure 2.14.

Thereafter, the paper implements three approaches to control the oxygen excess ratio of 2, to prevent oxygen starvation. This is the main control objective that the paper wants to tackle, by manipulating the fan's voltage, which affects the airflow rate supplied to the stack. The three approaches the paper used were static feed-forward control, state-feedback control and gain scheduling control, and their results can be seen in Figure 2.15. It was shown that the feed-forward controller used lookup table making it simple, but it was slower in transients. State-feedback controller was better, however it had stationary error in working points outside of the linearization point, as it had to linearize the non-linear fuel-cell model. Whereas the gain-scheduling controller showed better results over the entire working range of the fuel-cell. Here, it made linearized models for several nominal working points, and different controllers were then interpolated between each other. This paper properly covers controllers for the cathode air supply and the anode hydrogen supply subsystems, however the control of the cooling subsystem still remains.

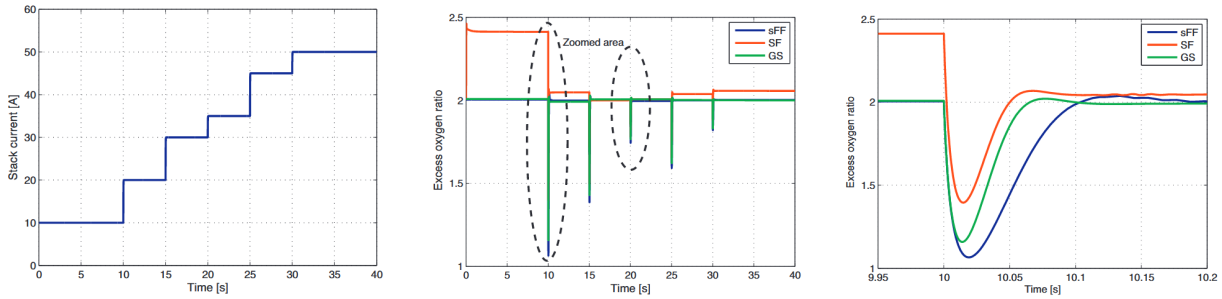

Figure 2.15: Input current profile and corresponding oxygen excess ratio results using three controllers [22]

Another paper is found to develop controllers on a simplified control oriented model for open cathode PEMFC, using only 3 states [23]. The model is simplified because it only has 3 states, namely the mass flow of oxygen, hydrogen, and water. They estimated some of the parameters using experimental data from a 1.2kW fuel cell. The main objective in the paper, was to maintain a fixed oxygen excess ratio to avoid oxygen starvation and to ensure that the required power can be supplied.

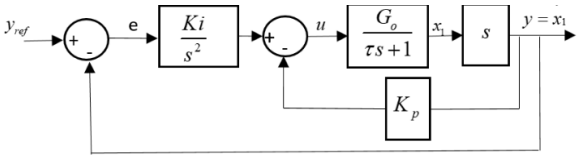

Fig. 1 PI-like Controller scheme for maintaining oxygen excess ratio.

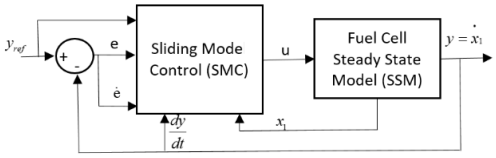

Fig. 2 Sliding Mode Control scheme for maintaining oxygen excess ratio.

Figure 2.16: PI and SMC control scheme comparison [23]

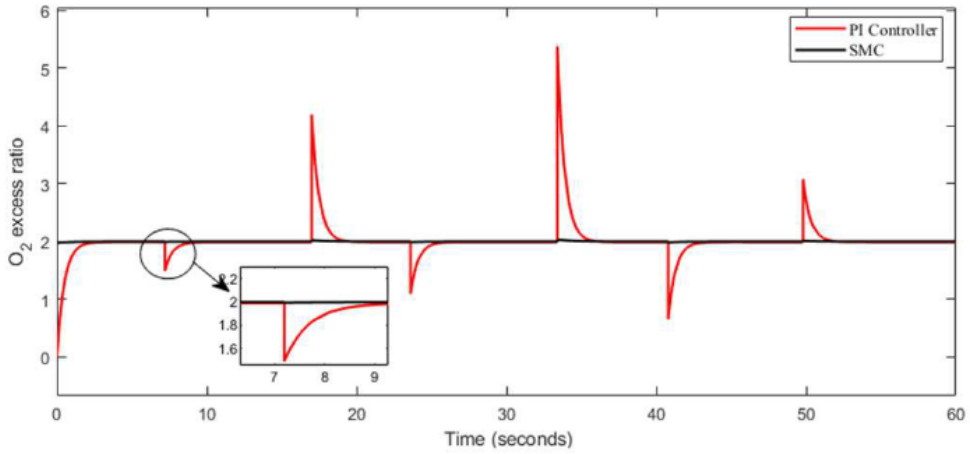

Figure 2.17: Comparison between PI and SMC controllers in maintaining excess oxygen ratio of 2 [23]

After creating a simplified model, they validated it with experimental results, saying model was accurate enough. It is actually a good balance between accuracy and response time of the PEMFC, with a simplified model reducing the response time. Then, they actually implemented two different control systems to be able to compare which one performs the objective better. Firstly, they implemented a PI (proportional and integral) controller, and secondly SMC (sliding mode control). The control diagrams of how both of these controllers were implemented in MATLAB Simulink can be seen in Figure 2.16. The results of both control systems trying to achieve their objective can be seen in Figure 2.17. As can be seen, the SMC controller

does a better job of maintaining the excess oxygen ratio of 2 in dynamic situations when the parameters change. Whereas, PI controller lets the ratio deviate quite a lot when parameters change, and with some delay it is able to bring it back to 2.

So it is shown in Figure 2.17, that the SMC controller performs better with this simplified model with the objective of maintaining a constant oxygen excess ratio of 2, avoiding degradation and ensuring required power can be consistently supplied. This may be useful later on, when deciding what kind of low level controllers to select for various objectives.

2.4.2. Control of Cathode Cooling Subsystem

Open-cathode fuel cells usually need to be operated at a target operating temperature, and overheating can cause degradation of the stack due to membrane dehydration. A paper is found which deals with implementing MPC to perform the temperature cooling control of an open-cathode PEMFC system [24]. Firstly, they create a thermal model of the fuel cell which is linearized by using the Taylor formula, and this model is validated. Thereafter they develop closed-loop feedback MPC according to linearized state-space model which is used to track 50°C as the target operating temperature. Then it is experimentally tested on a testrig, controlled via LabVIEW.

The effectiveness and performance of the MPC controller was compared with a PI controller, which can be seen in Figure 2.18 for a constant 20A load current. Here, the PI controller can be seen to have a steady state error, whereas the MPC simulation and experiment performed better, and seem to match each other. Underneath, the duty cycles produced by the MPC and PI can be seen, which corresponds directly to the PWM period, which affects the fan voltage and power, and thus the airflow rate. MPC duty cycle remains stable around a value, whereas PI duty cycle fluctuates a lot. Secondly, in Figure 2.19 the MPC performance can also be seen in a current ramp up from 18A to 25A during which the target temperature is also increased from 45°C to 50°C.The experimental and simulation of the MPC also seem to match quite well here, demonstrating the reliability of MPC.

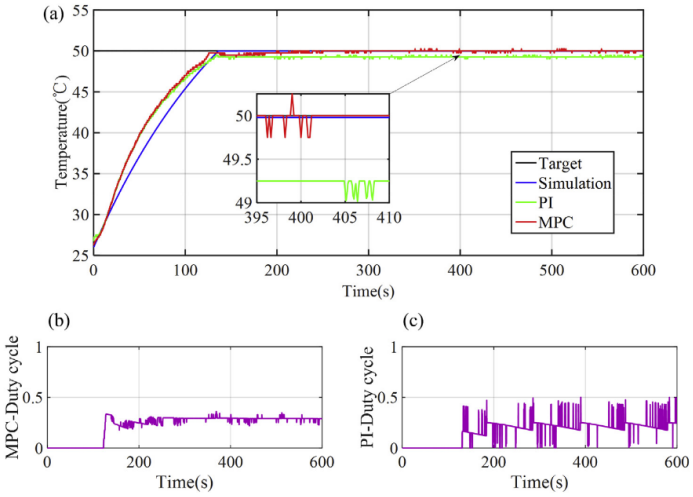

Figure 2.18: Temperature control during a constant 20A load current [24]

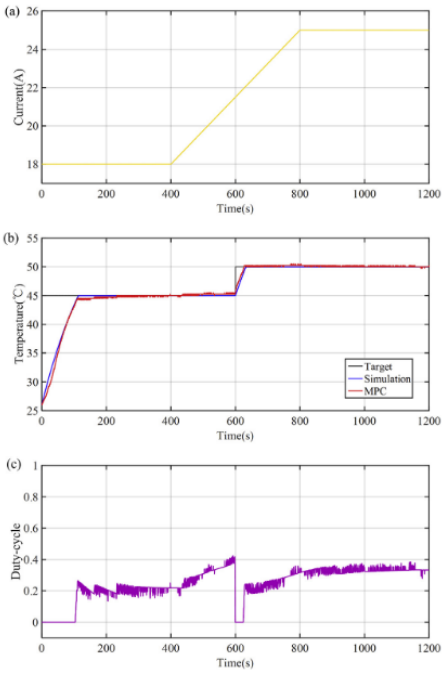

Figure 2.19: Temperature control during current ramp-up and varying target [24]

2.4.3. Control of Anode Purge Subsystem

The purging of the anode loop is important during fuel cell operation, also specifically in the startup and shutdown procedures. Anode purging prevents the degradation modes of anode starvation and high cathode potentials, however the frequency, duration and how much the purge valve should be opened in %, remains a control challenge. A paper was found that attempted to find the optimal purge strategy, which includes determining the purge duration and the purge interval, which relates to the frequency [25]. The paper tested on a fuel-cell with dead ended anode, which is similar to the Imponator fuel-cell stacks, as they also don't have an anode recirculation loop. This essentially means that the anode loop has an end, since the purge valve is not always opened. To get rid of the accumulating impurities, the stack needs to be purged, however suboptimal purge interval (valve closed) and purge duration (valve open) can cause excessive impurity accumulation, or low hydrogen utilization.

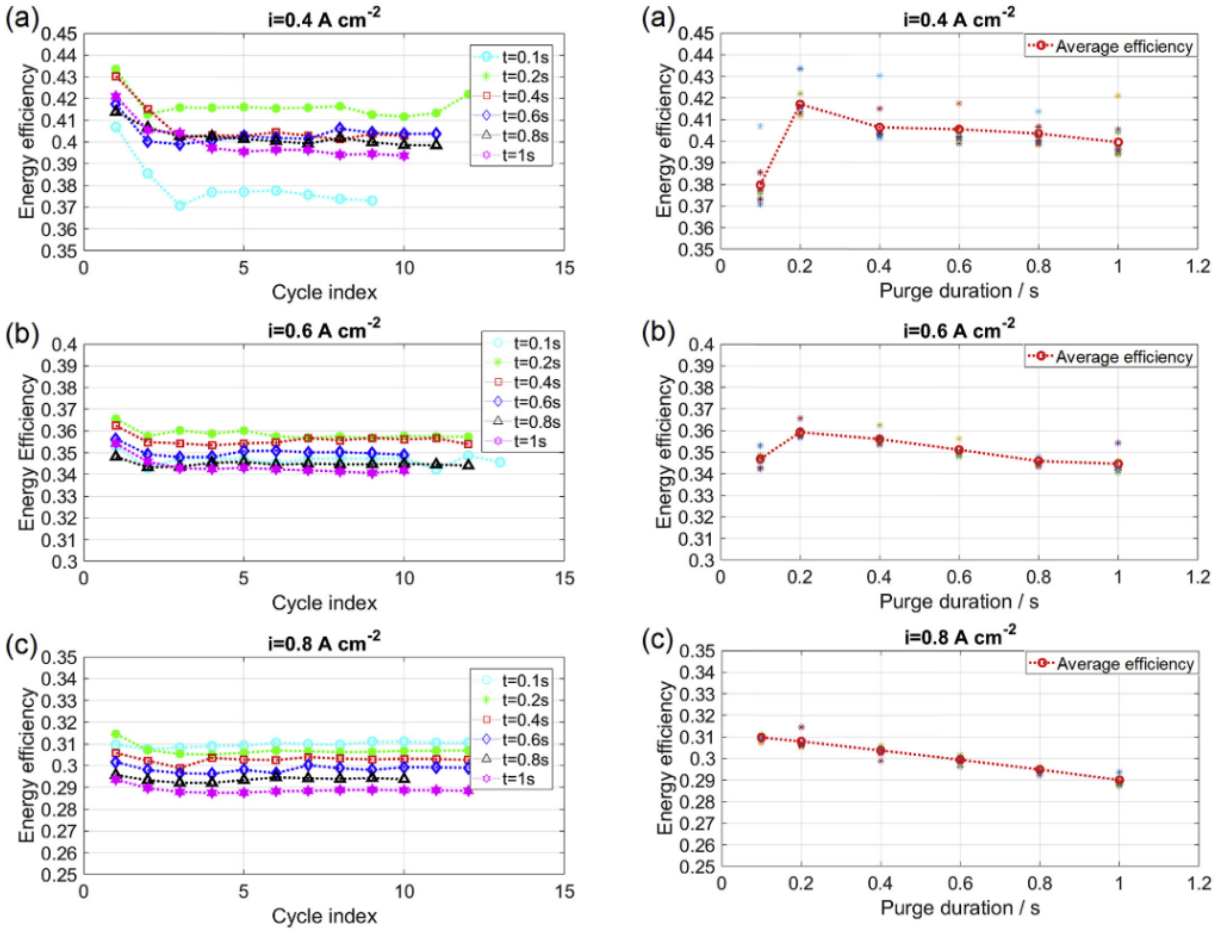

Figure 2.20: Energy efficiency of several purge cycles varying durations, for given current density [25]

The results of the tests with varying the purge durations for different current densities can be seen in Figure 2.20. As can be seen, for current densities of 0.4 and 0.6 Acm^{-2}, purge duration of 0.2s lead to highest energy efficiency. Whereas for current density of 0.8 Acm^{-2}, the optimal purge duration was 0.1s. The paper also provided a method to determine the optimal purge duration. This method assumes that if the entire anode volume is purged by fresh pure hydrogen, no impurities would remain. Using this, it calculates the volume of anode for a single cell (including double serpentine channels and gas diffusion layer), and then calculates the gas flow rate when valve is opened. With these two values, the time required to purge all gases out of the anode was found. However, since the paper also shows that impurities form near the outlet, and slowly propagate towards the inlet, and thus the entire volume does not need to be purged. Their study shows, that approximately 1/4th of the anode volume needs to be purged

to achieve optimal energy efficiency. This is a useful method which can be used in the optimal purging of the Imponator stacks, and the purge duration can be updated with changes in the anode pressure.

2.5. Research Plan

After a sufficient literature review to answer the primary and sub research questions, it is important to develop a research plan. This research plan shall include the research activities that shall take place to answer the research questions in detail, along with a timeline to indicate when they should be carried out in the thesis. There should also be a hypothesis for each research question, and this hypothesis should be used to determine the content of the research activities.

From the primary research question PRQ, several sub-questions were previously defined. From these sub questions, the literature review research was carried out. It is important now to bring it back to the research questions, and form an hypothesis or a relevant answer to them by summarizing the findings of the literature review. Section 2.5.1 to Section 2.5.4 serve as the answers or research activities linked to the research questions, with Section 2.5.5 giving the definite research activities up next along with the planning.

2.5.1. Control System Design Requirements

Sub Research Question 1

How can the control system design requirements be defined to ensure safe and reliable start-up and shutdown procedures?

As a result of understanding the Imponator fuel-cell system, the design requirements for its control system can be formulated. The requirements can be derived from the reliability, safety and operational considerations for category grouping. Some information is obtained from the publicly unavailable stack manual. These requirements can be seen in Table 2.3 and Table 2.4.

Table 2.3: Reliability requirements for the control system

ID	Requirement
CS-R1	The control system shall maintain the stacks' hydrogen pressure between 400–700 mbar.g.
CS-R2	The control system shall optimize anode purging to remove impurities whilst maximizing hydrogen utilization.
CS-R3	The control system shall maintain oxygen excess ratios of $\geq$2 during operation[26].
CS-R4	The control system shall keep the stack temperatures $\leq 50\,^{\circ}$C during operation.
CS-R5	The control system shall keep temperature within $\pm 1\,^{\circ}$C of desired value at maximum possible power.
CS-R6	The control system at startup shall purge anode before activating the load [27].
CS-R7	The control system at startup shall minimize the time in OCV [27].
CS-R8	The control system at startup shall ramp-up the fuel-cell system to the minimum power.
CS-R9	The control system shall maintain cell voltage between 0.5 V and 0.92 V when loaded.
CS-R10	The control system shall keep stack current within ± 1 A of demanded current.
CS-R11	The control system at shutdown shall purge anode after deactivating load [27].

In Table 2.3, CS-R1–R2 focus on preventing the anode starvation degradation mode, as they ensure that the stacks receive sufficient hydrogen at all times. CS-R3–R5 prevent the membrane dehydration, by ensuring that stacks don't dry from excess oxygen or by overheating. Whereas CS-R6–R11 focus on preventing high cathode potentials, by sequencing the purge appropriately and minimizing time in OCV.

Table 2.4: Safety requirements for the control system

ID	Requirement
CS-S1	The control system shall initiate emergency shutdown if the detected hydrogen leakage is ≥4000ppm [28].
CS-S2	The control system shall initiate emergency shutdown if stack core temperature ≥ 70°C.
CS-S3	The control system shall initiate emergency shutdown if unloaded OCV is <0.7V or >1V.
CS-S4	The control system shall initiate emergency shutdown if loaded cell voltage is <0.5V for >5s.

In Table 2.4, CS-S1–S4 all deal with ensuring that the control system will iniitate an emergency shutdown, in case any of these events occur. Notably, CS-S1 cannot be currently implemented into the real system due to absence of hydrogen sensors, however a suitable approach can be modelled as an improvement to real system.

2.5.2. Model & Controller Selection

Sub Research Question 2

What are the most relevant control-oriented model types and controllers in automating the startup and shutdown?

Model Selection

It useful to compare the researched model types, in terms of strengths and weaknesses to evaluate which model type combination is best suited for this research project. This evaluation can be seen in Table 2.5. Firstly, the three high level model types of MFM, PN and FSM are defined in terms of their strengths and weaknesses. This is followed by grouping the paper outlined in Section 2.3.4 into a category called low-level models, which describe a physical plant.

MFM can be defined as a high level conceptual model, which is intuitive to understand, and its holistic approach can be used for safety monitoring and fault diagnosis. However, it isn't directly executable as control logic, and its descriptions are more qualitative and less precise. Then secondly, PN can be described as a high level supervisory logic, which has the strengths of being executable logic for startup or shutdown procedures. However, the model can become non-intuitive as systems get large, and is not goal-oriented. Thirdly, FSM can be defined as also a high-level supervisory model, quite similar to PN, as it is also executable. Additionally, it is intuitive and has good integration within MATLAB, with its only weakness being that it may get complex with many concurrent systems.

As a result of investigating these model types, it seems that the MFM can be used as a high-level conceptual model that represents the systems goals and dependencies. These should cover the reliability and safety aspects of the Imponator system in a holistic manner, such that there is a good overview of operational constraints and risks. After developing such a conceptual model in a chart, these goals can be translated to the middle-level FSM which would act as a supervisory control-model. FSM can be used to make an intuitive model, that can be directly implemented in the Stateflow toolbox in the MATLAB/Simulink environment. FSM is a lot more intuitive than PN, and MATLAB also contains the tools to directly build a State Machine. Due to these reasons, FSM is chosen instead of PN. After this, low-level physical models can be used in combination with FSM in MATLAB. These are quantitative, and would be quite suitable for various kinds of linear or non-linear controller design and tuning. Therefore, the combination of MFM, FSM and low-level models, can be used to tackle the control-oriented modelling of the Imponator system.

Table 2.5: Comparing the researched model types

Model Types	Strengths	Weaknesses
Multi-level Flow Modelling (High level conceptual)	• Intuitive, goal oriented • Safety monitoring, fault diagnosis	• Not directly executable as control logic • More qualitative, so can be less precise
Petri Nets (High level supervisory logic)	• Executable supervisory model • Automating startup/shutdown	• Large systems become non-intuitive • Not goal-oriented
Finite State Machine (High level supervisory logic)	• Intuitive, integrated in MATLAB • Executable startup/shutdown procedures	• Complex with many concurrent subsystems
Low-level models (Low level modelling)	• Quantitative • Suitable for controller design and tuning (PID/MPC)	• Not suited for sequential logic

Controllers Summary
Regarding the controllers for the low-level models, the main subsystems were defined in Section 2.2. These subsystems also correspond to the physical models that need to be created. Firstly, literature was reviewed for the control of cathode air and anode hydrogen supply subsystem. Here, papers were found to use PI controllers to control the hydrogen supply, and SFF, SF, GS, PI and SMC controllers for the air supply. To control the cathode cooling subsystem, PI and MPC controllers were found to be effective. Lastly, papers on anode purging subsystem were found to include certain empirical optimization methods.

This gives a good overview of the relevant controllers that exist in this application. At this stage of the project, it is not necessary to chose a certain controller for a physical model, as the physical models have not yet been developed. It is useful for now, to simply be aware of the attempts approaches, to inspire choices later on in the project.

2.5.3. System Modelling

Sub Research Question 3

How can the fuel-cell system be modelled, along with its startup and shutdown procedures?

Sub Research Question 4

How can the accuracy of the model to the real system be measured?

These two sub research questions can be answered by developing a system model of the Imponator fuel-cell system. This would be an important phase called ”Modelling” of the system, as seen in Figure 2.21. Here, the Imponator can be represented by a combination of the three chosen model types. It will be a top-down approach, starting at an conceptual level first by doing Multi-level Flow Modelling to define goals and functions. Then, a supervisory Finite State Machine model will be developed, this goes a level deeper as it is an executable code that is to be developed in MATLAB. After this, the low-level physics models will be developed, depending on the requirements and the goals that are important. This phase would end in a model validation, which would mean comparing the model’s main behavior to experimental data. Existing experimental data can be used to keep planning controlled, however it is possible to gather experimental data if needed.

2.5.4. Control System Design

Sub Research Question 5

How can relevant model-based control systems be developed to automate the startup and shutdown?

Lastly, this sub research question can be answered by a research activity involving the design of ”Control Systems” as seen in Figure 2.21. This phase would firstly involve model-based controller design and developed, where each low-level models would have integrated controller(s), which aim to meet their respective control objectives. After this, the requirements of the control systems will be attempted to be verified in the model. Due to the limited time of the thesis, the integration of the controllers and requirement verification into the real system will be left as a stretch goal to keep planning feasible with margin. Therefore, if time permits, the controllers may be integrated in the real system and tested for demonstration purposes, however it is currently formulated as outside the main content of the thesis.

2.5.5. Research Activities & Planning

Based on the research questions and their hypothesis, the key main research activities are system modelling, and model-based control system design which can be seen in Figure 2.21. After the modelling phase, the mid-term review will be held, which is a good moment to evaluate the state of the model. Thereafter, green-light meeting can be used to evaluate the model validation, the control system design progress and the draft of the final thesis report. The green-light meeting will be held in the middle of April 2026, which means the thesis defense shall be planned within the month of May 2026. Therefore, 8 May 2026 is the date of the graduation, and the conclusion of this MSc thesis project.

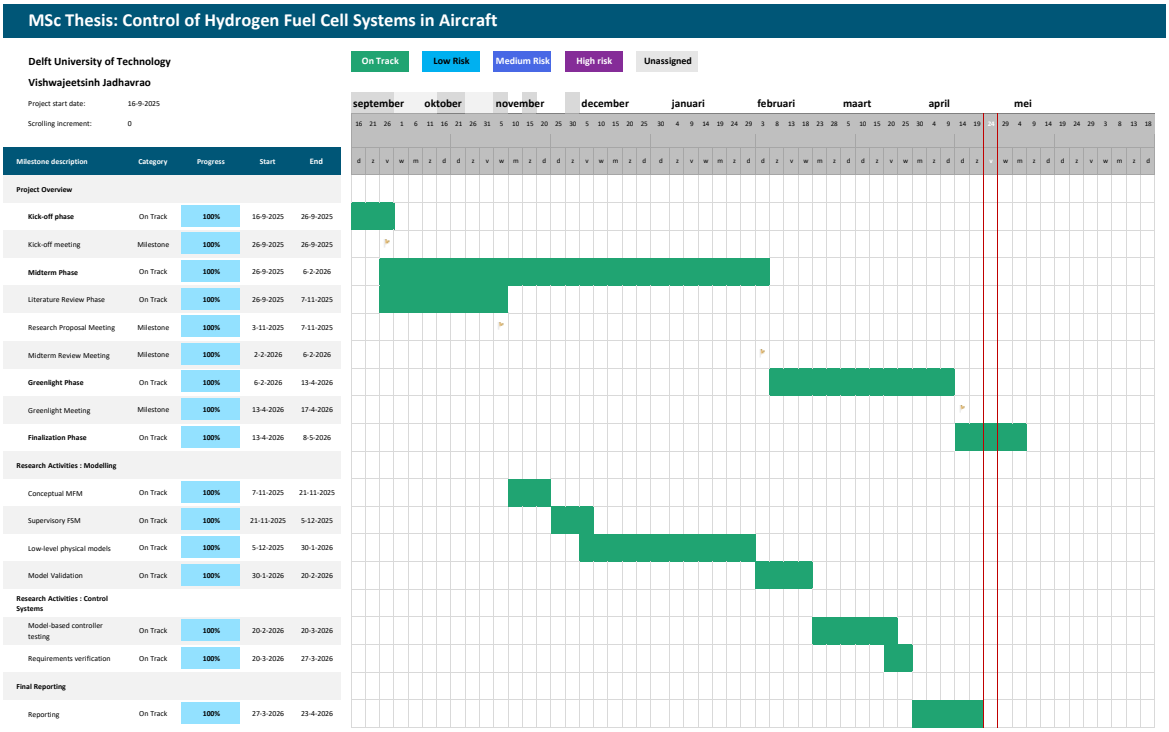

Figure 2.21: MSc thesis planning

3

Fuel-Cell System Modelling and Supervisory Control Design

As mentioned in the research plan which is the conclusion of the literature review, the first main research activity is the modelling of the fuel-cell system. The intention is to create a control-oriented model which answers the third sub research question, that can be later used to develop control systems. A top-down approach to modelling the fuel-cell system will be implemented. Therefore, firstly a conceptual model will be made with Multi-level Flow Modelling in Section 3.1, secondly a Finite State Machine model will be derived in Section 3.2 and lastly some low-level physics based models will be implemented from literature in Section 3.3.

3.1. Multi-level Flow Model

Firstly, a conceptual (high-level) Multi-level Flow Modelling is to be conducted to consider the overall system goals and functions. As seen from the P&ID diagram in Section 2.2.1, each of these flows can be modelled as functional subsystems that each serve sub functions, to achieve intermediate and end goals. Firstly, the mass and energy flow structures will be modelled to outline all the functions of the system in Section 3.1.1, after which the control flow structures will be built on top in Section 3.1.2 and then hazards modelling will be done in Section 3.1.3. Notably, Figure 2.6 showed all the symbol descriptions and Table 3.1 shows all the descriptions of the the functions and objectives seen in the following MFM charts, along with the components that achieve these functions.

Table 3.1: MFM functional structures with associated tags, descriptions, and components

Function/Objective	Description	Components
EFS1: Power Subsystem		
So1	Electricity	
tr1	Electrical energy transport to motor	Cabling
Si1	Motor (electrical sink)	Motor
O1a	Provide requested power to the electric motor	
CFS1: Current flow regulation		
R1	Regulate electrical load / load-switch actuation	Load switches& MCU
O1b	Keep current within ± 5% of requested	
H1a	Hazard: OCV < 0.7V or >1V (any cell)	Voltage sensors
H1b	Hazard: Loaded cell voltage < 0.5V for >5s	Voltage sensors
EFS2: Thermal Management Subsystem		
So2	Thermal energy	
tr2	Heat transport to storage	
Sto1	Heat storage (stack thermal mass)	Fuel-cells

Function/Objective	Description	Components
tr3	Heat dissipation (fan-driven airflow)	Fans
Si2	Ambient air (heat sink to environment)	
O2a	Maintain stack temperature $\leq$ 50°C	
CFS2: Thermal Regulation		
R2	Regulate fan speed (thermal management)	
O2b	Keep temperature within ± 1°C of desired	
H2	Hazard: Stack temperature $\geq$ 70°C	Temperature sensors
MFS1: Purging Subsystem		
So3	Exhaust gases	
tr4	Transport exhaust gases to anode outlet	
Sto2	Storage of exhaust gases a	Anode outlet
tr5	Exhaust-gas transport	Purge valves
Si2	Ambient air	
O3a	Remove all impurities	
CFS3: Purging Optimization		
S1	Steer the purging process	
O3b	Maximize hydrogen utilization	
MEFS1: Fuel-cell Subsystem		
So4	Conditioned hydrogen	Anode inlet manifold
So5	Conditioned air	Cathode air inlet
tr6	Transport hydrogen to anode inlet	Hydrogen manifold
tr7	Transport air to cathode inlet	Air manifold
C1	Electrochemical conversion (chemical $\rightarrow$ electrical + heat + exhaust)	Fuel-cell stacks
tr8	Transport electricity	Electrical output cabling
Si3		
tr9	Heat transport	
Si4		
tr10	Exhaust gases transport to anode outlet	Anode outlet manifold
Si5		
tr11	Transport air and water to cathode outlet	Fans and cathode ducts
Si2	Ambient air	
O4	Generate electricity via chemical reaction	
MFS2: Hydrogen Supply Subsystem		
So6	Hydrogen	Hydrogen tank
tr12	Hydrogen supply from tank to PRV	H_2 supply line
C2	Pressure change	Pressure reducing valve
tr13	Internal H_2 transport to all stacks	Supply valves
Si6	Fuel cell anode inlets	Anode inlet ports
O5a	Supply hydrogen pressure at 400–700 mbar.g	
CFS4: Hydrogen flow regulation		
R3	Regulate hydrogen supply / pressure	
O5b	Maintain hydrogen pressure ± 5% margin of desired	
H3	Hazard: Hydrogen leakage $\geq$ 4000 ppm	H_2 leak sensor
MFS3: Air Supply Subsystem		

Function/Objective	Description	Components
So7	Ambient air (mass source)	
tr14	Air transport to cathode (fan airflow)	Air fans / ducts
Si7	Fuel cells cathode	Cathode inlet ports
O6a	Maintain oxygen excess ratio $\lambda \geq 2$	
CFS5: Air flow regulation		
R4	Regulate air flow (fan duty)	
O6b	Monitor oxygen excess ratio [29]	

3.1.1. Mass and Energy Flow Structure Modelling

As explained before, it is easiest to first model the mass and energy flows taking place within the system, in a top to bottom approach [30]. It is important to note, that auxiliary power or energy will not be modelled here, as it is assumed that it would not aid the modelling and control, and would end up making the model too complex. In terms of control, the fuel-cell system has 2 main inputs and 3 main outputs. The electrical power generated is the main output of interest, as it achieves the overall process objective of the fuel-cell propulsion system, which is O1a to ”Provide requested power to the electric motor”, as seen in Table 3.1. Therefore, the functional structure EFS1: Power Subsystem sits at the top in Figure 3.1, along with the other controllable outputs. This is done to make the MFM hierarchical, starting at the top with the highest level (or the end), and descending justifies the means to reach the ends.

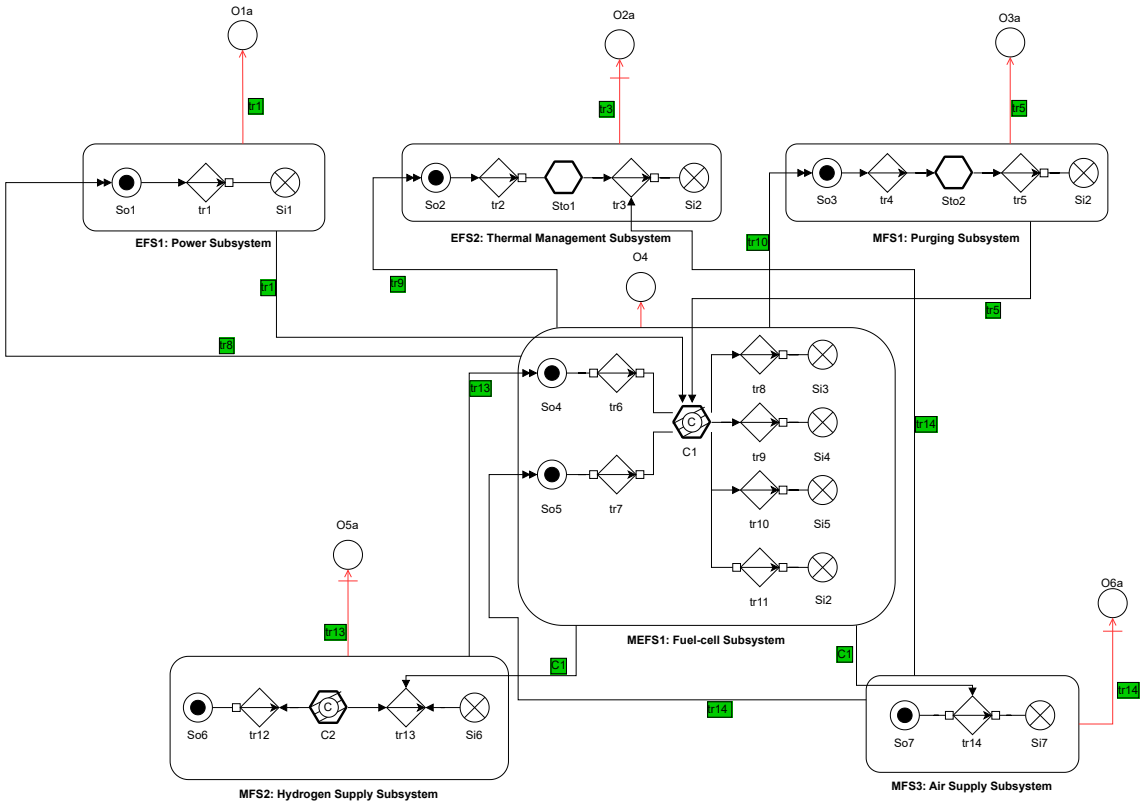

Figure 3.1: Mass and energy flows in MFM

The second output is EFS2: Thermal Management Subsystem which handle the heat process objective being to maintain the stack temperatures ≤ 50°C. The last output is MFS1: Purging Subsystem which has a process objective of removing all impurities (exhaust gases) trapped at the anode outlet, which are

limiting the hydrogen utilization and thus can lead to anode starvation. Below this layer, is the MEFS1: Fuel-cell Subsystem , which is a mass and energy functional structure, as it represents a conversion between the inputs and outputs. Inside MEFS1, the inputs are air and hydrogen, with the controllable outputs being electricity, heat, and exhaust gases, all of which are transported into the output subsystems at the top (tr8, tr9, and tr10 respectively). The process objective of MEFS1 is to generate electricity via a chemical reaction. Here, the inputs of hydrogen and air can be seen to be transported (tr13 and tr14) from the lowest layer MFS2: Hydrogen Supply Subsystem and MFS3: Air Supply Subsystem respectively, where their functions and processes are defined. The process objective of MFS2 is to supply the hydrogen at a requested pressure between 400-700 mbar.g, and of MFS3 is to maintain an OER of ≥ 2, to prevent membrane dehydration. These mass and energy flow structures show what are useful subsystems to define, in terms of functional groupings under a functional structure. Therefore, a total of 6 subsystems are identified, 3 output subsystems at the top, 1 middle conversion subsystem and 2 input subsystems at the bottom, all having process objectives that contribute to the propulsion process.

Influences of Subsystems
Now that the functional structures have been defined, these can essentially be the subsystems that can be individually modelled in FSM and lower level models. It is better to define a subsystem by these functional groupings in MFM, instead of just using a P&ID and grouping the components, as was done previously. However, it is also important realize the influences that subsystems can have on each other, which is seen by the influence arrows in Figure 3.1. Firstly, the Power Subsystem is using up the current it receives, and thus it influences C1 (the fuel cells) and its chemical reaction function, as more power is being requested. Secondly, the TMS can be seen as stand alone after it dissipates the heat, however the Purging Subsystem uses hydrogen to purge the impurities, which makes less hydrogen available in the transient for C1, and hence another influence.

The Fuel-cell Subsystem uses up the hydrogen and air that it is being provided, and hence, it influences the Hydrogen and Air Supply Subsystems functions that is transporting those masses. Notably, the Air Supply Subsystem's tr14 is used to transport air to the cathode inlet, however this also influences the TMS's tr3 function od heat dissipation, as both functions is achieved by the same component of fans. With results from modelling, it was seen that the OER objective is always met and only needs monitoring, whereas the temperature regulation is more constraining and thus the primary focus of the fans.

3.1.2. Control Flow Structure Modelling
Now that the mass and energy is defined, the control flows can be built on top of this to show how the process objectives can be met, as well as new control objectives which are based on desired performance [30]. Therefore, the updated MFM chart can be seen in Figure 3.2, with 5 new control functional structures added to the controllable 2 input and 3 output mass and energy functional structures.

Again going from the top-down approach, firstly there is the CFS1: Current flow regulation, as the main function of this controller (R1) is to regulate the electrical load, via requesting currents with the MCU and switching the circuit with load switches. It achieves the process objective, by actuating tr1, whose function is transport of electricity to the motor. It also has a control objective O1b to keep the current within ± 5% of the requested load. Secondly, there is CSF2: Thermal regulation, which is to regulate the fan to maintain stack temperature, with its control objective O2b being to keep within ± 1°C of desired. Thirdly, CFS3: Purging Optimization is there to steer the opening and closing of the purge valves to remove impurities, whilst having a control objective O3b of maximizing hydrogen utilization, which is how the optimization plays a role.

The MEFS1 does not have an associated control functional structure, because it is split up into the inputs and outputs. Therefore, CFS4: Hydrogen flow regulation, regulates the hydrogen pressure with supply valves and PRV, and has a control objective O5b of maintaining the pressure within ± 5% of desired. Lastly, CFS5: Air flow regulation, regulates the OER with the fans, and has a control objective O6b to simply monitor OER [29].

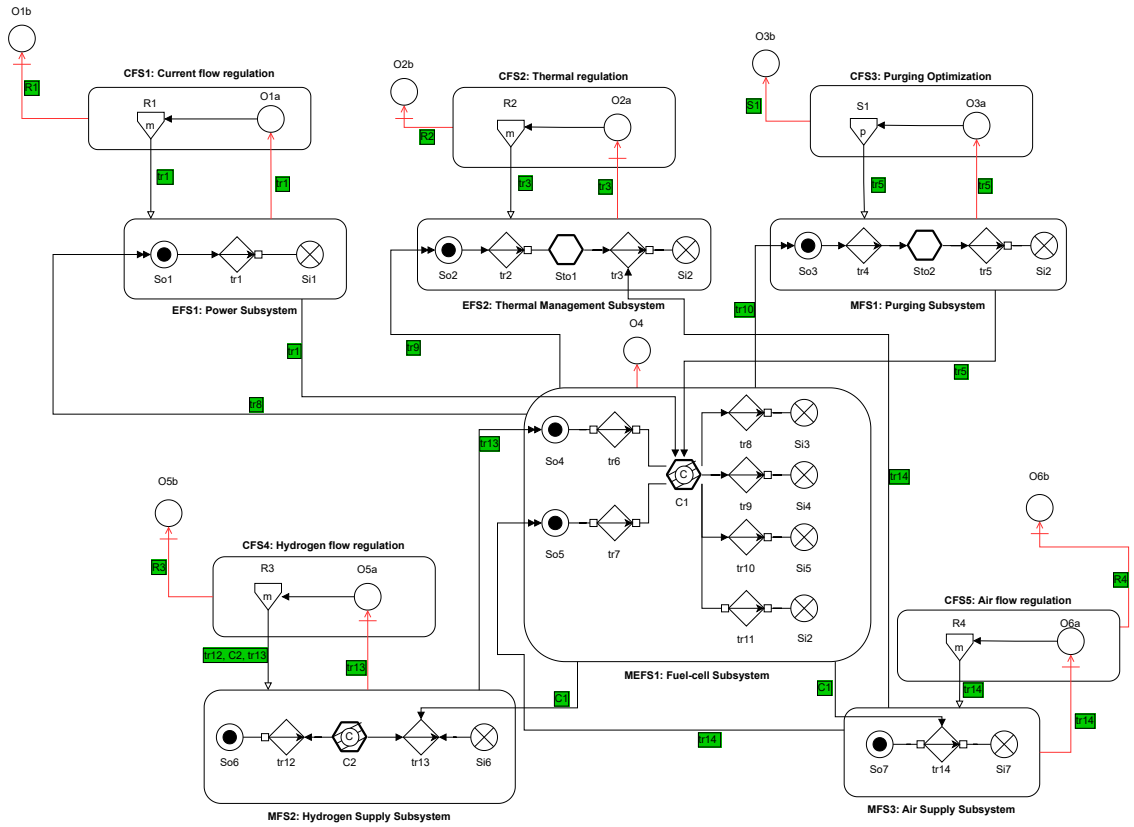

Figure 3.2: MFM model with control flow structures implemented

3.1.3. Hazard Flow Modelling

Lastly, besides goals, which are objectives that are desired, there are also hazards in MFM, which are another type of objective that is undesired [31]. Usually, processes and functions within the system can cause the occurrence of such hazards, and it is importance to recognize what can produce these hazards, and which control subsystem's responsibility it is to prevent them. In this context, hazards are defined as events that are safety-critical, and system should escalate to a full shutdown when they occur. Hence, the hazards are directly derived from the safety requirements as was seen in Table 2.4. For events that are suboptimal for a system, but don't require a shutdown (such as drifting away from OER range causing dehydration), won't be modelled as a hazard, but would be incorporated in the process and control objectives. The hazards (black circles) can be seen modelled in Figure 3.3, which is the total Multi-level Flow Model including all of its aspects.

There are the hazards H1a of OCV<0.7V for any cell and H1b of cell voltage being <0.5V for >5s, which are both produced by the tr1 function in Power Subsystem. As electrical energy being being transported to the motor, the fuel cell voltage typically starts dropping, and that's why this function is seen to produce these hazards. Both of these hazards are suppressed by R1, as it is current controller's job to limit ramp up rate, decrease the requested current or simply flip the load switch, to avoid the cell voltages from dropping too low or not running operation these hazardous events. Then there is H2 which is in case of overheating of the stacks when temperature $\geq$ 70°C. This is produced by Sto1 in TMS, as if more heat energy is stored than dissipated, then overheating can occur. Here, R2 controller is responsible to regulate the fan such that this does not occur, and hence is suppressing this hazard.

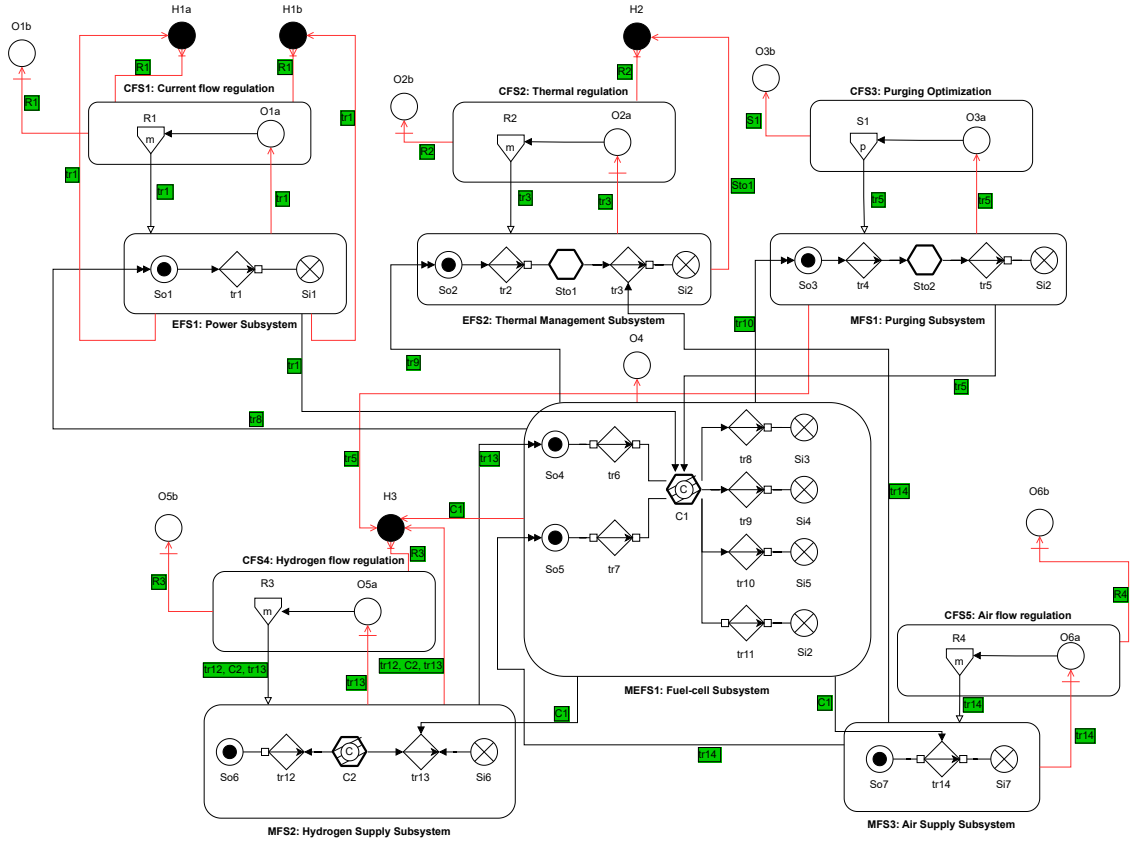

Figure 3.3: Total Multi-level Flow Model including mass, energy and control functions with their objectives and hazards

Lastly, H3 hazard of an excessive hydrogen leak $\geq$ 4000ppm that can cause a fire is modelled, which is perhaps the most safety critical. It is to be known, that detection of such a leak with a hydrogen sensor within the system does not exist currently, however since it is quite safety critical, it's prevention method is modelled here as a potential improvement to the current system. It can be seen that H3 is produced by functions tr12, C2, tr13 in the Hydrogen Supply Subsystem, by C1 in Fuel-cell Subsystem and by tr5 in the Purging Subsystem. These are the identified sources that can leak hydrogen during operation, which can be detected by a new hydrogen sensor. Thereafter, it is R2 controller's responsibility to shut off the supply valves and the PRV as it sees the leakage approaching 4000ppm, to suppress this hazard from occurring. In the meanwhile, purging can also be put to a halt to avoid releasing more hydrogen into the ambient air. With this in Figure 3.3, the stage of Multi-level Flow Modelling is concluded, and it is time to take the learnings about the subsystems, the what and why of the objectives, and use them in the next level supervisory model of Finite State Machines.

3.2. Finite State Machine Supervisory Controller

The Finite State Machine is meant to be an automatic discrete event controller, modelled on Simulink, which would regulate between the different states of the fuel-cell system, from the startup to the shutdown. It is important to recognize, that the FSM (like the MFM), does not exist with the real system. Therefore, when modelling it all together, it is important to visualize the interactions between the FSM and the existing real subsystems. The overall FSM chart and its interactions can be seen in Section 3.2.1, after which its startup and shutdown procedure sub-charts breakdown can be seen in Section 3.2.2. Notably, Table 3.2 describes the different operation modes of each subsystem that are commanded by FSM, and this can be used to understand all the FSM charts.

Table 3.2: Subsystem operation modes

Mode	Air Supply & Thermal Management Subsystem [aircommand]	Hydrogen Supply Subsystem [h2command]	Power Subsystem [powercommand]	Purging Subsystem [purgecommand]
0	Fans OFF	All H_2 valves CLOSED	Load switch OPEN	Purge valves CLOSED
1	Fans ON at fixed 10% for minimum OER	PRV ramp to STARTUP pressure	Load switch OPEN, OCV	Purge valves anode clean sequence
2	Fans regulated to also maintain T $\leq$50°C	Close main supply valve	Load switch CLOSED, rampup to 4A current	Periodic purge
3	Fans ON at MAX 100% for cooldown		Rampdown to 0A current, load switch OPENED	

3.2.1. Overall FSM Chart with Subsystems

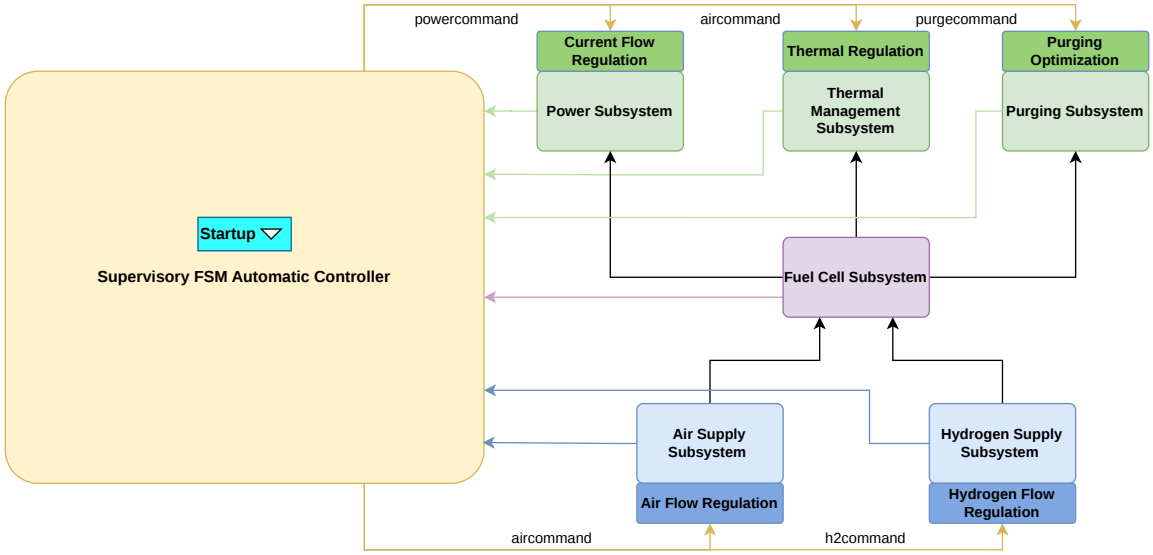

Figure 3.4: Simulink diagram with FSM and 6 physical subsystems integrated (Simulink Figure A.1)

The Simulink model with the FSM integrated with the 6 physical subsystems can be seen in Figure 3.4. Here it can be seen, that the 6 physical subsystems, as were previously identified in MFM, are placed in a

similar hierarchical order for consistency on the right side. The FSM chart block is placed on the left side, and this block takes inputs from all 6 subsystems (data), and outputs to the 5 controllable subsystems. The control subsystems receive the commands, as they are linked to the physical subsystems as seen in Figure 3.4, and they will be designed in Chapter 5. Additionally, the FSM needs 3 input commands from the user, for startup, to activate load to minimum power, and to shutdown.

The overall FSM chart of the Imponator describing its main states can be seen in Figure 3.5, all contained within the SuperState. Within the SuperState, there are 2 sub-charts namely MainFSM and SafetyMonitor which run in parallel. Within MainFSM seen in Figure 3.6, the main identified states of the Imponator fuel-cell propulsion system run exclusively, and are Off, Startup, Idle, Minimum Power, Shutdown and Emergency Shutdown. Within these states, sub charts can be made specifically to emphasize the sequencing order of events in the startup and shutdown procedures. These states are inspired from literature, as well as the scope of this project. It is important to note, that a ”Run” state isn't featured in this model, because that would involve another layer of control complexity, as it needs manual power inputs from user. Therefore, the model is kept focused to the automation of the startup and shutdown procedures.

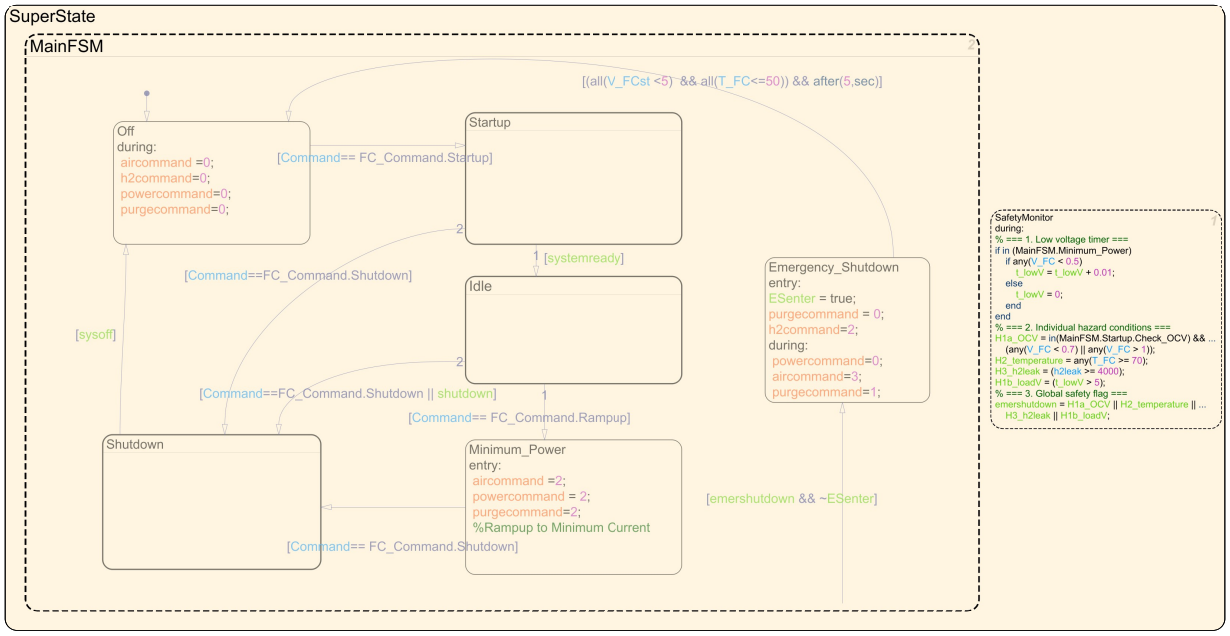

Figure 3.5: Finite state machine chart of the Imponator system

The Off state, is where the fuel-cell system stays in the beginning. This is where essentially everything is off or disabled, as seen by the commands sent to the 4 controllable subsystems. To elaborate, whilst the system is in this state, there are ”during” actions that are conducted. For example, the action ”aircommand = 0” is an output message sent to the Air Supply Subsystem, to engage its mode 0, as seen in Figure 3.4 and Table 3.2. Then, the system only transitions to the Startup state once it receives a Startup Command by the user (which would be a switch). Once startup checks are done, system would enter the Idle state, where it would rest and remain in OCV until it receives another Rampup command by user. If >10s have passed in Idle and hence OCV without any command, system enters Shutdown state. With a Rampup command, it enters Minimum Power state, which is to ramp up to a minimum current for all 6 stacks, after which it remains in a steady state. This means, that the system has finished starting up, and would be ready to draw more power. Thereafter, the Shutdown Command from user is needed to go into Shutdown state, where a safe and sequenced shutdown is done, after which system is allowed to transition to the Off state again.

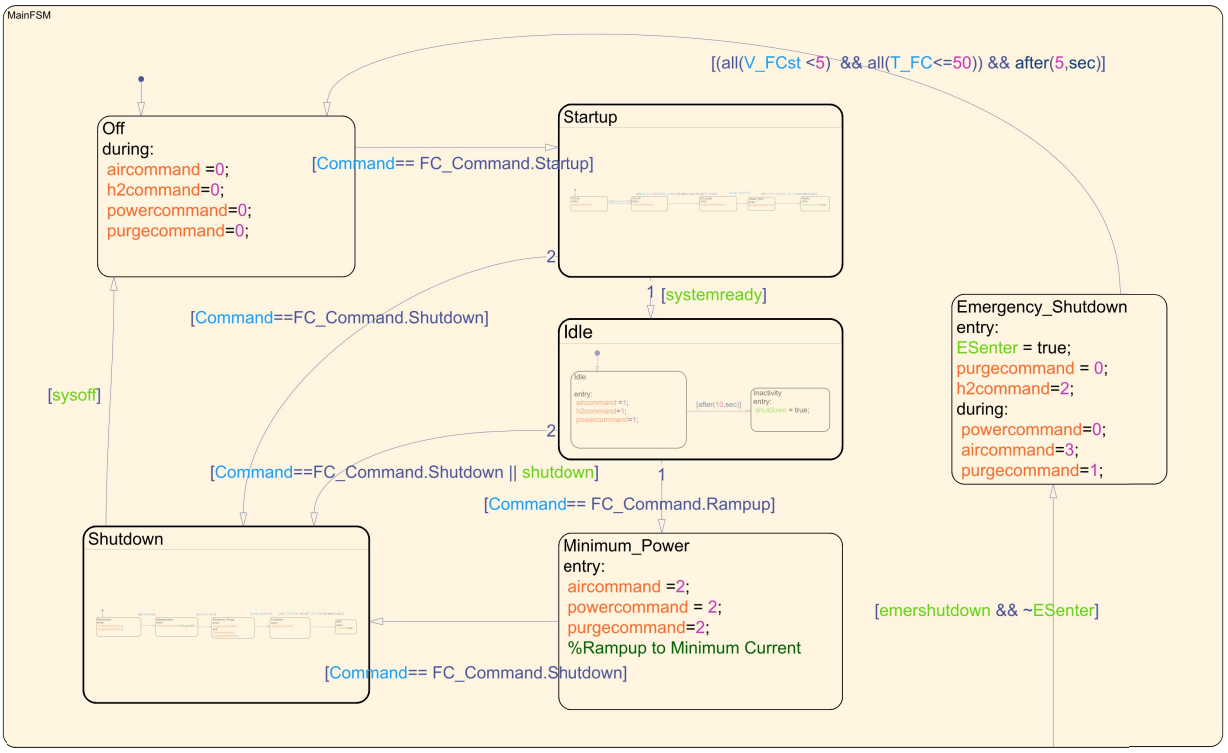

Figure 3.6: Main FSM Chart of the Imponator System

Whilst states are exclusively switched within MainFSM, SafetyMonitor is also running parallel to MainFSM, to detect any hazardous events that were previously identified in MFM. Once detected, the SafetyMonitor automatically engages Emergency Shutdown from any state within the MainFSM. Notably, OCV hazard (H1a) is only detected in a substate in Startup, and loaded low voltage hazard (H1b) in Minimum Power, since these are the only states in which they could occur. However overheating (H2) and hydrogen leakage (H3) are kept as global, as they can occur whenever.

3.2.2. Startup and Shutdown Sub-charts

Now, it is time to go more in depth into some of these states that need their own sub chart, particularly to show a clear defined sequence that is needed. The sub charts of the Startup procedure (including Startup, Idle and Minimum Power) can all be seen in Figure 3.7, and the Shutdown procedure sub chart can be seen in Figure 3.8. Most notably, a sequence of events or transitions between sub states can be seen for the Startup and Shutdown sub charts. This is the main power of FSM, that such a sequential logic can be created and easily visualized.

For example, inside Startup, the default transition is into Init air, where aircommand is set to mode 1, which means to start running the fans at a fixed rpm. Then, there is a transition condition that checks whether the fans are actually running (action is carried out), and thereafter the h2command is set to 1. This means that the supply valves are slowly opened and the PRV is ramped up to a startup pressure. The anode inlet pressure of all the stacks is checked to be within range, and then system enters the Init purge sub state. Here, the anode clean purging sequence is engaged, after which a cell voltage check in OCV is done. If it passes, system goes into ready sub state. However, if it fails in under or over cell voltage, then Hazard 1a sub state is entered, which calls for an emergency shutdown. In this way, all the hazards as found from MFM, are modelled here as sub states inside sub charts. Such that, whenever they are entered, an emergency shutdown is automatically triggered.

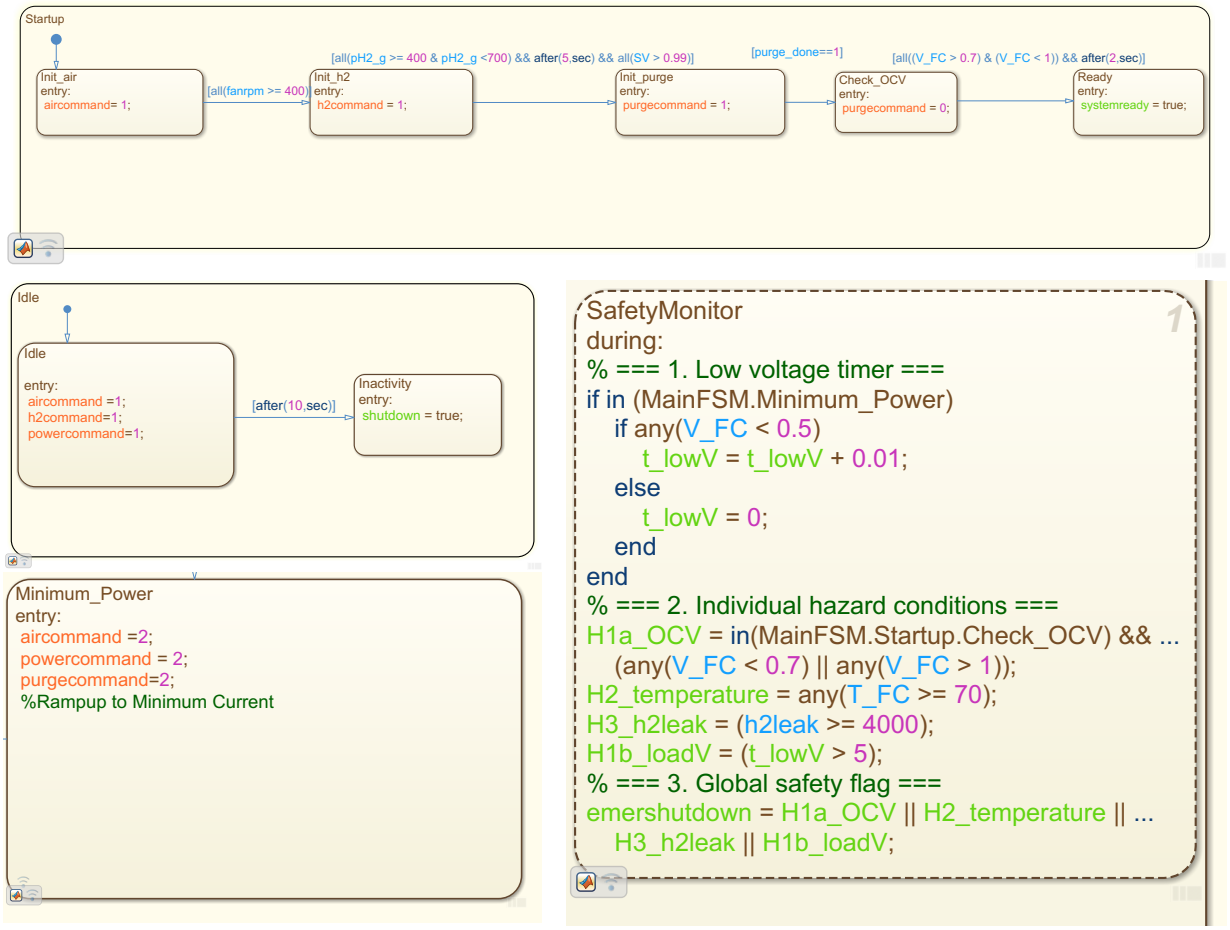

Figure 3.7: Startup procedure sub charts, including Idle and Minimum Power

Once system is ready, it enters Idle state, where there are a few new mode commands. Hydrogen pressure is meant to be stabilized at a fixed value, load switches are still open but now there is OCV, and purging is now in a periodic mode, instead of a single anode clean sequence. Here, there are a few hazardous events that can occur, such as OCV high or low potentials, hydrogen leakage and overheating. Additionally, since staying in OCV for too long can cause degradation, there is also a transition to an inactivity state when time in idle is >10s, after which the Shutdown procedure is initiated. However, if within the 10s there is a user command to Rampup, this transitions the state to Minimum Power, where the load switches are closed and the current is being ramped up to a minimum value of 4A. Due to this transient and dynamic behavior, the fans enter the regulation mode, to maintain the OER of 2 and keep stack temperatures $\leq$50°C. In this mode, the ramp up must also be done steadily, by monitoring the cell voltages remaining in range. The system shall then reach a steady state response, operating at a minimum power of around 1200W (200W each stack). During this, similar hazards to Idle can occur, except instead of OCV, cell voltages can drop below 0.5V for more than 5s, and this is a hazard that can be detected.

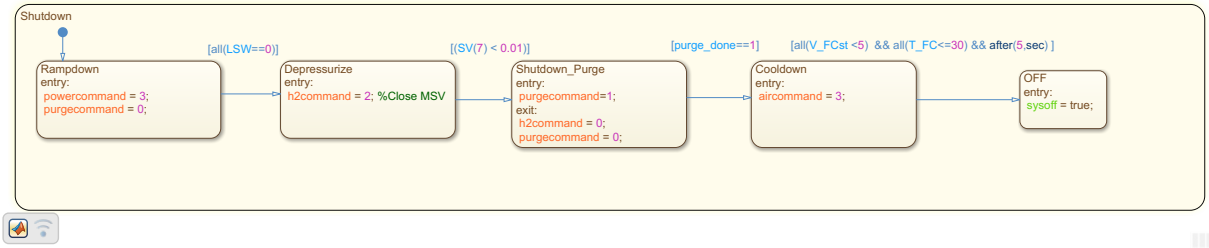

Figure 3.8: Shutdown procedure sub chart

From several states like Startup, Idle and Minimum power, the Shutdown state can be reached with a user Shutdown Command, or it is automatically triggered for reliability. The Shutdown sub chart can be seen in Figure 3.8, where it first enters the Deload sub state which opens the load switches. After checking that all load switches are open, system is depressurized by closing all the supply valves, and then initiating the anode clean sequence. Then, if all the supply and purge valves are closed, then it enters the Cooldown sub state, where the fans are set to a fixed low duty rpm to decrease the temperature if too hot. Thereafter, system transitions to OFF when all the stacks reach stack voltages <5V and temperatures $\leq$30°C. Once its in this sub state, it meets all the conditions to enter the global Off state, whether everything is turned off and disabled, just like it started.

3.3. Subsystem Physical Models

Now, the physical subsystem models can be built to be interconnected with each other and also with the previously created FSM automatic controller. The subsystems as seen in Figure 3.4 will be built up starting with the inputs, all the way until the outputs. Firstly, the Air Supply and Hydrogen Supply Subsystem Models are made in Section 3.3.1 and Section 3.3.2 respectively, with the junction Fuel Cell Subsystem Model made in Section 3.3.3. Then the Purging, Thermal Management and Power Subsystems are made in Section 3.3.4, Section 3.3.5 and Section 3.3.6 respectively.

3.3.1. Air Supply Subsystem Model

The air supply subsystem shall be modelled first, and it consists of a PWM controlled fan that will output a certain air mass flow, and therefore controlling OER. The objective of this subsystem is to maintain this oxygen excess ratio during ramp up, by regulating the PWM input. The PWM input specifies a control voltage, which determines the power of the fan, which affects its rpm speed. Depending on the fan characteristics, the rpm of the fan then influences the actual air mass flow over the stack. Additionally, the fan also has an influence on the temperature of the stacks, and this part can also be modelled later. Therefore, it is important to model all the different parts that are required to represent all the dependencies.

Firstly, the relation between the PWM input to the fan and the w rotational speed of the fan, can be modelled by fitting a polynomial in Equation 3.1 to existing data from the fan's manual. This is for the Sanyo Denki DC fan 9SG1224G101, based on their performance curve data and data digitalized as seen in Figure 3.9 [32]. Additionally, a first order lag transfer function with τ_{fan} fan time constant estimate of 0.2s, can be used to represent the fan dynamics needing some time to get to the target fan speed, as seen in Figure 3.11.

$$\begin{aligned} w(t) = {} & 7.80 \times 10^{-10}\, u^7(t) - 4.75 \times 10^{-7}\, u^6(t) + 9.87 \times 10^{-5}\, u^5(t) \\ & - 9.69 \times 10^{-3}\, u^4(t) + 0.49\, u^3(t) - 13.21\, u^2(t) + 237.26\, u(t) + 46.00 \end{aligned} \tag{3.1}$$

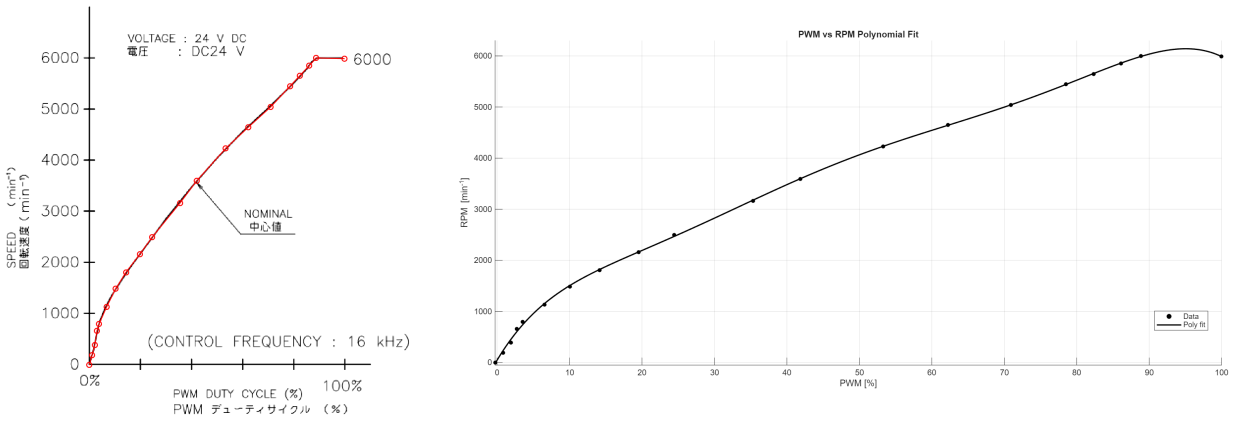

Figure 3.9: Polynomial fit of PWM versus fan speed data digitalized [32]

Now, from this point onward, it is important to determine the operating point of the fan and stack combination due to their pressure drop. This operating point is the intersection of the fan and stack performance curve, which shows their static pressure drop with increasing volumetric airflow. This can also be done with data digitization of the fan and stack performance curves, from their respective manuals, giving Figure 3.10 [33]. The operating point is for 100% PWM, giving $w_1 = w(u) = 6000rpm$, and the volumetric airflow at this point Q_1 is $5.85 \frac{m^3}{min}$. Equation 3.2 can be used to determine the Q resulting flow rate for any w is arbitrary fan speed, and Q_1 and w_1 are the fixed values from the intersection as found before [21].

$$Q(t) = w(t)\frac{Q_1}{w_1} \tag{3.2}$$

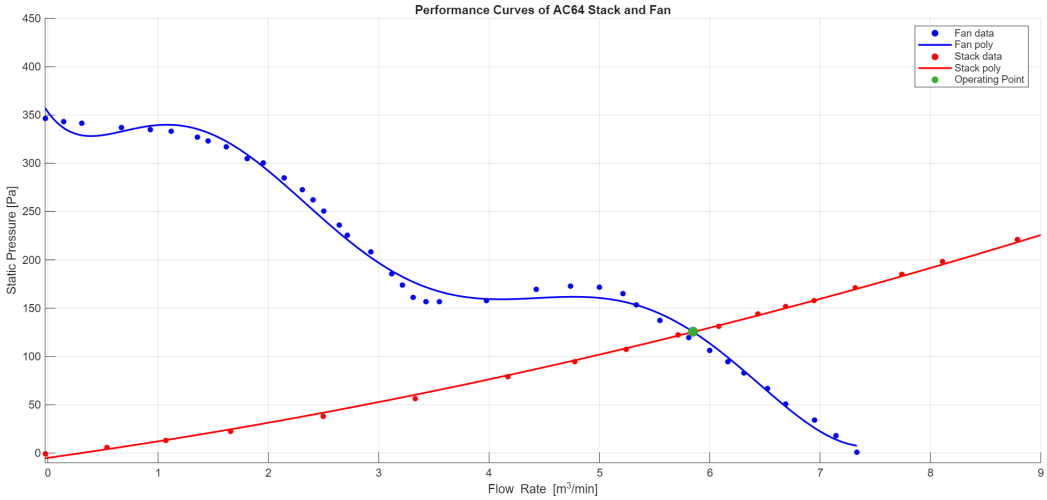

Figure 3.10: Performance curves [33]

From this, the air mass flow can be computed with Equation 3.3 [21]. Then the oxygen excess ratio of a stack can be computed with Equation 3.4 with $y_{O2} = 0.232$ and $M_{O2} = 0.032 \frac{kg}{mol}$, using a time varying current and air mass flow [34]. Finally, all of this is implemented in the Air Supply Subsystem Simulink Model as can be seen in Figure 3.11.

$$\dot{m}_{air}(t) = \rho_{air} Q(t) \tag{3.3}$$

$$\text{OER} = \frac{\dot{m}_{O2in}}{\dot{m}_{O2consumed}} = \frac{y_{O_2}\, \dot{m}_{\text{air}}}{\frac{I_{FC}\, N_{FC}\, M_{O_2}}{4F}} = \frac{4F\, y_{O_2} \dot{m}_{\text{air}}}{I_{FC}\, N_{FC}\, M_{O_2}} \tag{3.4}$$

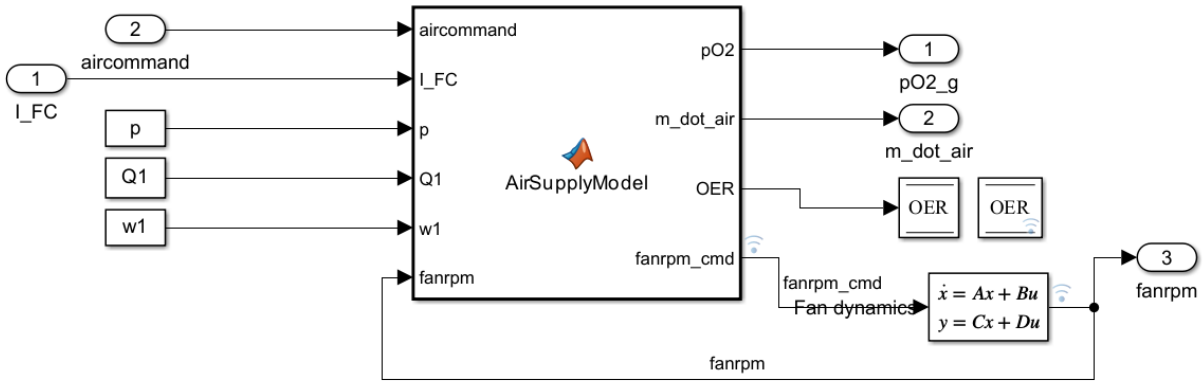

Figure 3.11: Air Supply Subsystem Simulink model

3.3.2. Hydrogen Supply Subsystem Model

The Hydrogen Supply Subsystem has a lot of dynamics that need modelling, since the anode loop consists of several components that bring about this dynamics. Unlike the cathode loop, the anode loop is pressurized and thus has several components in its manifold that need to be modelled when considering sequential operation. Out of the existing components in the anode loop, only the ones that can be electronically or digitally controlled are modelled here. There is firstly a main supply valve, then a mass

flow controller (with internal PID), and then the manifold splits into 6 pipes which have stack supply valves and then 6 purge valves. The sequential opening and closing of these valves and actuators is essential for a safe and reliable startup and shutdown, and hence must be modelled. To achieve this, a model derived from physics will be used as seen in Equation 3.5. This model essentially relates the change in pressure to the change in net mass flow of hydrogen, which is the combination of $\dot{m}_{H2in}$ incoming mass flow, $\dot{m}_{H2cons}$ mass flow consumed by fuel cells and $\dot{m}_{H2purge}$ purged mass flow. With $R_{H2} = 4124\frac{J}{Kmol}$ and $V_{total} = V_{man} + \alpha_{SV}V_{stack}$ with measured $V_{man} = 2.254 \cdot 10^{-4}m^3$ and $V_{stack} = 1.1 \cdot 10^{-4}m^3$ and α_{SV} is the stacks' supply valve positions.

$$\frac{dp(t)}{dt} = \frac{R_{H2}T_{amb}}{V_{total}(t)}(\dot{m}_{H2in}(t) - \dot{m}_{H2cons}(t) - \dot{m}_{H2purge}(t)) \tag{3.5}$$

Firstly, the incoming mass flow is assumed to be Equation 3.6, where it is directly controlled by the value of the main supply valve and the mass flow controller valve, which are both an element of [0,1]. Here, it uses $\dot{m}_{H2inmax} = 2.83 \cdot 10^{-4}\frac{kg}{s}$, which is the maximum hydrogen mass flow that can be allowed into the system by the Red-y mass flow controller when all valves are fully open [35]. A sanity check on this value can be done with Equation 3.7, which determines the maximum hydrogen mass flow that can be consumed at the maximum operating condition of the 6 fuel cell stacks running at their full rated power. Here, C_{st} is a stack hydrogen consumption value from manual, and maximum current $I_{FC,\text{max}}$ and voltage $V_{FC,\text{max}}$ of a stack is 40A and 50V respectively. Using both these values, a λ hydrogen excess ratio of 1.57 is computed, which shows that this value from the mass flow controller is sensible to take.

$$\dot{m}_{H2in}(t) = \alpha_{MSV}(t) \cdot \alpha_{MFC}(t) \cdot \dot{m}_{H2inmax} \tag{3.6}$$

$$\dot{m}_{\text{H2consmax}} = \frac{6C_{st}\left(\frac{I_{FC,\text{max}}\, V^{st}_{FC,\text{max}}}{1000}\right)}{1000} = 1.80 \cdot 10^{-4}\frac{kg}{s} \tag{3.7}$$

Now, the $\dot{m}_{H2cons}$ hydrogen consumption mass flow for a single stack can be calculated, and this is dependent on its power as seen in Equation 3.8. This logic can be combined with some first order valve dynamics for the supply valves, and therefore the total hydrogen supply subsystem model can be shown in Figure 3.12. Here, the left side has a logic function which takes the h2command and outputs which supply valves should be open. For example in startup, it first ramps up the main supply valve to fully open, and upon opening this enables the mass flow controller block which has a PID controller, which sees the error between reference pressure and anode manifold pressure, and outputs a valve value, which then leads to calculation of the incoming mass flow. Then a net of this mass flow is integrated to get a single pressure state inside the anode manifold. Since the real system has manifold pressure sensors and a stack pressure sensor, to simulate this, the stack pressures are modelled to follow the manifold pressure with a "Stack pressure lag", which plays a role especially when the stack supply valves open after a stable manifold pressure has been reached.

$$\dot{m}_{\text{H2cons}}(t) = \frac{C_{st}\left(\frac{I_{FC}(t)V^{st}_{FC}(t)}{1000}\right)}{1000} \tag{3.8}$$

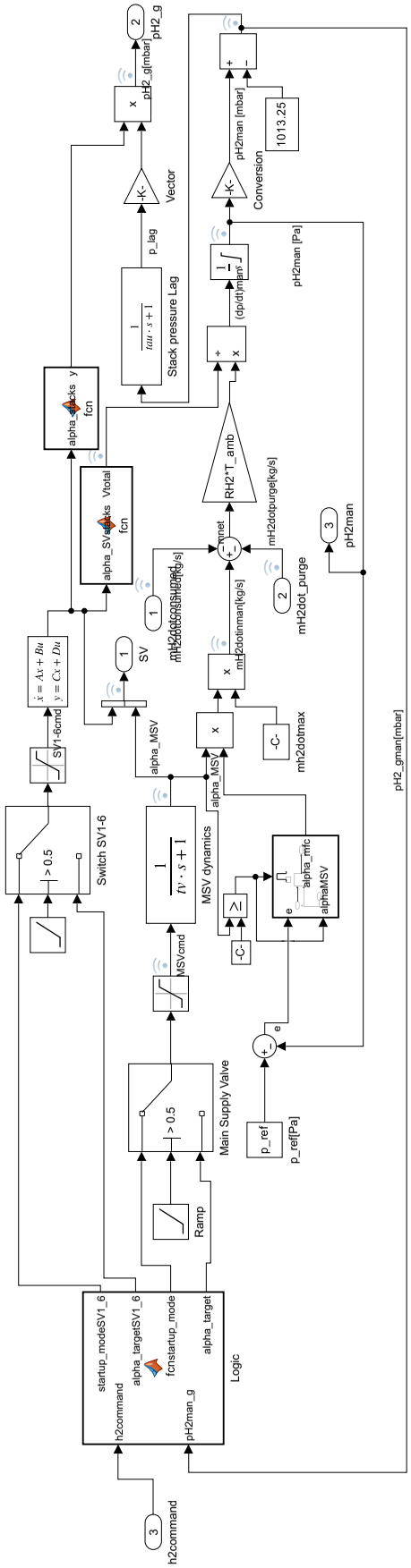

Figure 3.12: Hydrogen Supply Subsystem Simulink model

3.3.3. Fuel Cell Subsystem Model

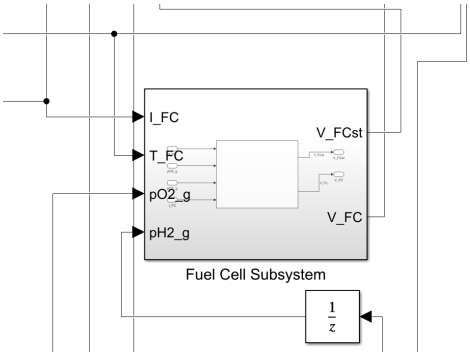

Figure 3.13: Fuel Cell Subsystem Simulink model

The Fuel Cell Subsystem voltage model can also be derived from control-oriented models literature [21]. Firstly, the total fuel cell voltage can be represented as a combination of 4 terms as seen in Equation 3.9. V_{oc} is the open circuit voltage of a cell which is calculated with the Nernst equation in Equation 3.10 using the partial pressures of hydrogen p_{pH_2} and oxygen p_{pO_2}. Here Δs entropy change of reaction is $-44.43 \frac{J}{molK}$, F Faraday's constant is 96485.34 $\frac{C}{mol}$, E^0 gibbs free energy change is 0.901 V, R universal gas constant is 8.315 $\frac{J}{molK}$, T^0_{FC} standard fuel cell temperature (thermodynamic reference temperature) is 298.15K and T_{FC} is the time-variant fuel cell temperature. Then there are voltage losses such as V_{act} activation over voltage, which is voltage lost to overcome energy barrier for the reactions. V_{ohm} ohmic over voltage is voltage loss due to resistance against charge transfer within a fuel cell, obeying Ohm's conduction law. Lastly, V_{conc} concentration over voltage is the voltage loss caused by poor mass transport in supplying and removing of reactants and products within the fuel cell.

$$V_{FC}(t) = V_{oc}(t) - V_{\text{act}}(t) - V_{\text{ohm}}(t) - V_{\text{conc}}(t) \tag{3.9}$$

$$V_{oc}(t) = E^0 + \frac{\Delta s}{2F}\left(T_{FC}(t) - T^0_{FC}\right) - \frac{RT_{FC}(t)}{2F} \ln\left(\frac{1}{p_{pH_2}(t)\, p^{1/2}_{pO_2}}\right) \tag{3.10}$$

The final fuel cell voltage equation that combines all 4 aspects can be seen in Equation 3.11 with current density $i_{FC} = \frac{I_{FC}}{A_{FC}}$, cell area $A_{FC} = 59.56cm^2$, and the total stack voltage with $N_{FC} = 72$ cells per stack in Equation 3.12. This model can be seen built up in Simulink in Figure 3.13, and this is the only subsystem that doesn't take any commands from the FSM, but it is the reaction hub of all the other subsystems, and hence exchanges time-varying signals with them.

$$V_{FC}(t) = V_{oc}(t) - \frac{RT_{FC}(t)}{2\alpha F} \ln\left(\frac{i_{FC}(t) + i_n}{i_o}\right) - R_{\text{ohm}}\, i_{FC}(t) - me^{(ni_{FC}(t))} \tag{3.11}$$

$$V^{st}_{FC}(t) = N_{FC}\, V_{FC}(t) \tag{3.12}$$

3.3.4. Purging Subsystem Model

In the Hydrogen Supply Subsystem model, only the purging mass flow needs to be modelled, and this will be done inside its own Purging Subsystem Model due to its specific goals designed in MFM. Whilst the $\dot{m}_{H2purge}$ is modelled, the effect of the impurities will not be modelled for simplicity. Based on the FSM, the purging subsystem will have 3 main modes that can be commanded as seen below.

1. Mode 0: Off
2. Mode 1: Anode clean sequence. 3 purges, can be commanded during startup and shutdown procedure.
3. Mode 2: Periodic purging. Purging during the minimum power state, purge intervals based on stack current, as advised by manual.

In Figure 3.14, a Purging Logic function sends the purge valve commands which go through purge valve dynamics to get an actual position of the valves. Then $\dot{m}_{H2purge,i}$ for a stack is calculated with the nonlinear purge valve model, which is based on information and equations given in Burkert's purge valve manual [36]. Firstly, the flow coefficient K_v is calculated in Equation 3.13 using an S-curve estimation

for its relation to the PWM input of PV, where K_{vs} is 0.055 $\frac{m^3}{h}$ [36]. Then Equation 3.14 calculates the volumetric standard flow rate, dependent on the constant p_{amb} of 1.01325bar, the varying p anode manifold pressure, constant T_{amb} of 293.15K and constant ρ_{H2} standard hydrogen density of 0.0899 $\frac{kg}{m^3}$. The final conversion to $\dot{m}_{H2purge,i}$ in SI units is seen in Equation 3.15, then this is summed up for all 6 stacks and subtracted from the pressure model in Equation 3.5.

$$K_{v,i} = K_{vs} \frac{1}{1 + e^{-11.5(PV_i(t) - 0.5)}} \tag{3.13}$$

$$Q_{N,i}(t) = 514\, K_{v,i}(t) \sqrt{\frac{p_{amb}(p(t) - p_{amb})\rho_{H2N}}{T_{amb}}} \tag{3.14}$$

$$\dot{m}_{H2purge,i}(t) = \frac{Q_{N,i}(t)\rho_{H2N}}{3600} \tag{3.15}$$

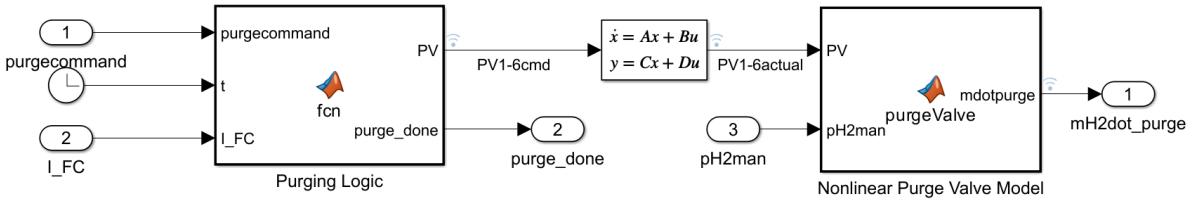

Figure 3.14: Purging Subsystem Simulink model

3.3.5. Thermal Management Subsystem Model

For the Thermal Management Subsystem, a lumped-parameter energy balance can be implemented, inspired from control-oriented models found in literature [21]. The energy balance can be seen in Equation 3.16, which shows how the total power, electrical power and heat removed cause a change in fuel cell temperature. Additionally, the initial fuel cell temperature condition is assumed to be $T_{FC}(0) = T_{\text{amb}}$.

$$C_t \frac{dT_{FC}(t)}{dt} = P_{\text{total}}(t) - P_{FC}(t) - \dot{Q}_{\text{coolant}}(t) \tag{3.16}$$

The total power, electrical power, and effective cooling power due to the fans can be calculated with Equation 3.17, Equation 3.18 and Equation 3.19. Here, $\Delta H = 285.5 \cdot 10^3$ [J/mol] is the enthalpy change of hydrogen. Additionally, η_{fan} fan efficiency and C_t thermal capacity of the stacks are parameters that need to be estimated with empirical data. The T_{FC} ambient temperature comes from a constant value sensor which reads 288.15K or 15°C. This thermal model can be seen implemented as the Thermal Management Subsystem in Simulink, as seen in Figure 3.15.

$$P_{\text{total}}(t) = \dot{M}_{\text{H}_2,\text{used}}\, \Delta H = \frac{N_{FC} I_{FC}(t)}{2F}\, \Delta H \tag{3.17}$$

$$P_{FC}(t) = V_{FC}^{st}(t)\, I_{FC}(t) \tag{3.18}$$

$$\dot{Q}_{\text{coolant}}(t) = \eta_{\text{fan}}\, \dot{m}_{\text{air}}(t)\, c_p\, (T_{FC}(t) - T_{\text{amb}}) \tag{3.19}$$

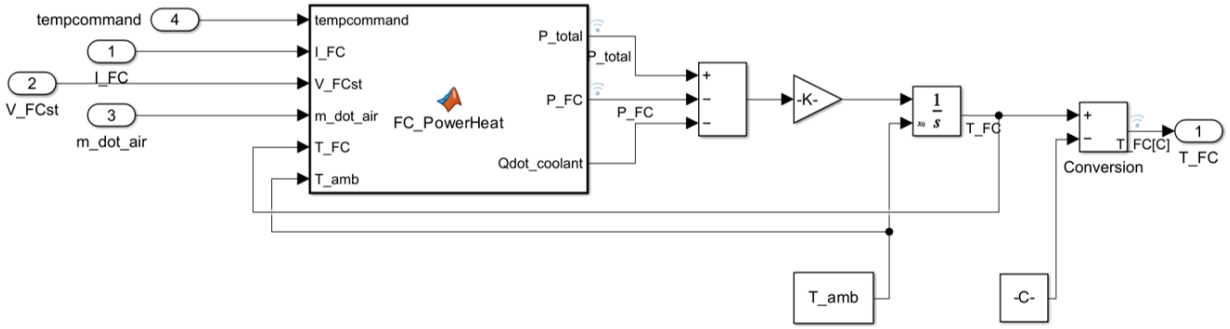

Figure 3.15: TMS Simulink model

3.3.6. Power Subsystem Model

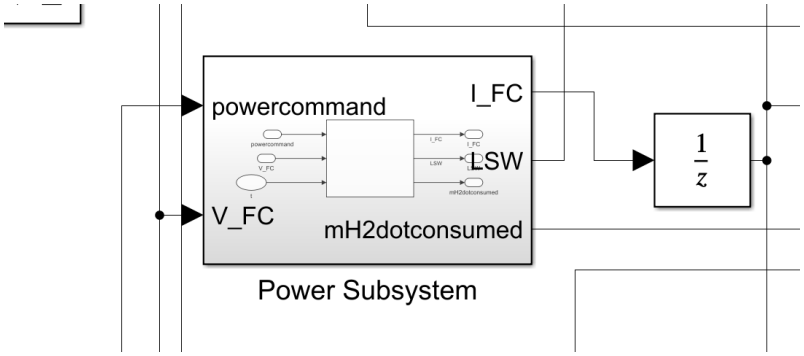

Figure 3.16: Power Subsystem Simulink model

Lastly, the power subsystem model needs to be made, as the last piece of the 6 subsystems, that together build the entire Imponator fuel cell propulsion system. This system is responsible for drawing current from the fuel cell, whilst adhering to the cell voltage range, and keeping stack temperatures below 50°C. In this control oriented model, current will be modelled as a demand signal, which essentially makes the assumption that the requested current is the actual current coming out of the stacks. This simplifies the model, and it means that this Subsystem simply needs to determine I_{FC} stack currents. For the startup sequence, the Power Subsystem needs to ramp up to a minimum current of 4A, and in shutdown it needs to ramp down from 4A to 0A, all safely and reliably. This minimum current value of 4A, to show that the system is on and ready to pull larger loads, has been chosen as per DLR experimental standards. Therefore, the Power Subsystem Simulink model can be seen in Figure 3.16.

4

Model Verification & Validation

In this chapter, the entire model including FSM and physical subsystems will be verified in Section 4.1. Then, parameter estimation on the subsystem physical models will be performed in Section 4.2. Lastly, these estimated subsystem physical models will be validated in Section 4.3. All Simulink graph results have simulation Time[s] on their x-axes, and y-axes units in the legend

4.1. Model Verification

Now it is time to run the model with its FSM automatic controller, and display the results. After an iterative process of Simulink debugging, and ensuring all dependencies as discovered in MFM are properly modelled and integrated, the results of a full startup and then shutdown sequence can be seen in Figure 4.1. With this, the proper operation of the FSM automatic controller is also verified, as it can be seen switching states in the right order, in the bottom left graph of Figure 4.1. This corresponds well to behavior of the subsystems, as it takes the appropriate actions and transitions based on the data from the physical models.

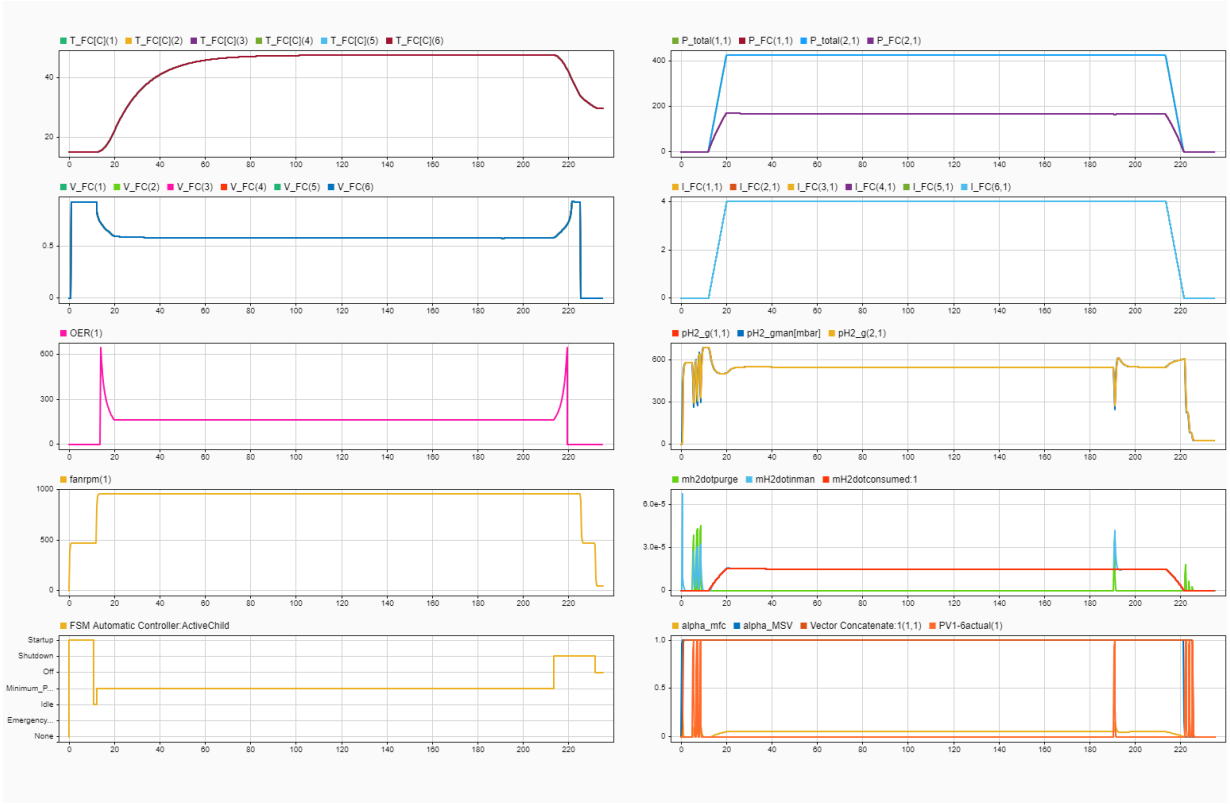

Figure 4.1: Full run with startup and shutdown sequence

The results from several physical subsystems can be seen in Figure 4.1. Firstly, the system is in Off state after which it is commanded to enter Startup state. Here, firstly, the fans are commanded to run at a fixed power (in this case 2% PWM), which can be seen by the fanrpm graph. Then once there is sufficient fan speed, the hydrogen values are opened and the pressure in the manifold and at the stacks rise to around 550mbar.g which is the reference. Then the hydrogen pressure, mass flow and valve graphs show a 3 cycle anode cleaning purge taking place, after which system enters the Idle state after ensuring voltage is within range. The effect of these 3 purges onto the hydrogen pressure and voltage is inherently modelled and can be seen in a close-up in Figure 4.2. After this, a manual Rampup command is issued, which happens within 10s so there isn't an inactivity shutdown. After this, system enters Minimum Power state after which fans speed is increased to 5% PWM, current is being ramped up to 4A, and periodic purging along with temperature control is enabled. At the top is the temperature profile of the stacks from the TMS, and it can be seen to rise from 15°C ambient temperature to around 45°C, the OER is seen to stabilize at around 160, the cell voltage dips to 0.6V, and then the electrical power is seen to be around 180W and total power just above 400W per stack. The pressure also remains controlled at 550mbar.g by the PID mass flow controller. A single periodic purge can also be seen at around 190s to remove the impurities that would be built up, after which Shutdown is commanded, causing system to enter Shutdown state.

Once entering the Shutdown state, the current can be seen beign ramped down from 4A to 0A. And after all the load switches are opened, the main supply valve can be seen to be closed, after which the anode clean sequence during shutdown is initiated. This consists of 3 purges which can be seen in the hydrogen pressure, mass flow and valve graphs, most notably the hydrogen pressure can be seen to get depressurized towards 0 mbar.g. After this all anode valves are fully closed and purging is stopped, and Cooldown is commenced where fans run at a fixed fan speed, and only when all stack voltages are less than 5V and temperatures less than 30°C for 5s, then only the system enters the Off state, and then the simulation is stopped.

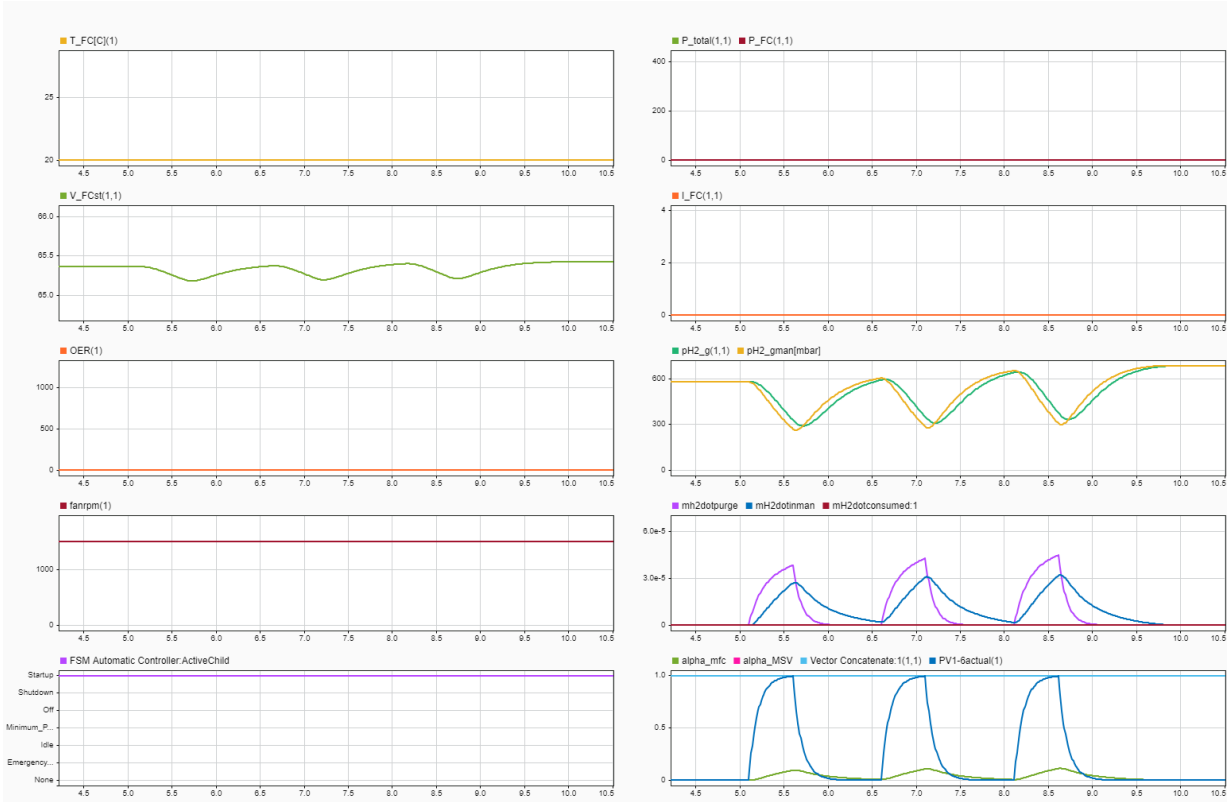

Figure 4.2: Startup purging effect

4.2. Subsystem Physical Model Parameter Estimation

In this section, certain parameters from the previously developed physical models will be estimated with experimental data. Specifically, the fuel-cell temperature and voltage models have parameters, that as of now, were taken directly from literature [21]. However, to achieve high model fidelity with the Imponator system itself, these parameters need to be estimated Imponator empirical data. From DLR, only an entire test run data from startup to shutdown exists which is 2896s ($\approx$ 50 minutes) long, and it is decided to use the first half (1448s) for parameter estimation. Firstly, the temperature parameters will be estimated in Section 4.2.1 and the voltage in Section 4.2.2.

4.2.1. AS and TMS Model Estimation

The temperature model has 2 parameters that need to be estimated, namely the η_{fan} fan efficiency and C_t thermal capacity. It was found from the temperature data of the stacks, that sometimes each stack was operated differently in terms of current demanded or fan power provided. To prevent adding complexity and preserve homogeneity, as discussed with the supervisors, it was decided to base the parameters on a single stack measurements, and assume that the temperature response of all stacks would be similar. To do this, stack 6 measurements were chosen arbitrarily. The ambient temperature sensor seemed to have an error, as its temperature fluctuated a lot, starting at higher than stack temperatures and then getting quite cold. This variation was likely because the window was kept open in November during the test run. The temperature sensor might be accurate locally, but it can't be assumed to represent the ambient temperature of the entire room. Therefore, it is assumed that the ambient room temperature was a stable 20°C after consulting with the DLR test team, and this value is used instead of the fluctuating sensor measurement. Of course, the main limitation of this assumption is that it doesn't take into account the outside cold air cooling the stacks. Therefore the calculated stack temperature may be slightly higher than the measured. After several optimization iterations to minimize the non-linear least square error cost function, the estimated parameter values can be seen in Table 4.1, with its model and sensitivity results in Figure 4.3. As seen in the sensitivity results, η_{fan} seems to have double the correlation than C_t, but most importantly it shows that both parameters have an influence on the temperature, when plotting minimum and maximums of the ± 10% of the optimal parameter values.

Table 4.1: Estimated temperature parameters and sensitivity range

Parameter	Estimated value	Sensitivity range ± 10%
C_t [J/K]	2630.40	[2367.36 , 2893.44]
η_{fan} [-]	0.57	[0.52 , 0.63]

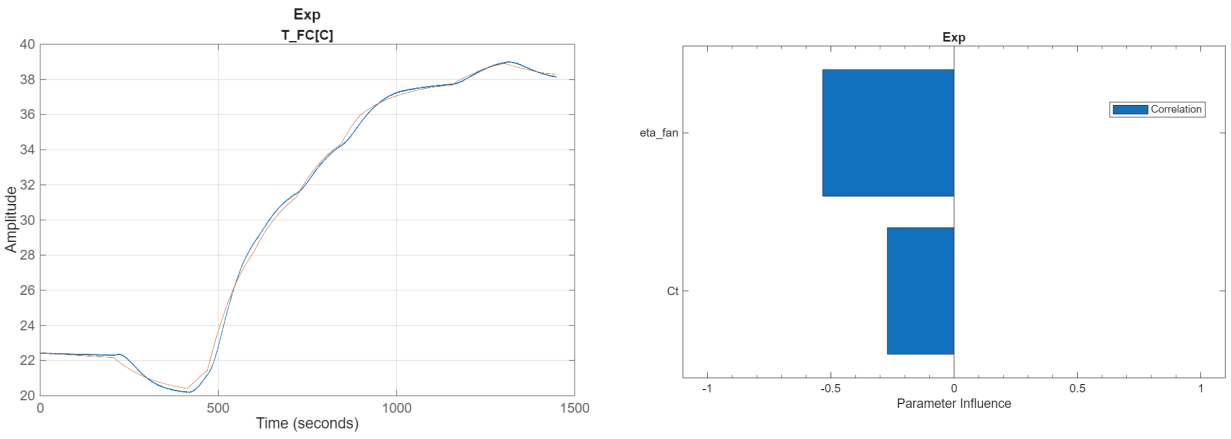

Figure 4.3: Temperature model parameter estimation & sensitivity results

The temperature response along with it's measured input signals of stack current, voltage, power and fan PWM can be seen in Figure 4.4. The data resembles a clear startup and ramp up, as current starts at 0A and rises to around 8A in this time. The fan and stack voltage also show startup behavior, but most importantly, the temperature response of the model can be visually seen to match quite well with the

experiment, which means the estimated parameters are good.

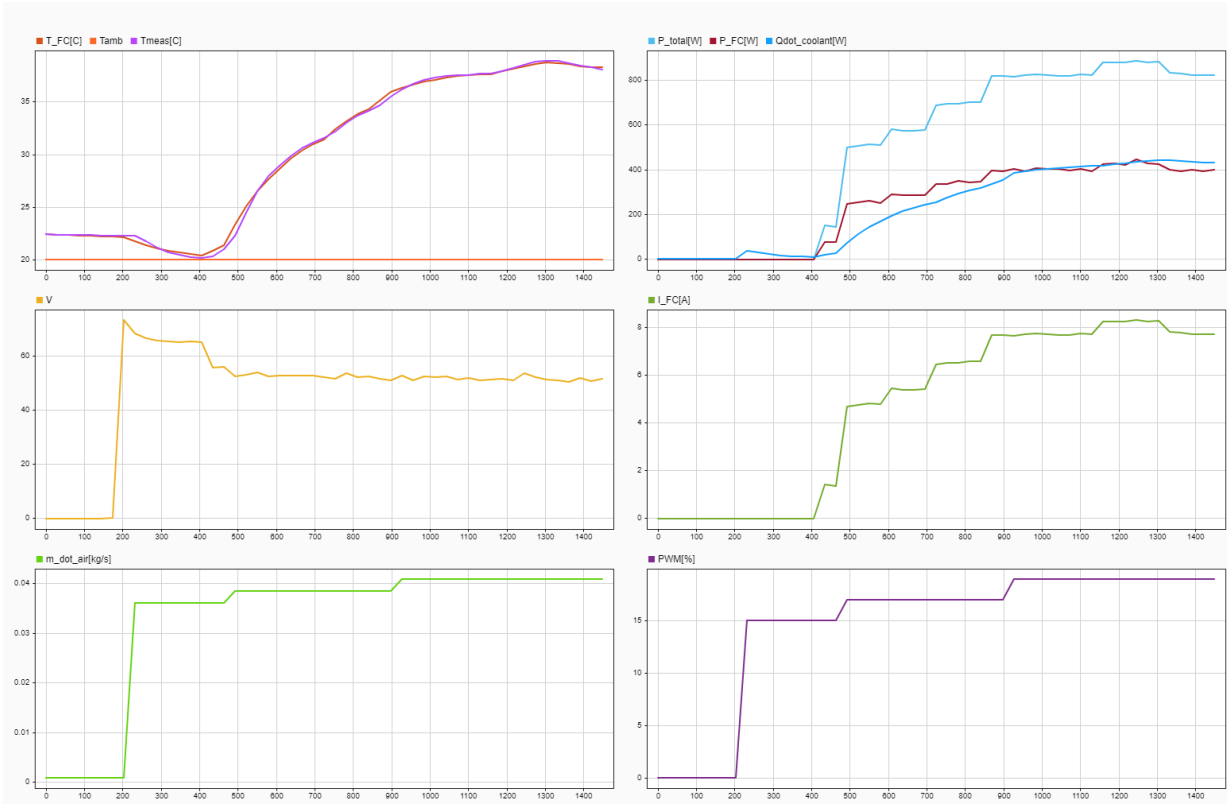

Figure 4.4: Temperature model parameter estimation with input signals

4.2.2. FCS Model Estimation

Similarly as for the temperature, the voltage model parameters will be estimated with the first half of the experimental data (1448s), and it has been decided to also be based on stack 6. This makes the assumption, that all stacks would have a similar voltage response, and thus only a single set of 6 parameters will be estimated based on stack 6. However, the voltage data was more noisy than the temperature as seen in Figure 4.5, and therefore a 4th order low pass filter was applied to the measurements, with a ω cut-off frequency of 0.3 $\frac{rad}{s}$. The data was filtered before starting parameter estimation.

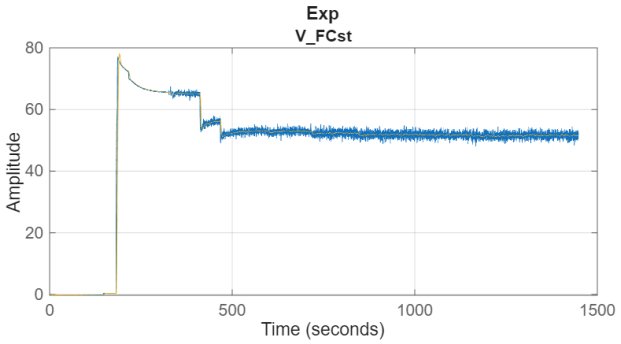

Figure 4.5: Low-pass filtering of the voltage estimation data

Table 4.2: Estimated voltage parameters and sensitivity range

Parameter	Estimated value	Sensitivity range $\pm 10\%$
$R_{\text{ohm}}[\Omega cm^2]$	0.0528	[0.048 , 0.058]
$\alpha[-]$	0.382	[0.344 , 0.421]
$i_n[\frac{A}{cm^2}]$	4.434×10^{-4}	[4.000×10^{-4} , 4.879×10^{-4}]
$i_o[\frac{A}{cm^2}]$	26.332	[23.699 , 28.965]
$m[V]$	0.428	[0.385 , 0.470]
$n[\frac{cm^2}{A}]$	4.849×10^{-11}	[4.364×10^{-11} , 5.334×10^{-11}]

The parameters to be estimated are the R_{ohm} ohmic resistance, α charge transfer coefficient, i_n exchange current density, i_o limiting current density, m concentration over-voltage coefficient, n concentration over-voltage constant. Their estimated values along with their sensitivity range can be seen in Table 4.2, achieved with the same non-linear least squares optimization. With this, the model and sensitivity results can be seen in Figure 4.6, where it can be seen that the model follows the filtered experiment quite well, except for the small initial spike, and also when the voltage dips and recovers. However, this behavior was also seen from literature and is accepted for control-oriented physical models [21]. Notably, only m, i_n, α, i_o are seen to have some correlation near their estimated values, whereas R_{ohm} is significantly smaller and n is zero. This essentially means, that at around these estimated values, only the former 4 have a noticeable correlation. Lastly, the voltage response along with the measured input data of hydrogen pressure, stack current and temperature can be seen in Figure 4.7.

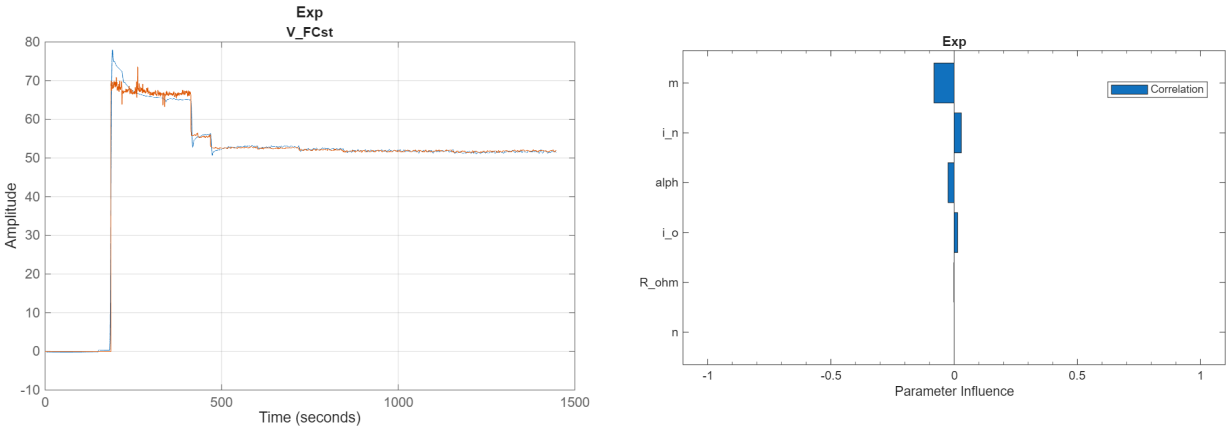

Figure 4.6: Voltage model parameter estimation and sensitivity

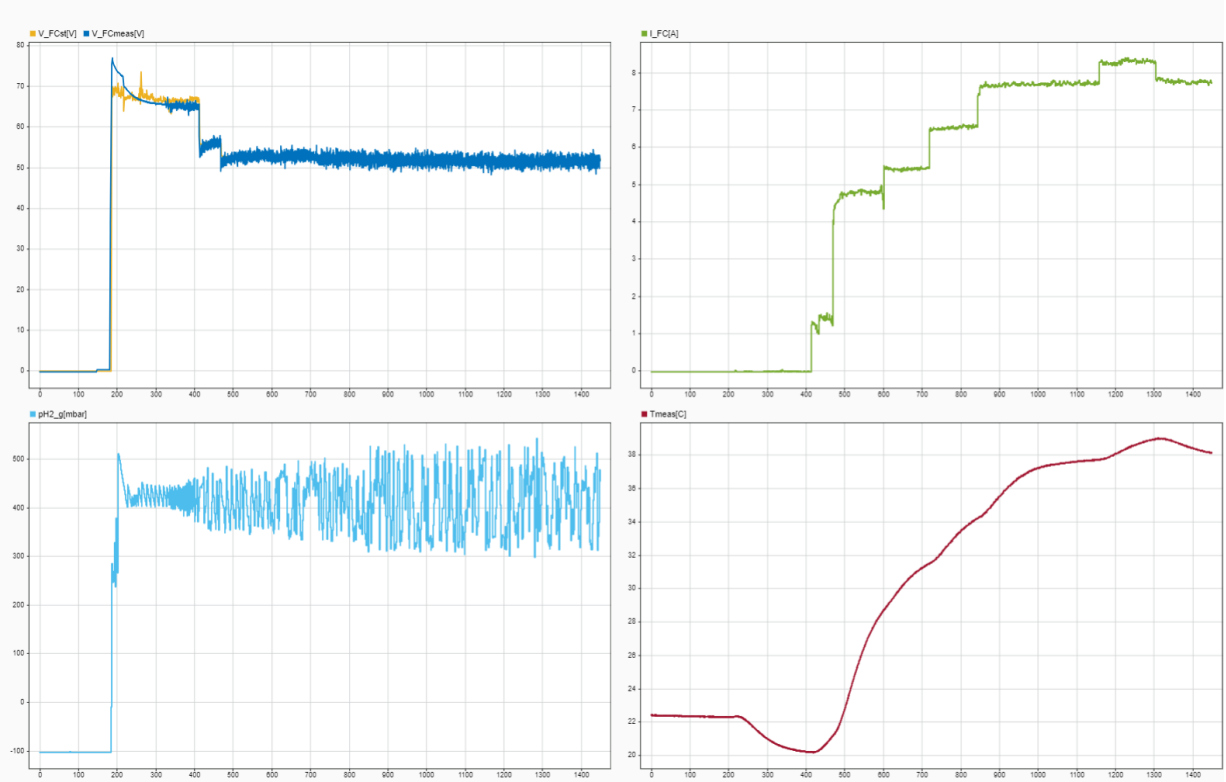

Figure 4.7: Voltage model parameter estimation with input signals

4.3. Subsystem Physical Model Validation

When it comes to validation, the second half of the experimental data can be used. This will be first done for the temperature and voltage models with the estimated parameters in Section 4.3.1 and Section 4.3.2 respectively. Then the hydrogen pressure response will be validated, which takes into account the hydrogen supply and purging subsystems, in Section 4.3.3. Lastly, the temperature, voltage and hydrogen pressure responses can all be plotted together against the experimental data, to get a sense of the overall model fidelity in Section 4.3.4.

4.3.1. AS and TMS Model Validation

The temperature model response plotted against the validation data ($1448s \leq t \leq 2896s$) along with the residuals graph can be seen in Figure 4.8. The model generally follows the shape of the data, however it can be seen that the error keeps increasing with time, and it seems that the model over estimates the temperature. This can be due to the model not accounting for the cooling caused by the wind flowing into the room due to the open windows in the experimental data. This is the limitation of the assumption that the room temperature was a stable 20°C, and the results show that perhaps the cooling term should be larger. The results of the validation metrics can be seen in Table 4.3, where the R^2 and RMSE values are acceptable, however the MBE shows that there is a constant shift, which is also observed in Figure 4.8.

Table 4.3: Temperature model performance metrics

Metric	Value
$R^2[-]$	0.81
RMSE[°C]	1.18
MBE[°C]	-0.92

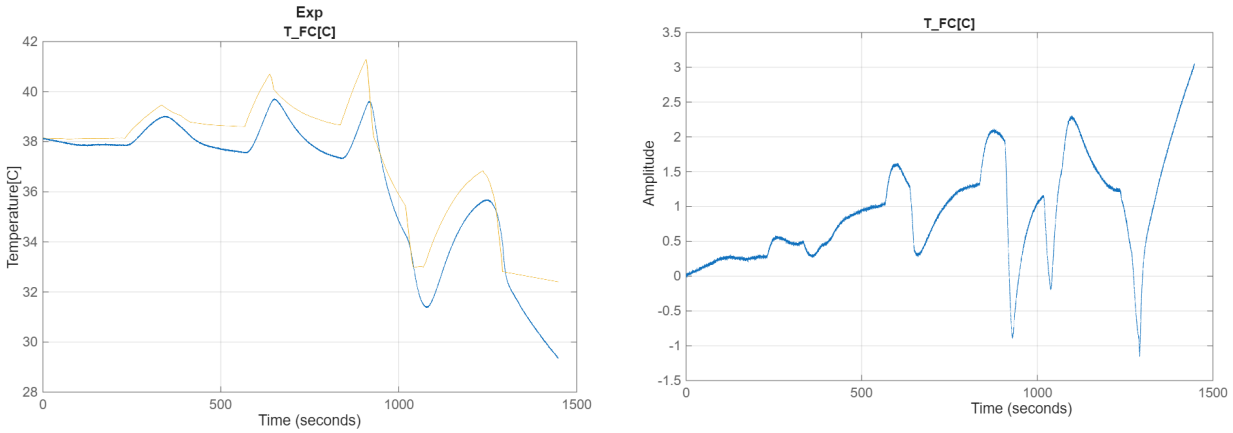

Figure 4.8: Temperature model validation with residuals

The results along with the input validation data can be seen in Figure 4.9. Most notably, it can be seen at the end that the model and experiment deviate when the current and fan PWM is put to zero. Here, since the model does not calculate any passive cooling due to the room or wind, and only calculates for the fan, the model temperature is seen to decrease with a shallower slope than the experiment. All in all, due to the limited data, these temperature model parameters show a good overall level of validation, and thus are acceptable to be included in the control-model.

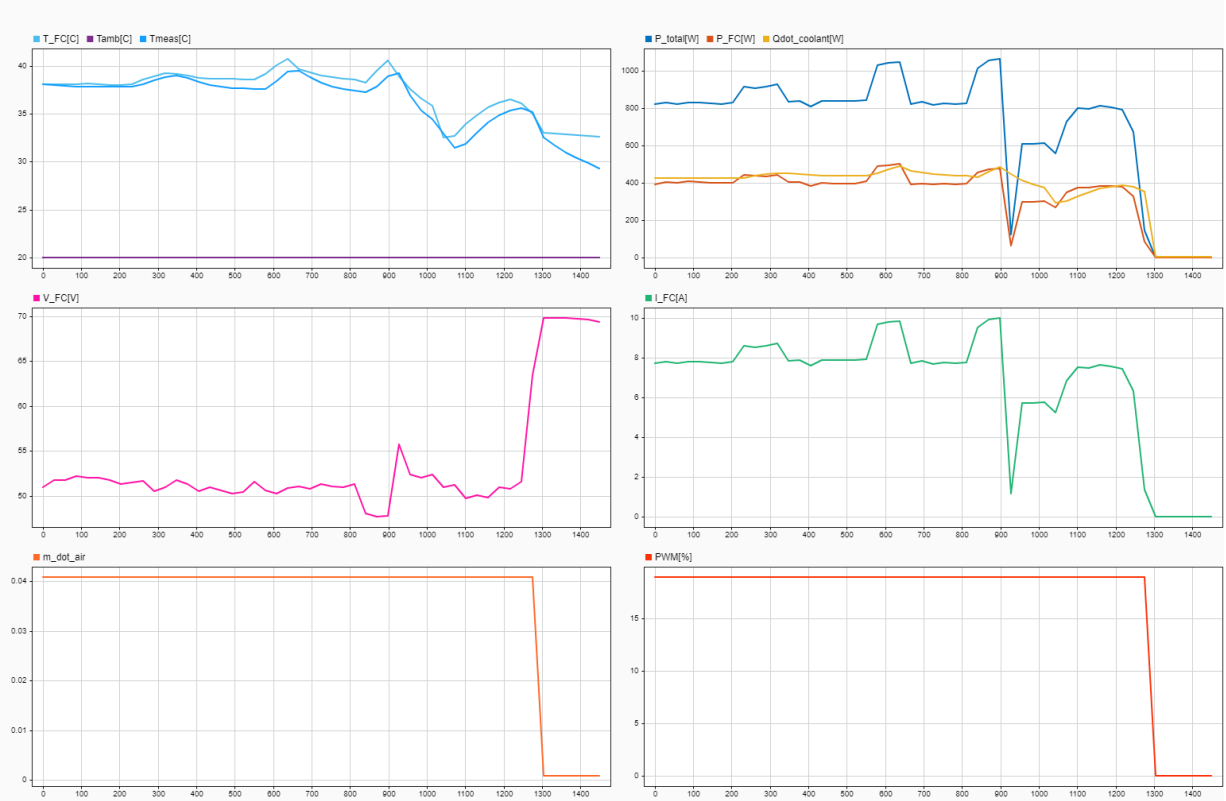

Figure 4.9: Temperature model validation along with input data

4.3.2. FCS Model Validation

Table 4.4: Voltage-model performance metrics

Metric	Value
$R^2[-]$	0.93
RMSE[V]	1.60
MBE[V]	-0.28

Similarly as for the temperature, the voltage model response plotted against the validation data ($1448s \leq t \leq 2896s$) along with the residuals graph can be seen in Figure 4.10. Here it can be seen that the model follows the shape and the magnitude of the experiment (in blue) extremely well, and the residuals oscillate around 0. The only exception is at the end, where the model puts the voltage to 0, whereas the experiment holds a non-zero value. This is likely because there is some remaining hydrogen at the anode inlet, however the model does not see this, and simply puts voltage to zero when the hydrogen pressure is zero. Therefore the boundary residual can be ignored when calculating the validation metrics, giving Table 4.4. The R^2 value is very good showing a close match, RMSE is also acceptable for the given range in voltages, and MBE shows a small bias error which is acceptable.

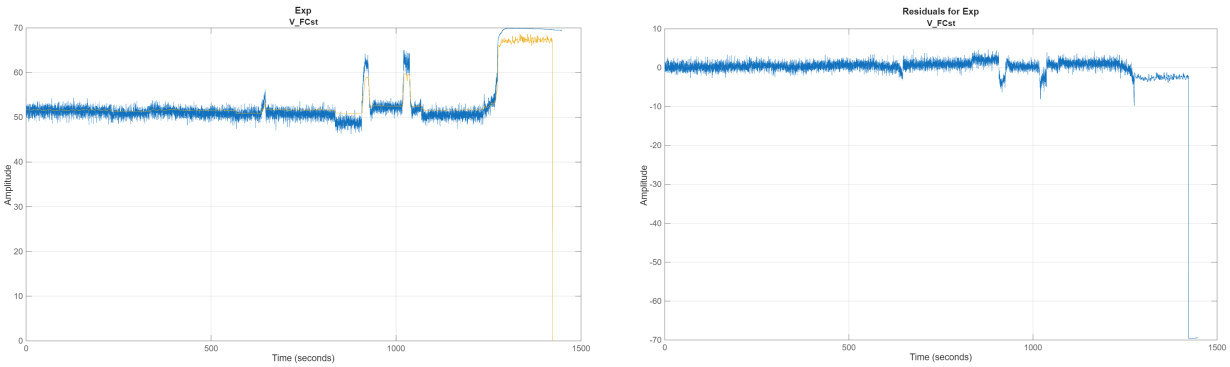

Figure 4.10: Voltage model validation with residuals

Then the voltage model response can be seen alongside input validation data in Figure 4.11. Here it can be seen that the voltage model reacts to the demanded current profile, for example the voltage dips when there is an increase in current and vice versa. The hydrogen pressure fluctuates a lot but manages to stay around 400mbar.g to provide for the stack voltage. Notably, the stack temperature is seen to decrease as the current is ramped down, which is also logical.

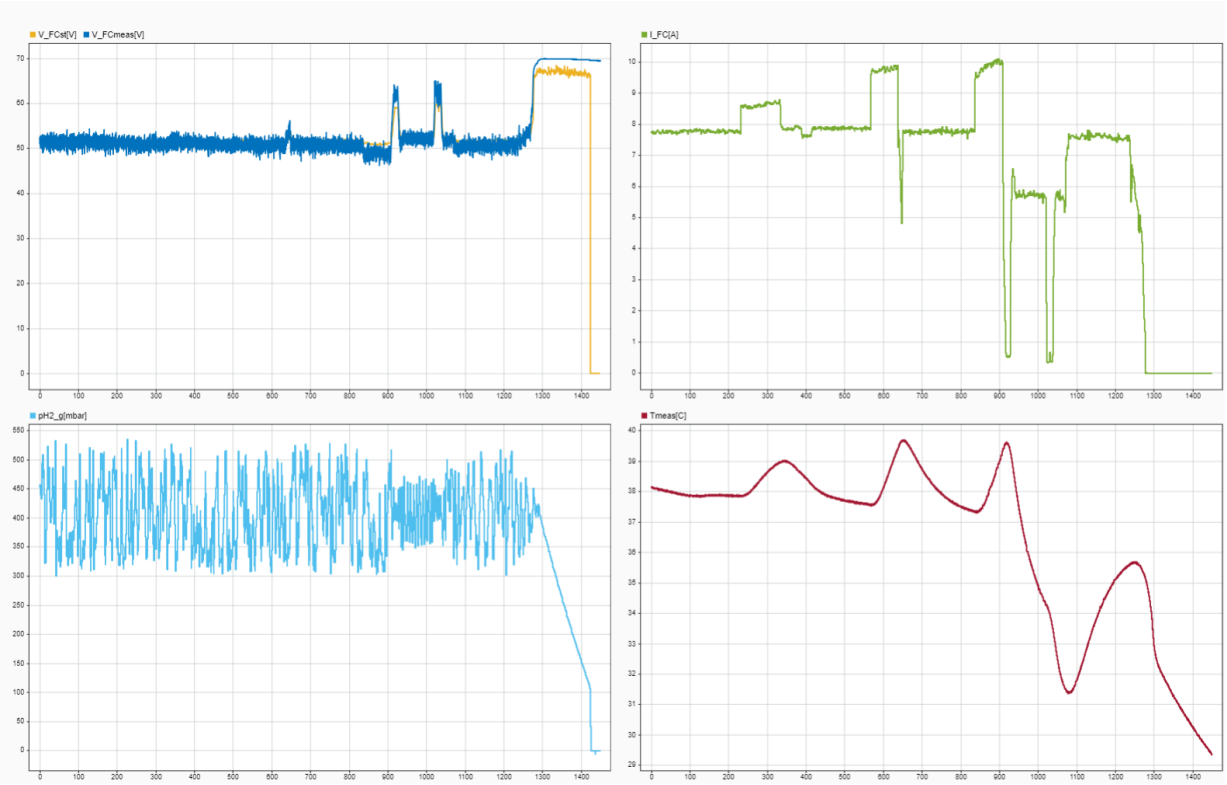

Figure 4.11: Voltage model validation along with input data

4.3.3. HSS, PS and PWS Model Validation

Now the hydrogen pressure model can be validated against the measured stack 6 pressure, and this time the entire data range is considered from startup to shutdown, because the pressure model is tuned and designed to start from 0mbar.g. The results can be seen in Figure 4.12 and Figure 4.13. Most notably, it can be seen that the model follows the measured data quite well from startup to steady state holding at 400mbar.g. Whilst testing, it was seen at the end that the model deviated a bit, and this is due to the purging influence. Essentially, the model overestimated the mass flow that is purged because it previously assumed a linear purge valve, causing a linear purge mass flow. It can be seen that the purge valve is kept to a command of 50% most of the time, and it purges to 70% periodically. The DLR test team reported that the valves actually only really open at 70% command and thus are non-linear, which explained why the pressure doesn't drop as fast as what the model calculates. Thereafter, with these learnings a non-linear purge valve was modelled with a deadzone till 50% as shown in Section 3.3.4, which is what the results show in Figure 4.12. Additionally, experimental data shows that hydrogen pressure can become negative at the beginning due to vacuum buildup, as hydrogen is still being consumed as air is still available at the open cathode. The model is built such that the stack pressures just follow the manifold pressure, and purging a stack doesn't locally reduce stack pressure just reduces the overall manifold pressure. Due to this, at the end, the model pressure drops a bit later than the measured, and the rate at which it decreased depended on the estimated anode volume. Therefore, the anode volume was physically measured, since it greatly

Table 4.5: Hydrogen pressure model performance metrics

Metric	Value
$R^2[-]$	0.81
RMSE[mbar.g]	62.24
MBE[mbar.g]	0.49

affects the pressure's response to purging and pressurizing, as a smaller volume would be purged out faster than a larger one.

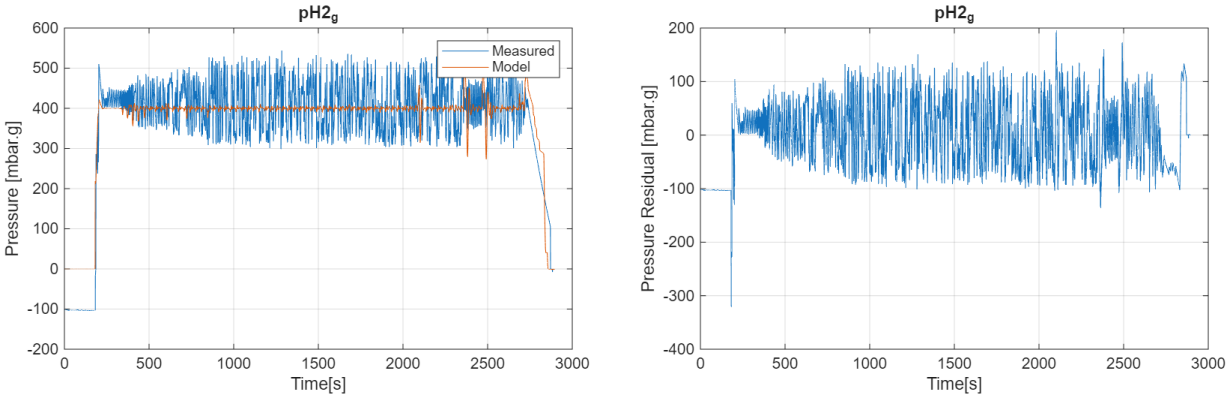

Figure 4.12: Hydrogen pressure model validation with residuals

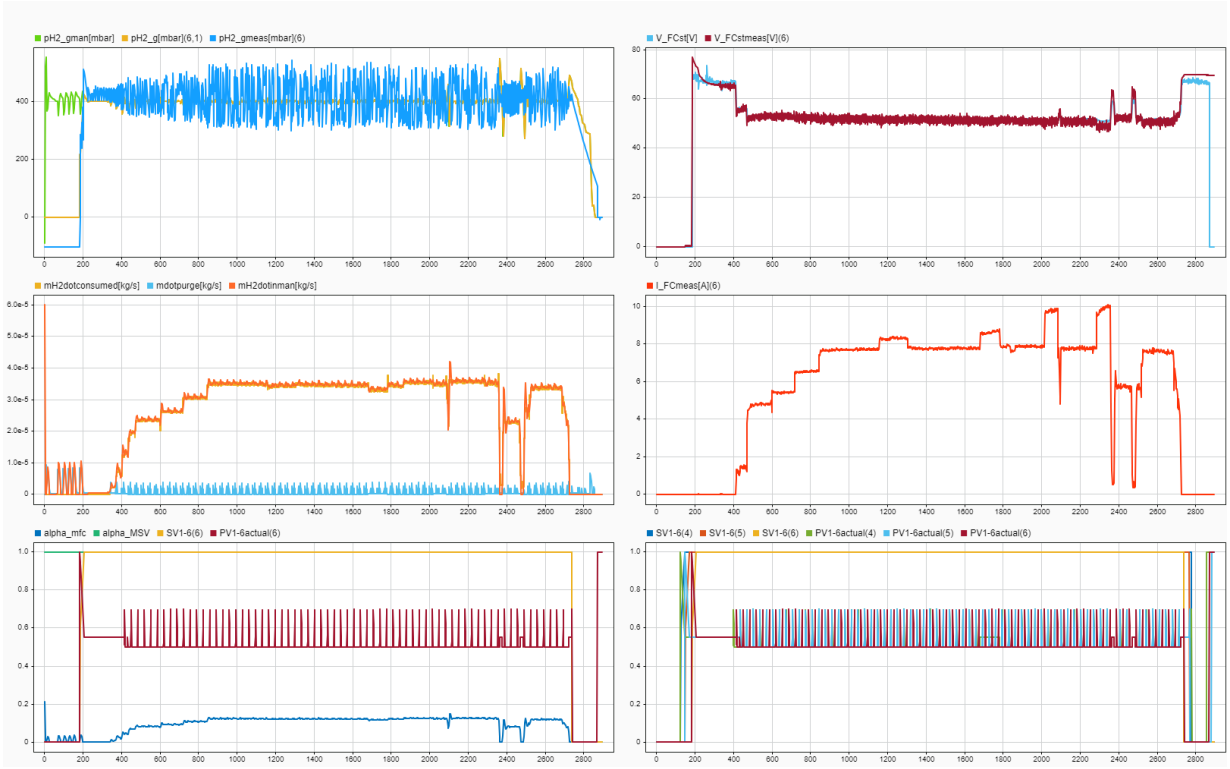

Figure 4.13: Hydrogen pressure model validation along with input data

For the validation metrics, the R^2 and MBE values are acceptable, however the RMSE is quite larger relative to the data range. This can also be visually seen for most of the time in Figure 4.12, since the measured pressure fluctuates a lot compared to the model. It can be seen that the model pressure also oscillates quite a bit, however it performs better in maintaining the target pressure and thus the magnitude of oscillations is smaller. It is predicted that this arises from the difference in PID gains of the real and model mass flow controller which will be further discussed in Section 5.1. It is known that the real PID controller was never tuned for this application, whereas the model PID controller was, which supports this reasoning. Additionally, the difference can come from the mass flow controller's internal valve dynamics which is not modelled. This information is not available, and the only way to build a higher fidelity mass flow controller model would be to use measurements from the anode manifold such as the manifold

pressure, and the manifold mass flows, which were not available in this dataset. This will be kept as a recommendation to improve the mass flow controller model fidelity when more data is available, but for validation it is sufficient to accept the model and take note of this difference.

4.3.4. Overall Model and Experiment Comparison

A single comparison plot can be made for the entire experimental run data used in estimation and validation. Here the model temperature, voltage and pressure can be showed alongside their measured values as well as measured input signals and their interpretations in Figure 4.14. This is for the entire experiment data range, from startup all the way to shutdown. It can be seen, that the model responds well to the input signals, and output signals of temperature, voltage and pressure that generally match the measurements. Therefore, this model is now deemed acceptable to begin subsystem controller design to achieve operational automation.

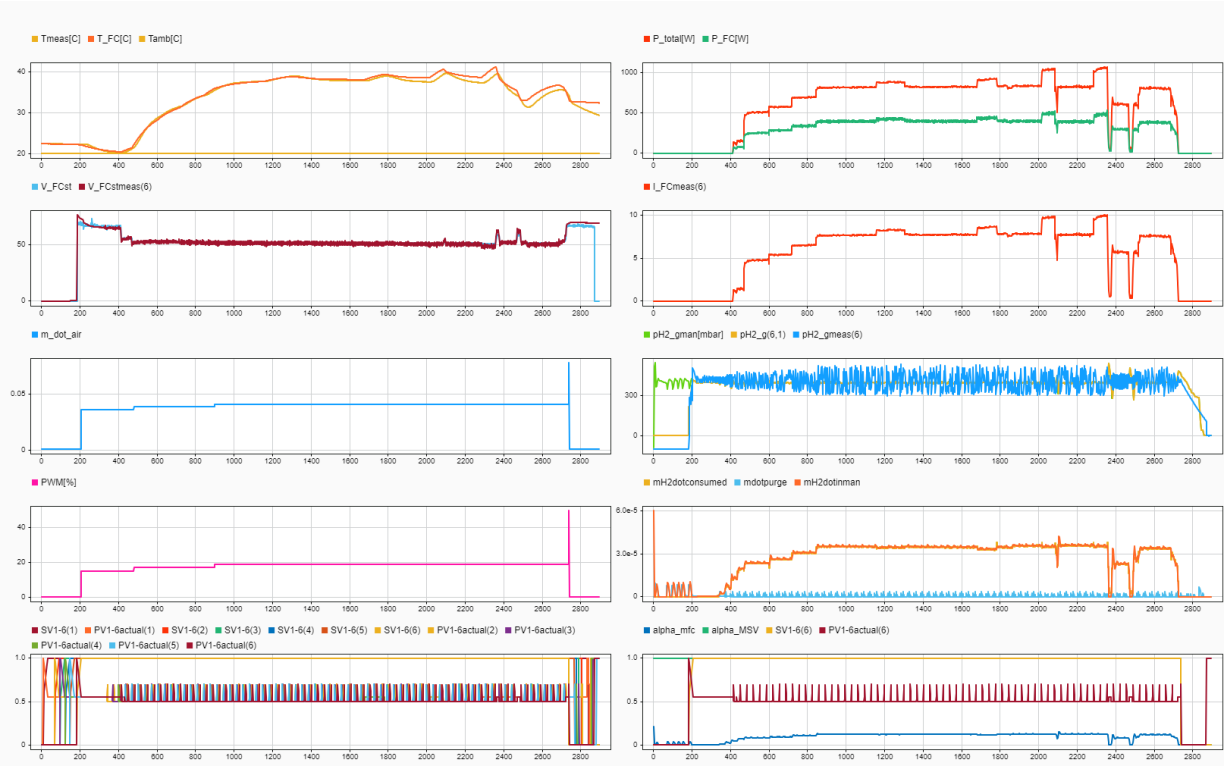

Figure 4.14: Entire test run comparison between model and experiment

5

Fuel-Cell Controller Design & Verification

The FSM supervisory automatic controller had already previously been designed along with the physical models. In this chapter, the required model-based subsystem controllers will be designed, to achieve the automation of the startup and shutdown procedures of the Imponator as defined in MFM and FSM. These subsystem controllers make up the control subsystems as defined in MFM Figure 3.3. Firstly, an existing mass flow PID controller (part of Hydrogen Flow Regulation) will be investigated to better match with experimental data in Section 5.1. Secondly, temperature (Air & Thermal Regulation), current (Current Flow Regulation) and purging (Purging Optimizer) controllers will be designed and their control reliability requirements verified in Section 5.2, Section 5.3 and Section 5.4 respectively. Thereafter, the remaining control safety requirements for emergency procedures will be modelled and verified in Section 5.5. All the results used for verification, are generated by running the entire FSM and subsystem models with their designed controller, from startup to shutdown. Additionally, all Simulink graphs have simulation Time [s] on their x-axes, and y-axes units in the legend.

5.1. Hydrogen Flow Regulation - Mass Flow PID Controller

The MFC is part of the Hydrogen Flow Regulation control subsystem within HSS, and its control block diagram can be seen in Figure 5.1. It has an input error signal e, for the difference between reference pressure p_{ref} (400mbar.g in the experiment) and the actual manifold pressure p. The PID outputs valve position α_{MFC} [0,1], which affects $\dot{m}_{H2in}$ and thus p, with the goal of making error signal 0. This MFC has a PID controller which was tuned by modelling a simple condition where there was a constant $\dot{m}_{H2cons}$ and $\dot{m}_{H2purge}$, and the controller just had to get to a stable value of 400mbar.g pressure, without any dynamic changes. As mentioned before, it needs to be checked that the oscillatory pressure response difference between model and measurements come from the model PID gains being different than the real PID. This oscillatory frequency is believed to come from the purging frequency, which is something the controller reacts to. It is hypothesized, that the magnitude of these oscillations is related to how well the PID gains are tuned for this purpose. It was previously seen, that the model pressure does respond to purging and oscillates, but the magnitude is way smaller. Therefore, the model PID gains need to be estimated to try to replicate this oscillatory response in magnitude and frequency. If this can be replicated, it means that the model isn't missing dynamics, and this is not sensor's white noise measurement error.

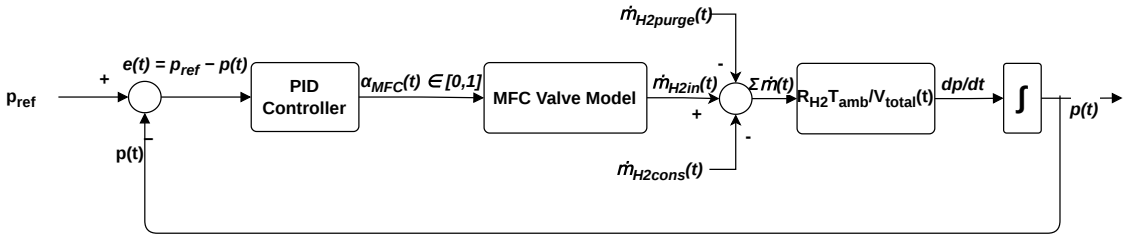

Figure 5.1: Mass flow PID controller block diagram

The results of changing the gains of the model PID controller can be seen in Figure 5.2. Doing parameter estimation of PID gains to match the measurement data was a difficult and computationally demanding task, thus the gains were simply altered manually to check if the responses can be similar. Here it can be seen that the magnitude of the model oscillations can be made to match the measurements, after some manual tuning of the gains. The match is not perfect, since the gains could not be tuned optimally, and the model magnitude seems to increase by a lot at the end, right after the current dipped twice, lowering the consumption mass flow. It was also seen, that the oscillatory frequency of the model depended on the gains of the PID. Additionally, it is known that the internal valve dynamics of the controller are not modelled, and it is assumed to be a linear proportional valve causing linear increase in mass flows. Due to limited information from the manual, and also no measurements from the mass flow controller itself, it was not possible to build a more accurate model. If measurement data from the manifold pressure sensor and mass flow controller were available, the $\dot{m}_{H2in}$ plot can be directly compared and model can be improved, as they have a direct relationship, and pressure is integrated.

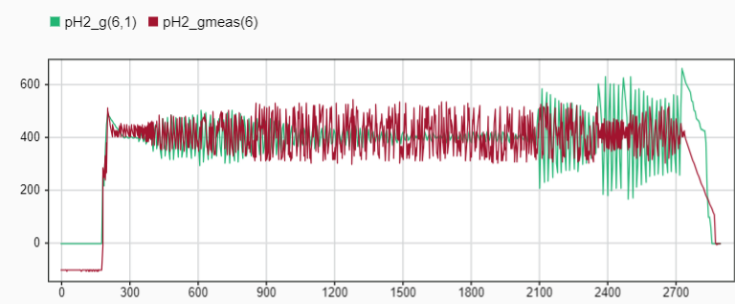

Figure 5.2: Model MFC PID tuning to match real MFC PID pressure behavior

Therefore, now it can only be said that the difference in pressure responses can be due to linear and fast internal valve assumption (missing dynamics) and differences in PID gains. The recommendation to improve fidelity here, would be to gather the mass flow controller's experimental data and real PID gains, so that model can be better matched and compared. And then if the responses are still different, then it would mean some other dynamics would be missing. However, since the goal was not tune the real PID controller, the pressure response is acceptable to design other new controllers as per MFM and FSM.

5.2. Air & Thermal Regulation - Temperature PID Controller

The stack temperatures need to be controlled during operation, especially during Minimum power state. The Air & Thermal Regulation control subsystem requirements can be formulated as a combination of previously defined control system requirements (CS-R4, CS-S2) and certain goals and hazards from MFM (O2b, H2), giving Table 5.1. To suffice these requirements, a simple PID controller was chosen and tuned, as can be seen in Table 5.2 and Figure 5.3 [37]. Specifically, the temperature PID controller block diagram can be seen in Figure 5.4, and for further details about TMS and AS models please refer to Section 3.3.

Table 5.1: Air & Thermal Regulation control subsystem requirements

ID	Requirement
CS-R3	The control system shall maintain oxygen excess ratios of $\geq$2 during operation[26].
CS-R4	The control system shall keep the stack temperatures $\leq 50\,^{\circ}$C during operation.
CS-R5	The control system shall keep temperature within $\pm 1\,^{\circ}$C of desired value at maximum possible power.

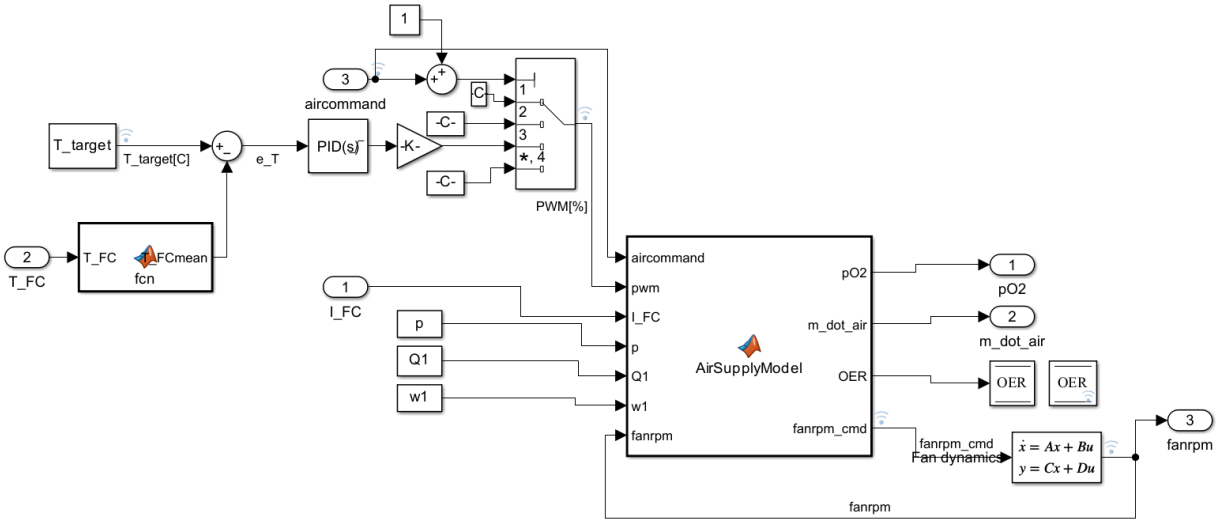

Figure 5.3: Temperature PID controller setup

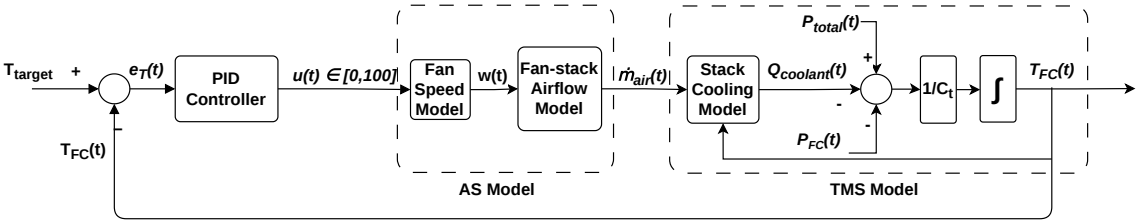

Figure 5.4: Temperature PID controller block diagram

Table 5.2: Temperature controller PID gains

Gain	Value
K_p	-49.79
K_i	-1.49
K_d	-133.87

The results of running the simulation at the maximum possible power with 31A current, can be seen in Figure 5.5. This is below the maximum rated current, because running the simulation for a rated 40A current resulted in a temperature overshoot as seen in Figure 5.6. Here, the fans are operating at maximum 100% power, however the cooling simply isn't sufficient to keep the stack temperatures $\leq 50°C$. Since the TMS was validated (which accounts for cooling), with an R^2 of 82%, this would be the validity of this result. Therefore, it can be said that the Imponator with its existing fans cannot sustain pulling 40A rated current without overheating. Hence, the maximum possible steady-state current is 31A without overheating, giving 1.29kW electrical out of 3.3kW total reaction power, which is 39.1 % efficiency. Since the maximum rated electrical power of stack is 2kW, this is only 65% of total power.

It can be seen in Figure 5.5, the temperature PID controller performs quite well to keep the stack temperatures $\leq 50°C$, and at the maximum possible power it keeps it within this desired value of $\pm 1°C$. Additionally, the OER of the stacks can be seen to be ≥ 2 in operation, verifying CS-R3, CS-R4, CS-R5. Notably, Figure 5.3 demonstrates how the air-commands from the FSM are interpreted and how the logic switching occurs during the entire run, constant blocks are used for the 0%, 10%, and 100% PWM.

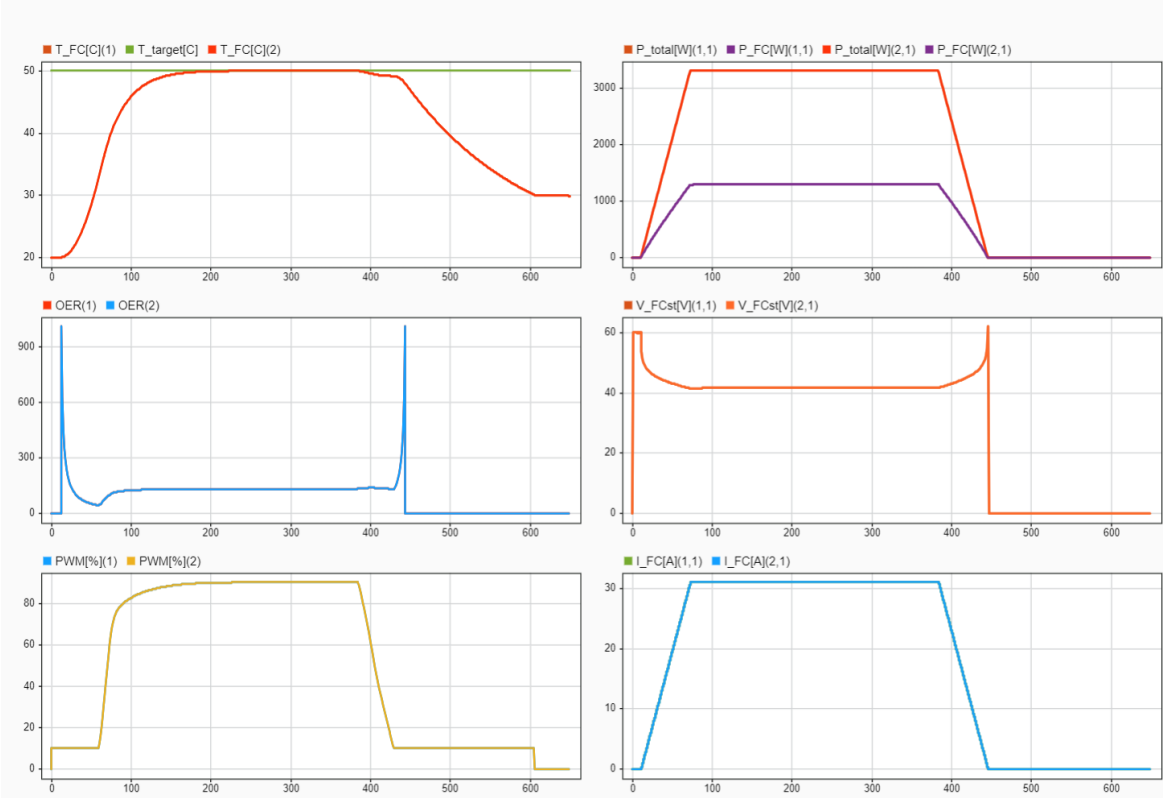

Figure 5.5: Temperature PID controller response for 31A load

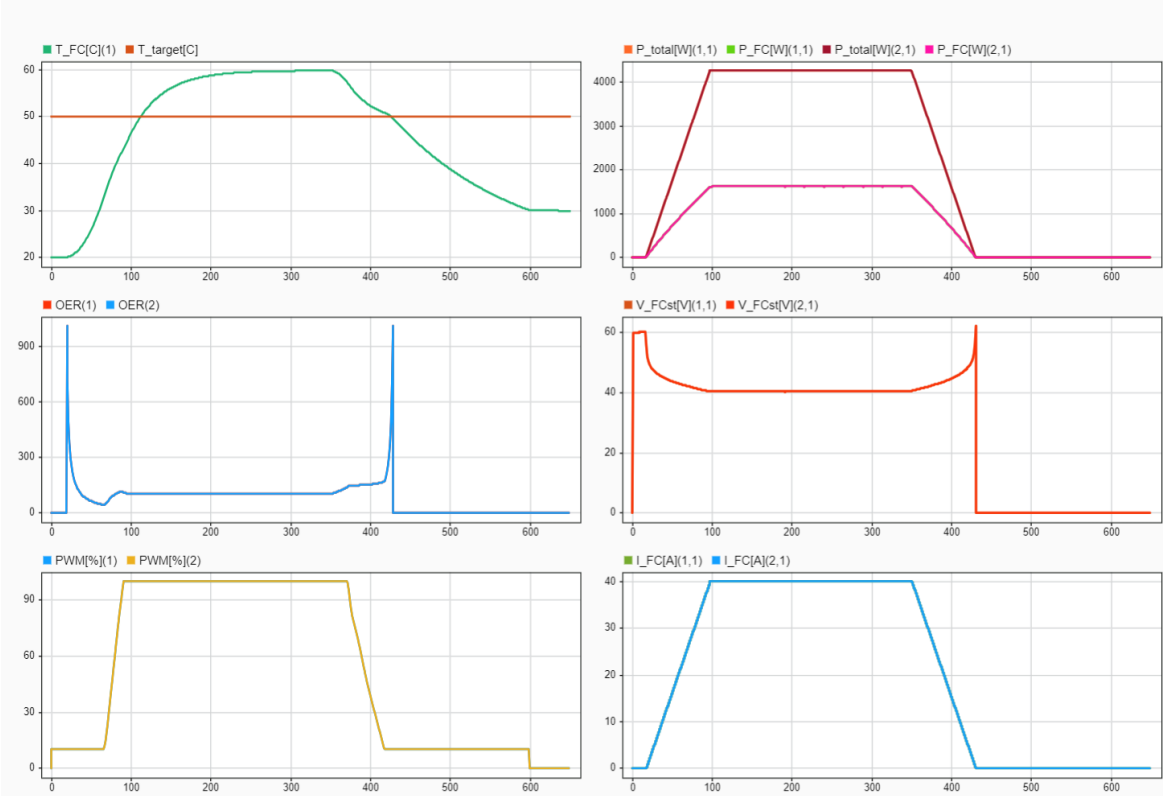

Figure 5.6: Temperature PID controller response for 40A maximum load

5.3. Current Flow Regulation - Current Nonlinear Reference Governor

In this section, a current controller will be designed to suffice the requirements as summarized in Table 5.3. The current needs to be ramped up to a minimum current of 4A during startup, and then ramped down to 0A and OCV state during shutdown. It is desirable to ramp the current up and down as fast as possible to the commanded value, to achieve a fast and responsive system, required for aircraft propulsion. The reason the commanded value cannot be directly met in an instant, has to do with the hydrogen pressure and thus the fuel cell voltage response. During the Minimum Power state, whilst the current is ramped up, hydrogen is being consumed and therefore the hydrogen pressure initially decreases before the MFC can react to maintain the 550mbar.g. The initial pressure decrease also causes a cell voltage drop due to V_{oc} decreasing, however the biggest drop comes from the voltage model's response to an increase in current, since the V_{act}, V_{ohm}&V_{conc} terms get larger as seen in Section 3.3.3.

Table 5.3: Current Flow Regulation control subsystem requirements

ID	Requirement
CS-R1	The control system shall maintain the stacks' hydrogen pressure between 400–700 mbar.g.
CS-R7	The control system at startup shall minimize the time in OCV [27].
CS-R8	The control system at startup shall ramp-up the fuel-cell system to the minimum power.
CS-R9	The control system shall maintain cell voltage between 0.5V and 0.92V when loaded.
CS-R10	The control system shall keep stack current within ± 1A of demanded current.

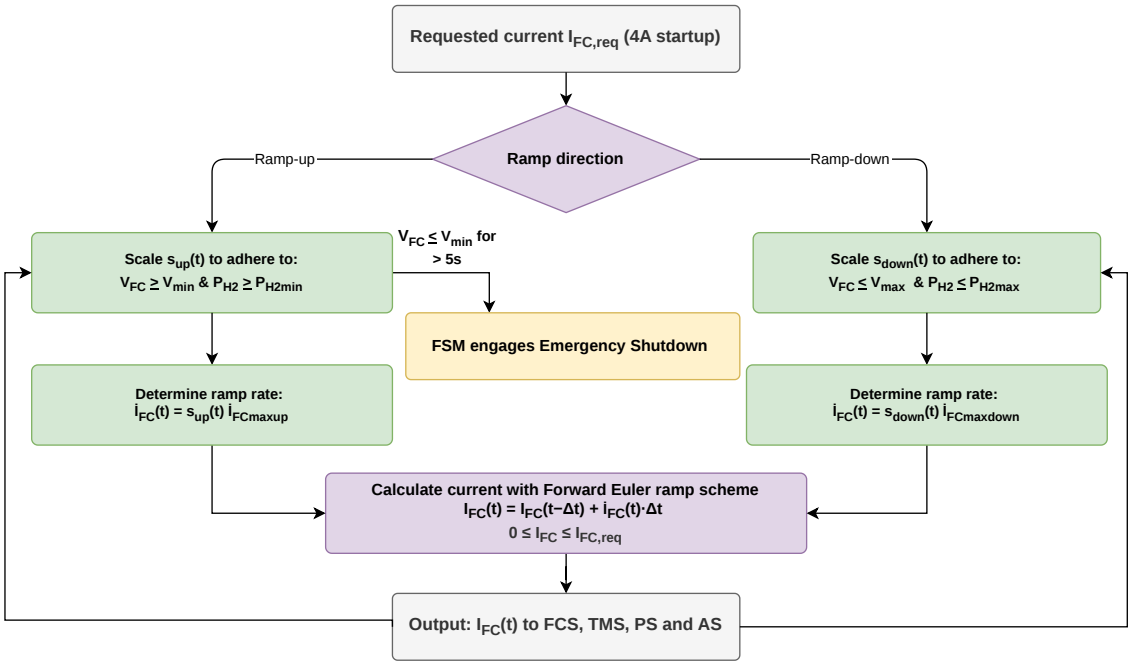

Figure 5.7: Current NRG Diagram

Table 5.4: Current NRG parameter values

Parameter	Value
$I_{FC,req}$ [A]	[4,31]
$\dot{I}_{FCmaxup}$ [A/s]	1.4

Parameter	Value
$\dot{I}_{FCmaxdown}$ [A/s]	1.9
V_{min} [V]	0.5
V_{max} [V]	0.92
V_{buffer} [V]	0.05
P_{H2min} [mbar.g]	400
P_{H2max} [mbar.g]	700
P_{buffer} [mbar.g]	20

The current controller chosen to meet the Table 5.3 requirements is a nonlinear reference governor, and its a forward Euler scheme with timestep Δt and can be seen in Equation 5.1 and its workflow in Figure 5.7. Here the $\dot{I}_{FC}$ current ramp rate has a scaling as seen in Equation 5.2. The s scale is between 0 and 1, but its values differ based on ramping up or ramping down as its constraints are different as seen in Equation 5.3. Here it can be seen, that ramping up rate is constrained by the lower voltage and pressure limits whereas ramping down rate is constrained by the upper voltage and pressure limits, and their values seen in Table 5.4. Specifically, the values for $\dot{I}_{FCmaxup}$ and $\dot{I}_{FCmaxdown}$ were determined by manually running the simulation, and an edge value was chosen, which means ramp rates higher than this value would lead to the current actually switching directions for a moment, to allow the voltage or pressure to reenter the allowable range. This is deemed undesirable in ramping up or down, and thus this value is the maximum where the fastest and smoothest current profile is achieved, and its result for 4A can be seen in Figure 5.8 verifying requirements CS-R1,8,9,10, and CS-R7 is handled by the FSM which forces a Shutdown if inactivity in OCV (Idle) >10s. For pulling this low load, it can be seen that voltage and pressures are not constraining, and thus the ramping up and down can be done the fastest reaching 4A (190W) in 2.8s and 2.1s respectively. For higher ramp rates, it can be seen than the pressure would be come constraining as it quickly approaches the limits. Since the purging is yet to be controlled, ignore the pressure dips at the startup.

$$I_{FC}(t) = I_{FC}(t - \Delta t) + \dot{I}_{FC}(t)\Delta t \quad 0 \leq I_{FC} \leq I_{FC,req} \tag{5.1}$$

$$\dot{I}_{FC}(t) = \begin{cases} s_{up}(t)\, \dot{I}_{FCmaxup}, & \text{ramp-up} \\ -\, s_{down}(t)\, \dot{I}_{FCmaxdown}, & \text{ramp-down.} \end{cases} \tag{5.2}$$

$$s_{up}(t) = \min\left(\frac{V_{\text{FC}} - V_{\text{min}}}{V_{\text{buffer}}}, \frac{P_{H2} - P_{H2min}}{P_{\text{buffer}}}\right) | s_{down}(t) = \min\left(\frac{V_{max} - V_{\text{FC}}}{V_{\text{buffer}}}, \frac{P_{H2max} - P_{H2}}{P_{\text{buffer}}}\right) \tag{5.3}$$

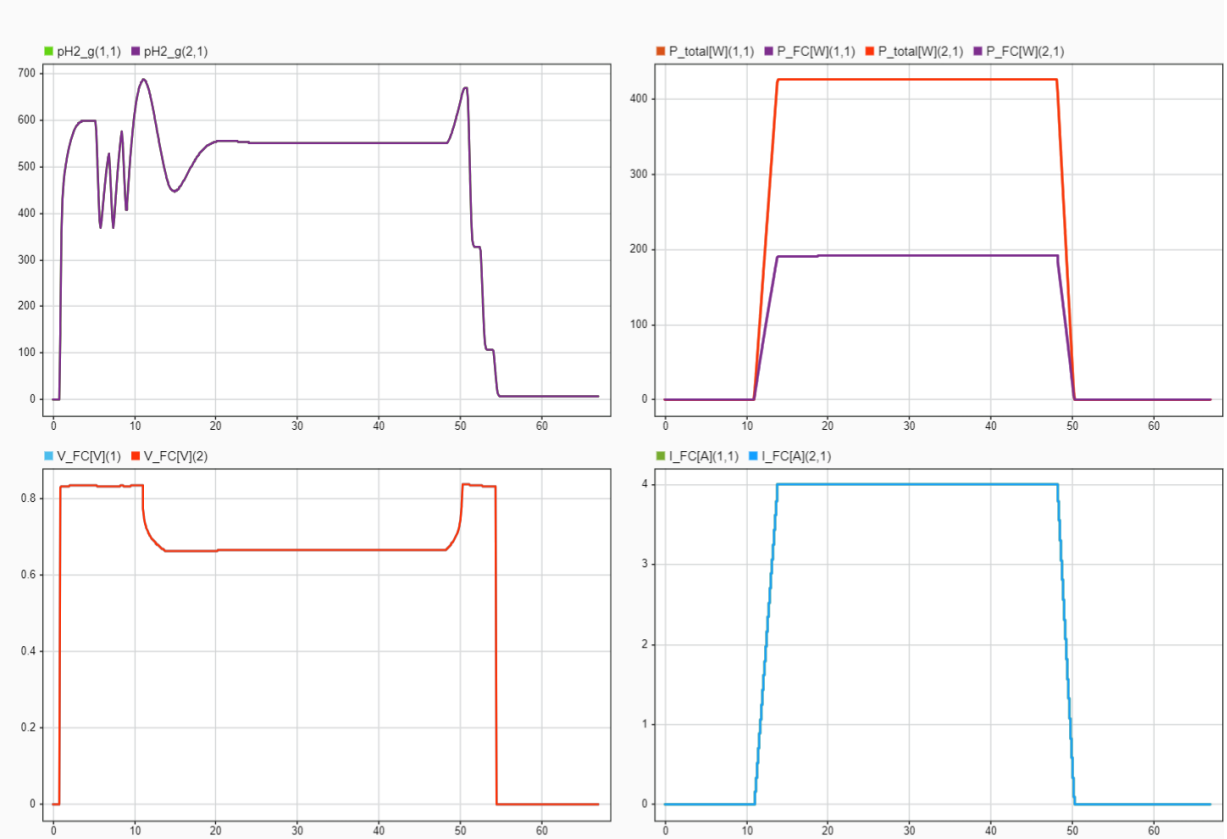

Figure 5.8: Current ramp controller response to 4A demand at minimum 0.5V cell voltage

Similarly as for the temperature controller, it is interesting to ramp up to the maximum possible current, which is now 31A without overheating. Since the manual mentioned a recommended minimum cell voltage of 0.6V and an absolute minimum cell voltage of 0.5V, the simulation was ran for both of these constraints can can be seen in Figure 5.9 and Figure 5.10 respectively. For the 0.6V case, for a current requested of 31A, the current can be seen to only reach a maximum capacity of 21.5A in 150s, which is equivalent of 930W. The current can be seen to decrease its ramping up rate, constrained by only the minimum cell voltage of 0.6V, where the pressure seems to maintain its target of 550mbar.g throughout the run. These results are quite different from the beginning of life rated values of cell voltage 0.7V at 40A. However, it is known that the stacks have been degrading and they haven't been able to run at the rated power in recent times, as confirmed by the DLR test team. When the same simulation was ran for a lower constraint of 0.5V, the results in Figure 5.10 show that the requested 31A current (1.29kW) is met in about 23s, and ramp down in 21s. Here, the pressure is constraining, but as seen the controller does a good job to keep the pressures within range using a margin. After discussion with DLR, it was decided to use the absolute minimum cell voltage constraint of 0.5V, since the stacks have already degraded, and thus it is most useful currently to draw the highest possible currents. This maximum possible current is still 31A, limited by overheating.

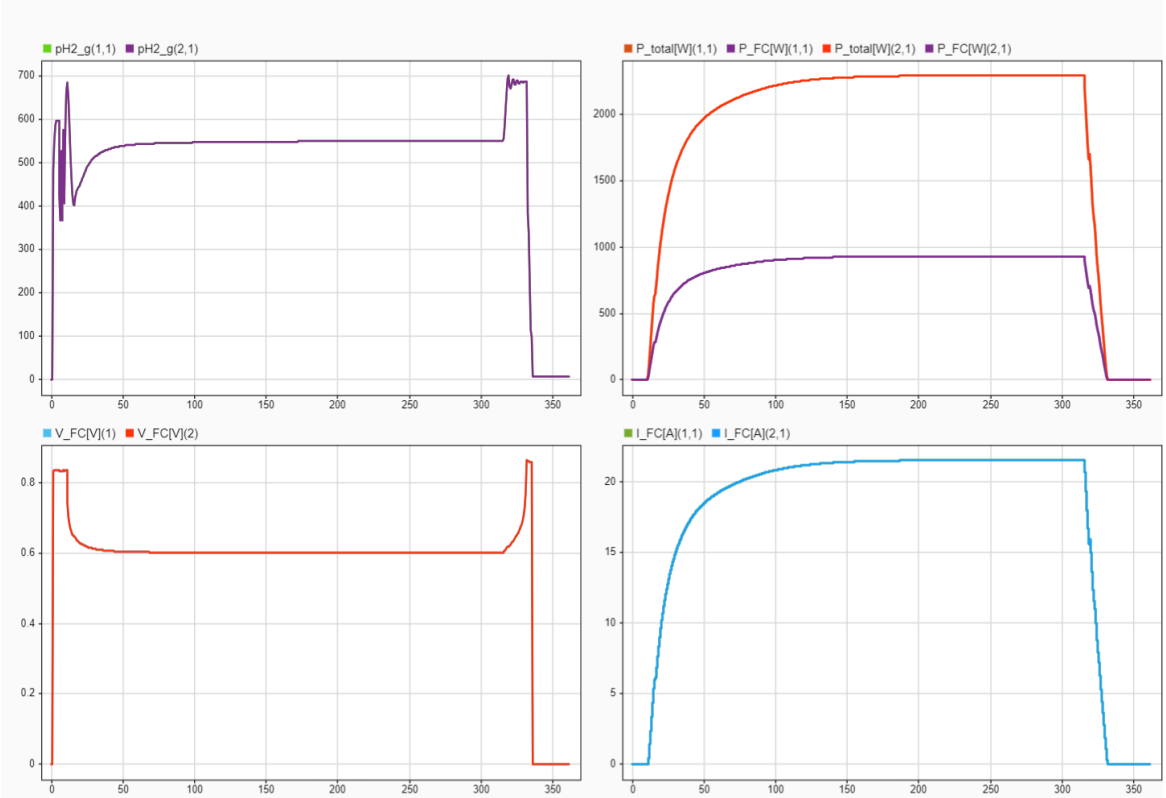

Figure 5.9: Current ramp controller response to 31A demand at minimum 0.6V cell voltage

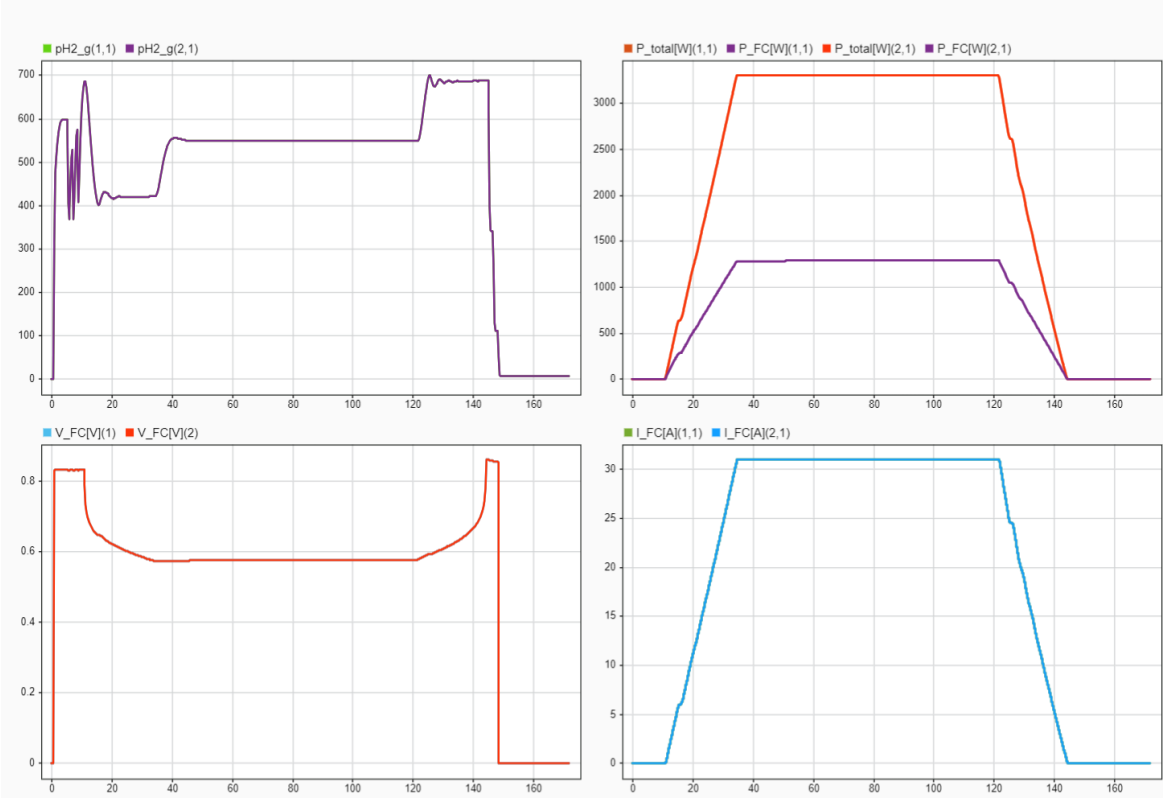

Figure 5.10: Current ramp controller response to 31A demand at minimum 0.5V cell voltage

5.4. Purging Optimization - Purge Controller

In this section, a purging controller will be designed to meet the control requirements shown in Table 5.5. In purging, there are 2 main parameters that can be controlled: purge interval and purge duration. The setup of the purging control system along with the purging model can be seen in Figure 5.11. The idea is to purge the impurities whilst maximizing the hydrogen utilization, which as calculated in Equation 5.4, with the molar reactant flow in Equation 5.5. Since the formula without integrals would calculate the instantaneous hydrogen utilization, which would be low during purging but then 100% otherwise, it is more useful to calculate an accumulated hydrogen utilization over the entire time using the integrals. Purge interval will be controlled by a feedforward scheduling law covered in Section 5.4.1, purge duration will be controlled by an integral threshold law in Section 5.4.2, and lastly the results will be shown in Section 5.4.3.

Table 5.5: Purging Optimization control subsystem requirements

ID	Requirement
CS-R6	The control system at startup shall purge anode before activating the load [27].
CS-R2	The control system shall optimize anode purging to remove impurities whilst maximizing hydrogen utilization.
CS-R1	The control system shall maintain the stacks' hydrogen pressure between 400–700 mbar.g.
CS-R11	The control system at shutdown shall purge anode after deactivating load [27].

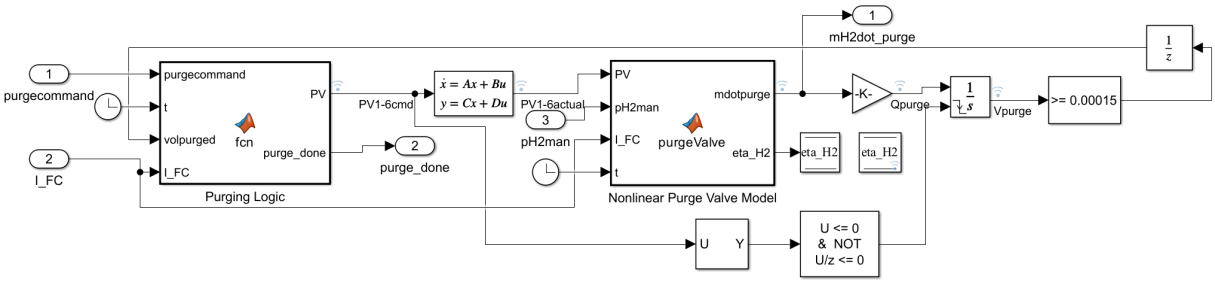

Figure 5.11: Purge controller setup

$$\eta_{H2}[\%] = \frac{\int_0^t \dot{n}_{reactant} dt}{\int_0^t (\dot{n}_{reactant} + \dot{n}_{purge}) dt} \tag{5.4}$$

$$\dot{n}_{reactant} = \frac{I_{FC} N_{FC}}{2F} \tag{5.5}$$

5.4.1. Feedforward Scheduling of Purge Interval

Table 5.6: Purge feedforward scheduling parameter values

Parameter	Value
$T_{ref}[s]$	60
I_{ref}[A]	16
T_{min}[s]	15
T_{max}[s]	180

In terms of determining the purge interval, looking at Equation 5.4, it is apparent that decreasing the freqeuncy of purges, or using large purge intervals will lead to maximizing hydrogen utilization. Purging should only occur, when enough impurities build up. The publicly unavailable stack manual gives some reference current and temperature data on maximum purge intervals based on requested current, which can be seen in Table 5.6. Using this recommended reference linearly, the purge intervals can be calculated with Equation 5.6 along with its arbitrary bounds.

$$T_{\text{interval}} = T_{\text{ref}} \frac{I_{\text{ref}}}{I_{FC}} \qquad T_{min} \leq T_{\text{interval}} \leq T_{max} \tag{5.6}$$

5.4.2. Integral Threshold Control of Purge Duration

Secondly, the purge duration needs to be controlled, and this can be done with an Integral Threshold controller. It was found from literature, that highest energy efficiency for dead ended anode is achieved when purging $1/4^{th}$ of the anode stack volume [25]. This total target volume for all stacks can be calculated with Equation 5.8, where V_{stack} is $10^{-4}m^3$, and the volume being purged can be calculated with Equation 5.7 where the mass flow is known and ρ_{H2} is 0.089 $\frac{kg}{m^3}$. With this, the idea is that once the purge interval is determined, and that time has passed, the Purging Logic in Figure 5.11 opens all 6 purge valves, and once the target purge volume is reached as seen in Equation 5.8, the purge valves are commanded to close again. Notably, since the $V_{H2purged}$ needs to be recalculated for each purge, the integral is with a $d\tau$ since the integral is made to reset to 0 each time the purge valves are closed. With this, the hydrogen utilization simply needs to be monitored to ensure that it is above a 97% threshold, which is recommended by the manual.

$$V_{\text{H2purged}}(t) = \int_0^t Q_{\text{H2purge}}(\tau)d\tau = \int_0^t \frac{\dot{m}_{\text{H2purge}}(\tau)}{\rho_{H2}}d\tau \tag{5.7}$$

$$V_{\text{H2target}} = \frac{V_{stack}}{4}6, \quad V_{\text{H2purged}} \geq V_{\text{H2target}} \tag{5.8}$$

5.4.3. Purge Controller Results

Now that both of the controllers have been designed and implemented, it is time to look at the results after a few runs of controller testing. Firstly, the results of an entire run ramping up to a minimum power of 4A can be seen in Figure 5.12. Here, the anode clean sequence consisted of 3 purges with a fixed interval of 1s, and purge duration of 0.53s. This was mainly constrained by the purging required to empty the anode manifold at the shutdown, and the same anode clean sequence is used for startup too. The hydrogen pressure remains within range during these anode clean sequences. Thereafter, the periodic purging begins, and due to the low 4A minimum power current, purge intervals have a maximum width of 180s, and each commanded purge duration lasts approximately 0.27s at a constant 550mbar.g pressure. The hydrogen utilization found at the end of the run is 99.4%, which is well above the 97% threshold, and thus it has been maximized. This entire run verifies all the purge control requirements defined in Table 5.5.

Secondly, ramping up to a maximum possible power of 31A can be seen in Figure 5.13. Here it can be seen that the temperature is at the limit with a near maximum fan power, and thus is still constraining to maximum possible current. After the startup anode clean sequence, the periodic purge begins, and here it can be seen that the purge intervals are a lot shorter, as they scale with the requested current. Here the average purge interval is about 30s, and each purge duration is still 0.27s. The reason the purge duration stays the same despite changing current, is because the anode pressure remains 550mbar.g in both scenarios. Similar to before, all purging ensures the hydrogen pressures stay within the range, and the hydrogen utilization here is also 99.4%, complying with all requirements.

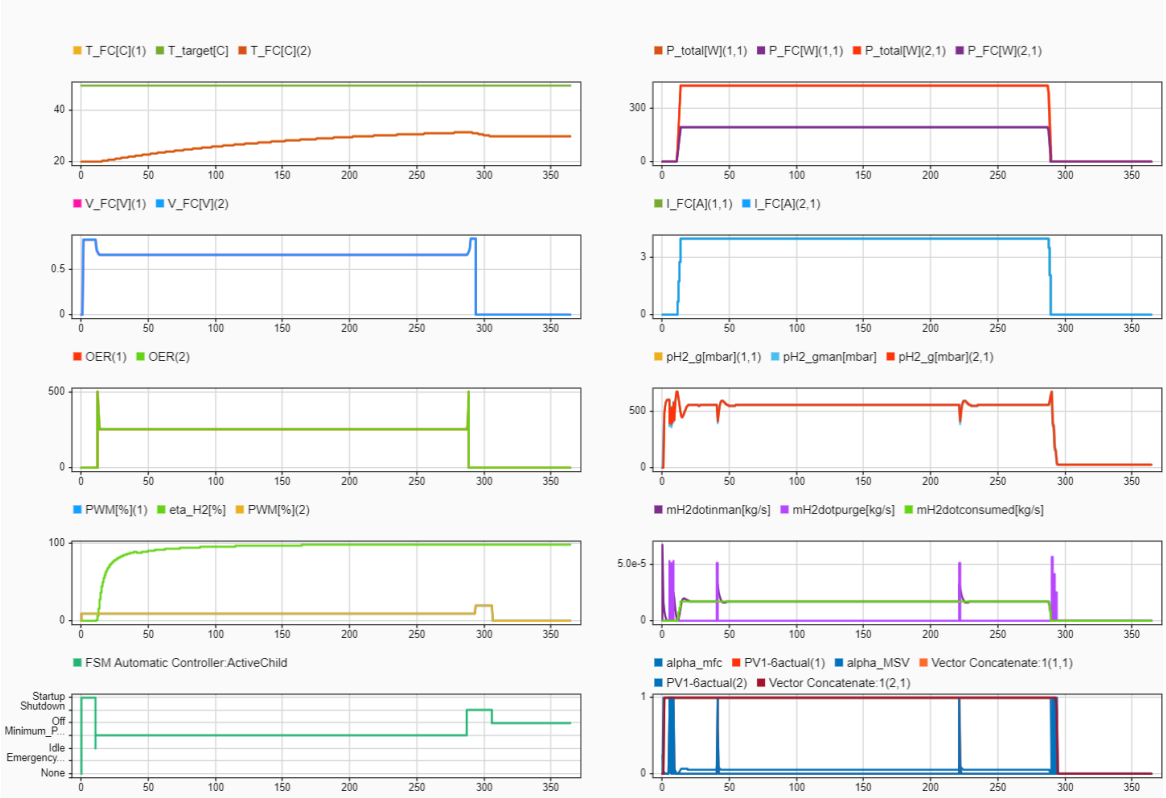

Figure 5.12: Purging controller entire run response at 4A requested current

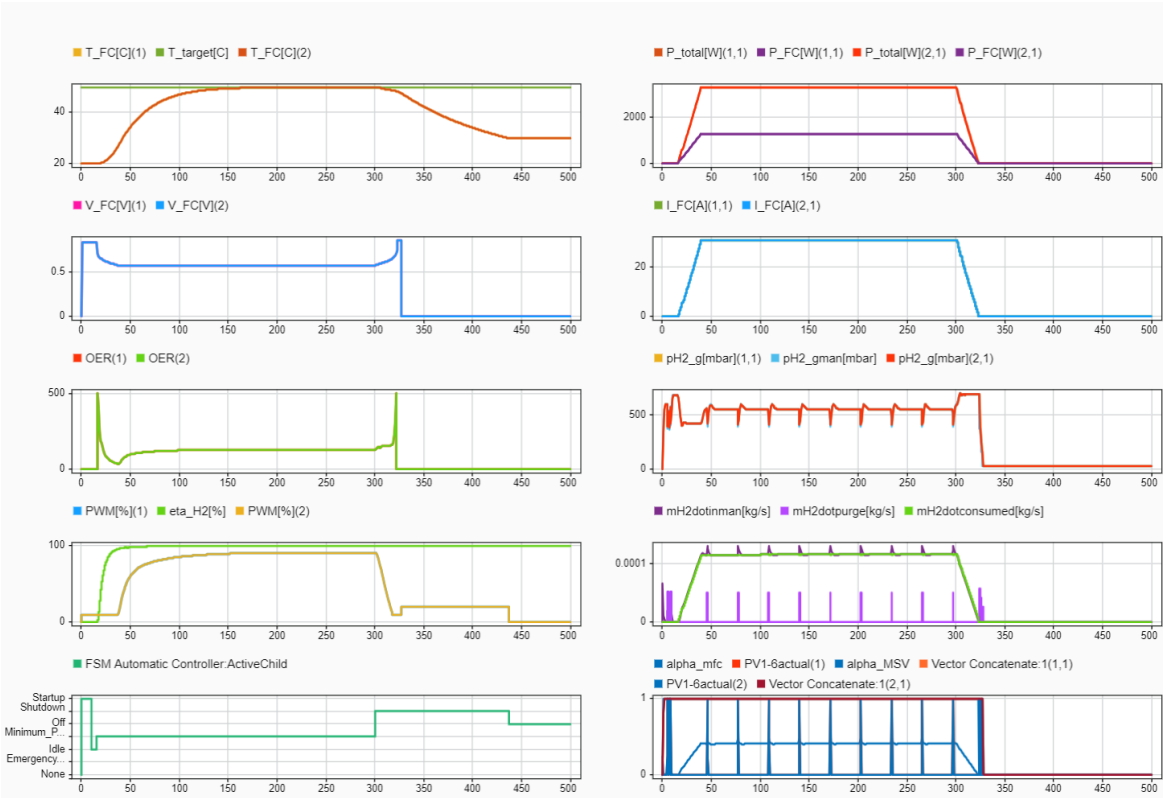

Figure 5.13: Purging controller entire run response at 31A requested current

5.5. Safety Requirements Verification

Now that all the control reliability requirements have been verified in the previous sections, it is important to consider and test for all the safety requirements by running the entire model including FSM and subsystem models with its controllers. Safety requirements were previously defined in Table 2.4 for hazardous events that could occur during operation, so that the control system initiates an emergency shutdown. There are 4 main hazardous events that need to be modelled, and an appropriate emergency shutdown response needs to be taken by the FSM. As of now, the emergency shutdown state was not fully developed due to the lack of physical models and controllers. However, now that this has been fully developed, emergency shutdown sequences will be created for each of the hazardous events, namely hydrogen leakage in Section 5.5.1, overheating in Section 5.5.2, OCV under and over voltage in Section 5.5.3 and loaded under voltage in Section 5.5.4.

5.5.1. Hydrogen Leakage Response

Firstly, the hydrogen leakage needs to be modelled, and the emergency shutdown response analyzed against the safety requirements. To model the hydrogen leakage, a model sensor sends the hydrogen leakage values in ppm to the FSM (which is similar to how a real sensor would be utilized), and as per the safety requirement if its $\geq$4000ppm the emergency shutdown needs to be initiated. So the model sensor starts at 0, and once the hydrogen pressure in manifold starts rising, hydrogen leakage ramps to a value of 1000 ppm/s to demonstrate a moderate leak in the manifold as in Figure 5.14. As seen from the FSM output, the system entered the Startup state for the first 4.5 seconds, where it is transitioning inside its sub states to ensure system is ready. Here the fan is running at 10% and the voltage and hydrogen pressure is also being built up. As soon as the hydrogen leakage hits 4000ppm, hydrogen leakage hazard (H3) is detected, forcing the system to enter the Emergency Shutdown state. The main supply valve is closed and the anode purge clean sequence is initiated to purge the hydrogen safely to environment, to prevent buildup of leaked hydrogen. Here it is critical, to design the purging exhaust to purge to an open environment, instead of a closed volume. This causes a decrease in pressure and voltage, after which supply valves are all closed and system enters the Off state. In total, it remained in the Emergency Shutdown state for 5s before switching fully Off, and it took 3.5s for the anode to be depressurized since the hazard was detected, as the hydrogen leakage flattens at around 7000ppm at 8s. Based on this result, the CS-S1 safety requirement is verified for an appropriate emergency shutdown initiation and response.

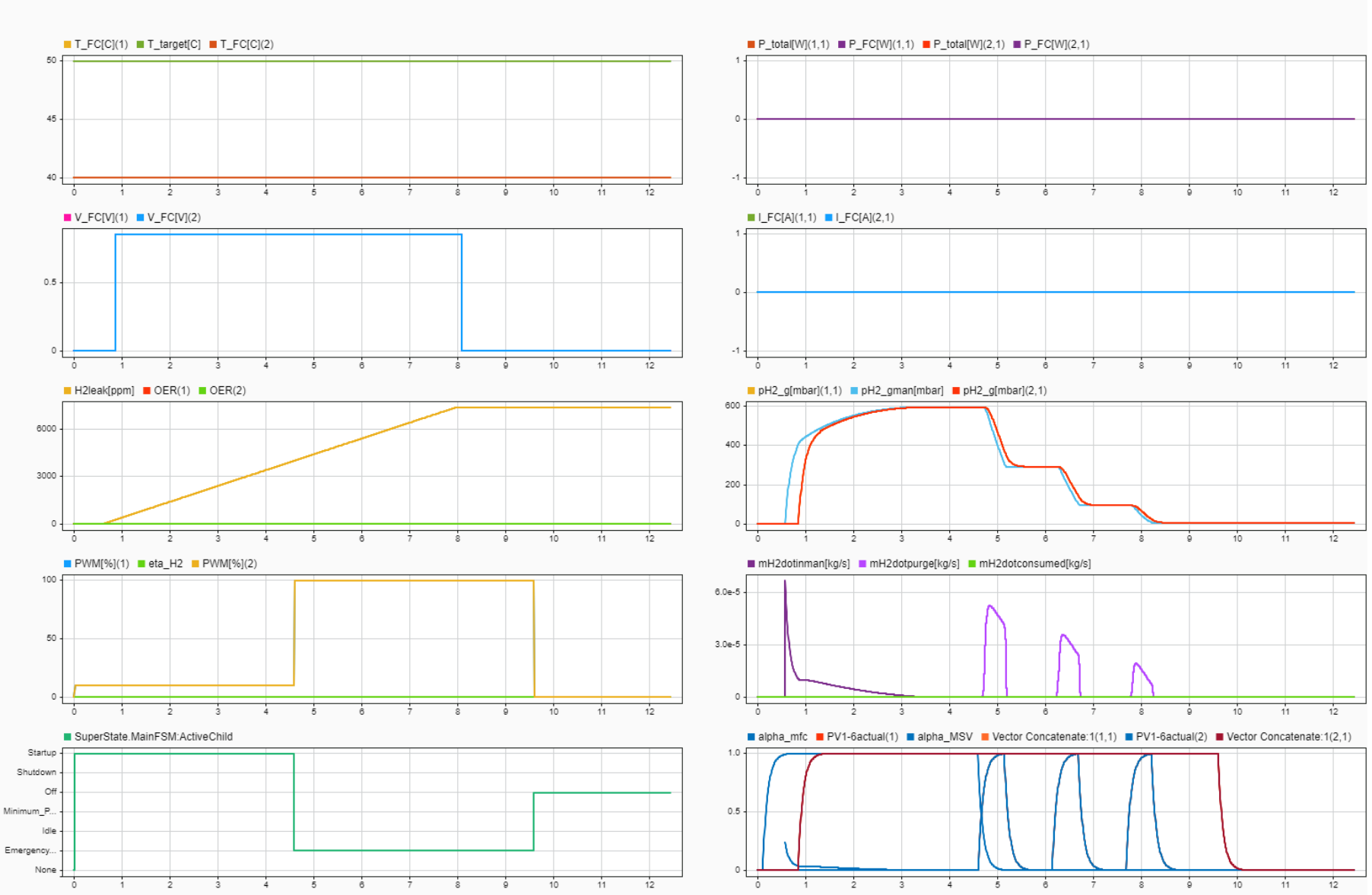

Figure 5.14: Response to constant hydrogen leakage of 4000ppm from model sensor

5.5.2. Overheating Response

The overheating was modelled by setting ambient temperature to $40°C$ and ramping up to 31A, causing temperature to hit $70°C$ at around 220s. This hits the overheating limit of $70°C$, and as seen in Figure 5.15, the emergency shutdown was immediately initiated. The emergency shutdown procedure is the exact same as before, so thus firstly the main hydrogen supply valve was closed, after which current was immediately brought to zero, fans were set to max 100% power and the shutdown anode clean sequence was initiated to depressurize the anode. The stack temperatures was lowered to $50°C$ from $70°C$ with the help of 100% fan PWM, taking around 40s. Thereafter, FSM enters the Off state where everything is set to 0 and system is at rest. These results verify the overheating safety requirement CS-S2.

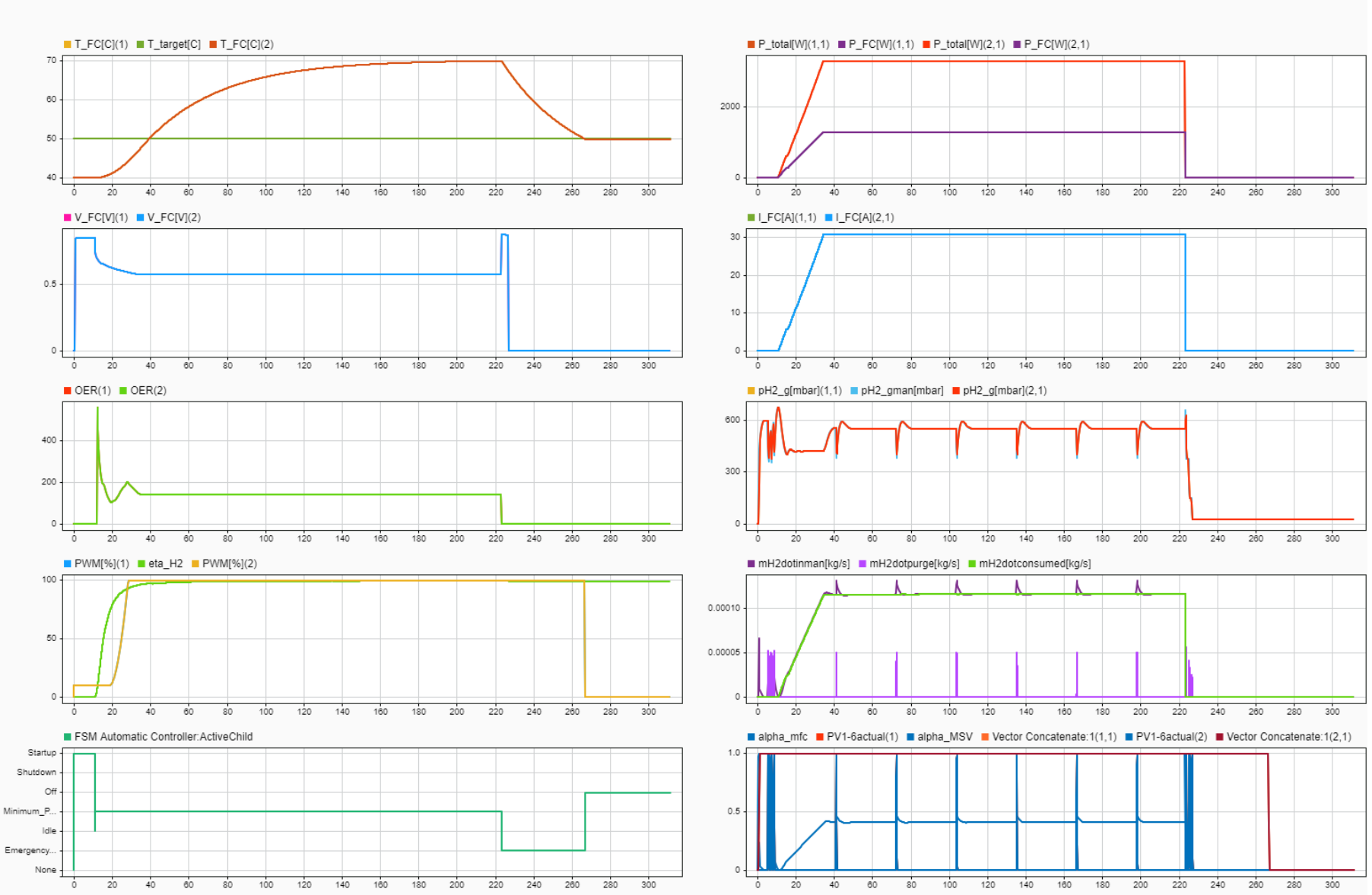

Figure 5.15: Response to stack temperature suddenly overheating to $70°C$

5.5.3. OCV Under and Overvoltage Response

Now the OCV safety requirements need to be tested for under and over voltage. OCV over voltage can cause high potential spikes, and under voltage would mean cells are damaged and not working properly so power should not be drawn. The manual only defines the under voltage as a hazard, therefore only this is shown in Figure 5.16 with a cell voltage of 0.65V, and notably over voltage produced a similar response. It can be seen that after 10s in the Startup state, Emergency Shutdown was immediately entered lasting 5s. With the same emergency shutdown sequence as before, the fans were set to maximum power and the anode was depressurized to bring the voltage back down to 0, as system was never ready to start drawing power. This is an appropriate and safe response which verifies the CS-S3 OCV under voltage safety requirement.

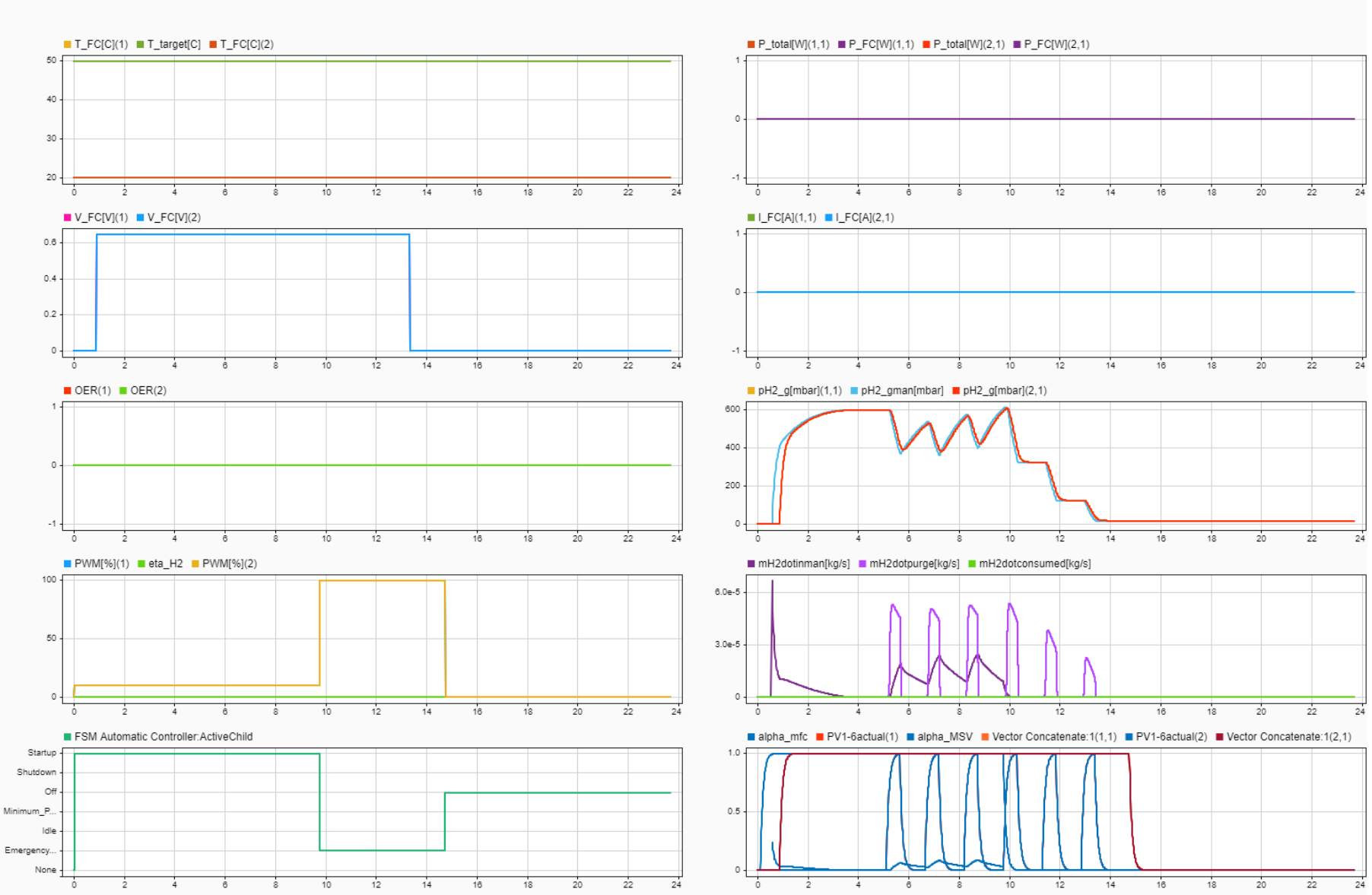

Figure 5.16: Response to OCV under voltage of 0.65V

5.5.4. Loaded Under Voltage Response

Lastly, the under voltage when loaded requirement needs to be tested, and here the cell voltage is purposefully dipped to 0.49V at around 37s as seen in Figure 5.17. Up until this point, the stacks have been loaded to a current of 31A. And as per the requirement, as the cell voltages remain <0.5V for >5s, at around 42s the Emergency Shutdown state is entered. Here, the main hydrogen supply valve was closed, current was immediately brought to 0 and fans were set to 100%. Then the anode was successfully depressurized with the anode purge, and it took approximately 10s to decrease temperature below $30°C$ and to exit out of Emergency Shutdown to Off state. The loaded under voltage could also occur whilst ramping up, however the current NRG prevents this and can regulate the current. It can also be seen, that for the first 5s of loaded under voltage at a continuous 31 current, the NRG was working to lower the current to push voltage higher, however the voltage was modelled to be a fixed 0.49V here to test the emergency shutdown. Additionally, for the real case purging is done to flush out the impurities to keep the cell voltage high. Therefore, the under voltage may not occur the way it is modelled here, but what's important is that the system commences a safe emergency verifying CS-S4.

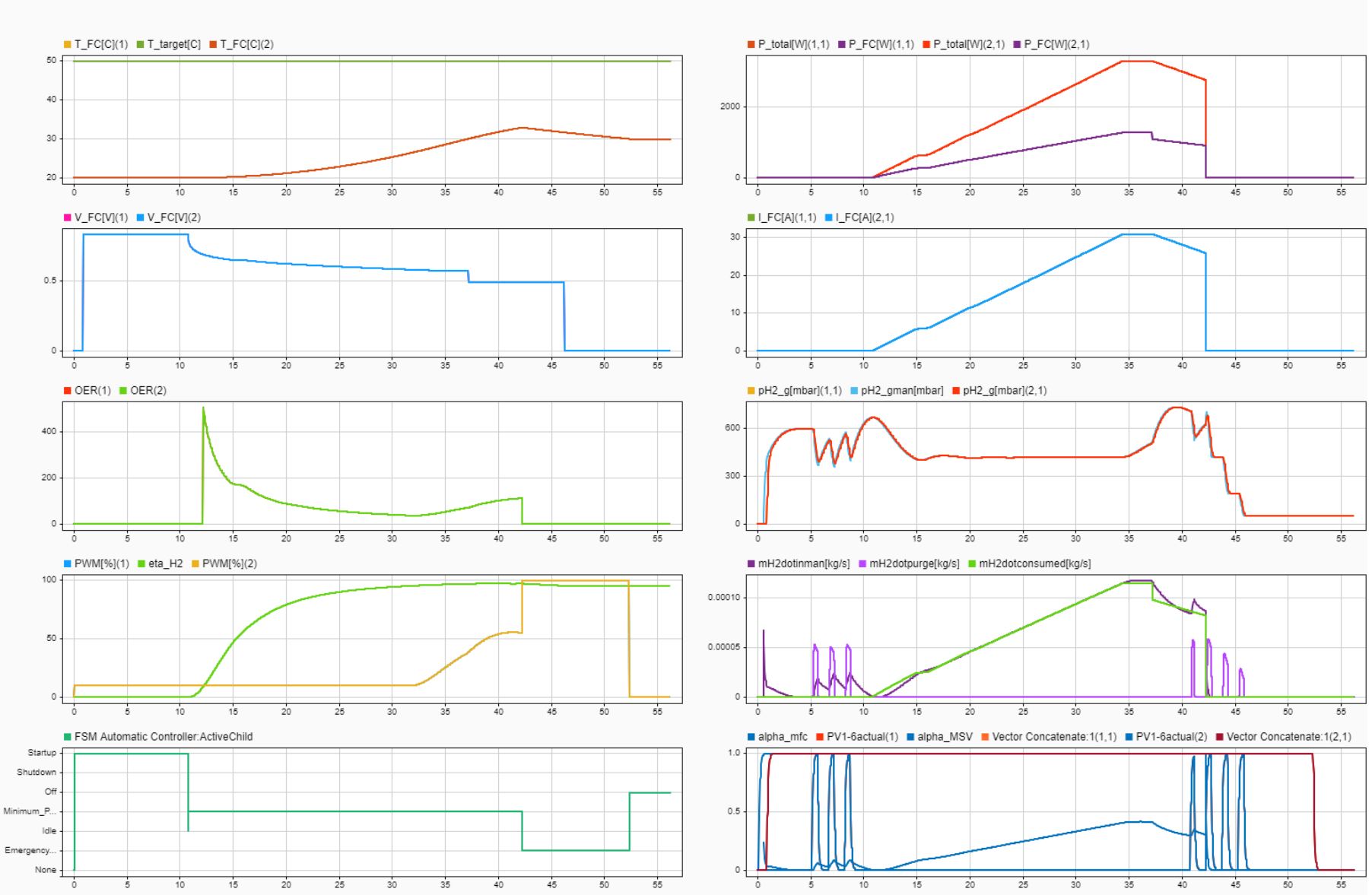

Figure 5.17: Response to loaded under-voltage of 0.49V for >5s

6

Final Results

This chapter serves as a synthesis of the key results developed from this thesis. The final results of this thesis can be summarized within the two categories of the research activities that were carried out. Hence, the results of the modelling is summarized in Section 6.1, whereas the results for the controller design is summarized in Section 6.2.

6.1. Physical Models and Validation

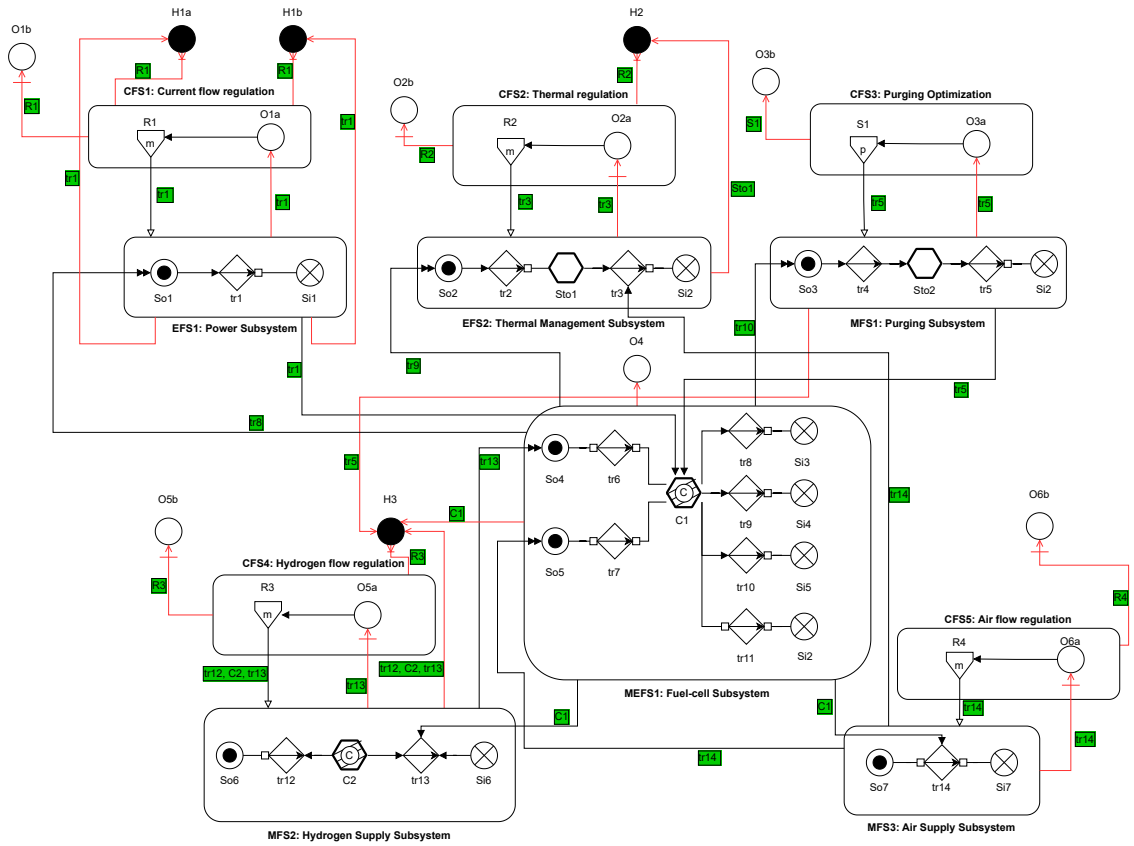

Figure 6.1: Total Multi-level Flow Model including mass, energy and control functions with their objectives and hazards

In order to develop a control system that can automate the Imponator, a model needed to be designed. There are several types of existing models, however the ones that are most relevant for this thesis were

control-oriented models. Since reliability and safety were core principles that were desired in automating the startup and shutdown sequences, it was decided to implement a top-down modelling approach. Firstly, it was decided to build a conceptual-level Multi-level Flow Model for the Imponator as seen in Figure 6.1, to describe the energy and mass flows that exist within the system. This way functional groupings were made, which were described as subsystems. Additionally, control functions (either existing or desired) were also defined for some of the subsystems, and hazardous events were identified. Most importantly, the causes of hazardous events were identified, and therefore requirements for the respective control subsystems were determined. This allowed to visualize all the interactions between the functional subsystems, as well as their goals and hazards, which help when creating physical and control subsystems.

Secondly, the physical subsystems needed to be designed. In the research process, firstly a preliminary FSM was made to understand the inputs and outputs needed from the physical subsystems, but the results of the FSM will be discussed in Section 6.2 to keep the focus on the models. From the MFM, 6 functional subsystems were identified, and hence these were modelled in Simulink as seen in Figure 6.2. The layout is kept the same as the MFM to define key input and output interactions. The Air Supply (AS) and Hydrogen Supply Subsystems (HSS) are the 2 inputs for the Fuel Cell Subsystem (FCS), which has 3 outputs of Power (PWS), Thermal Management (TMS) and Purging Subsystem (PS). For these, the temperature (TMS) and fuel cell voltage (FCS) models were taken from literature about control-oriented models. Whereas the Air Supply Subsystem was built based on fan manuals, and Purging Subsystem based on purge valve manuals. The Power and Hydrogen Supply Subsystems were designed from physical understanding and the stack manual, where HSS is the most complex accounting for several valve dynamics.

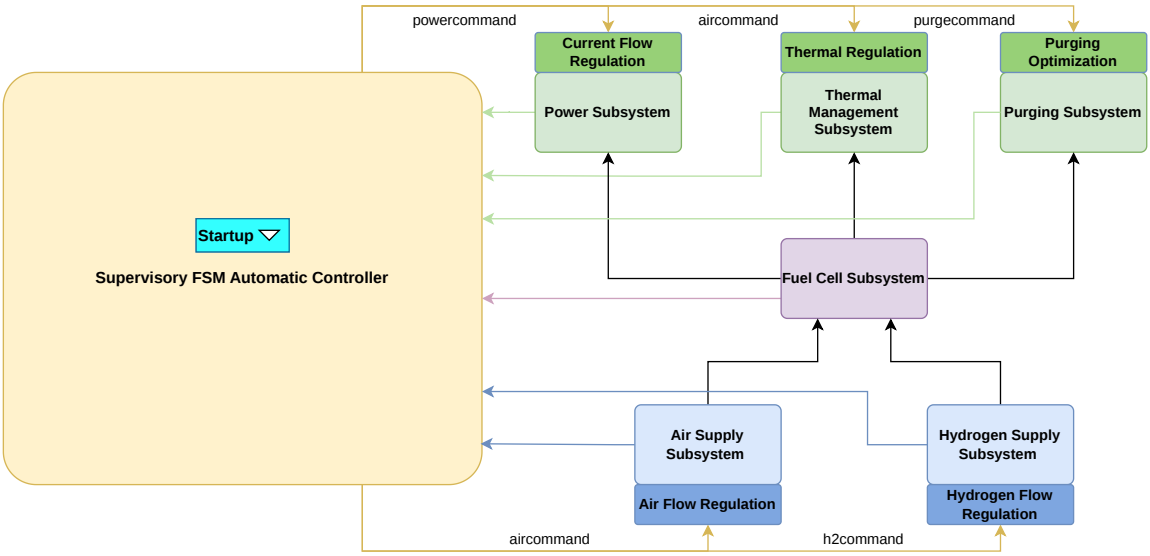

Figure 6.2: Simulink diagram with FSM and 6 physical subsystems integrated (Simulink Figure A.1)

Validation analysis was performed on these physical models based on the experimental data that was available, and their results can be seen in Table 6.1. The temperature covers TMS and AS, voltage covers FCS, and hydrogen pressure covers HSS, PS as well as PWS (due to consumption). The metrics show that the voltage model performs the best, whilst the temperature model is also acceptable. The temperature model has a high MBE for its range, and this could be due to experimental data having an environmental wind influence. So it is left as a recommendation, to do parameter estimations and validation from an experiment where wind does not play a role. The hydrogen pressure model has a high RMSE for its range, and this has to do with the MFC model fidelity, as little information was known about its valve dynamics and its sensor data was not available. This leads to a recommendation, to gather data from the MFC so that the valve behavior of mass flows could be validated directly. Air Supply Subsystem is the only one

that could not be directly validated due to fan sensor data unavailability, however the manual plots are assumed reliable in Figure 3.9 and Figure 3.10.

Table 6.1: Model performance metrics comparison

Metric	Temperature	Voltage	H_2 Pressure
$R^2[-]$	0.81	0.93	0.81
RMSE	1.18 °C	1.60 V	62.24 mbar.g
MBE	-0.92 °C	-0.28 V	0.49 mbar.g

6.2. Supervisory FSM and Subsystem Controllers

Now that the physical models were designed and found to be acceptable, the controller design was commenced. This is split into 2 types of controllers, a supervisory FSM automatic controller in Section 6.2.1 and low-level subsystem controllers in Section 6.2.2.

6.2.1. Role of FSM

The FSM is a supervisory automatic controller designed to automatically switch states and sub states in order to perform a startup and shutdown sequence for the Imponator. It is the highest level controller which determines operation modes and sequentially activates lower-level controllers as seen in Figure 6.3, Figure 6.4 and Table 6.2, and it is meant to supervise the physical models and its subsystem controllers. For example, within the Startup state, it determines the modes of the 5 controllable subsystems, and sends these commands to their respective controllers.

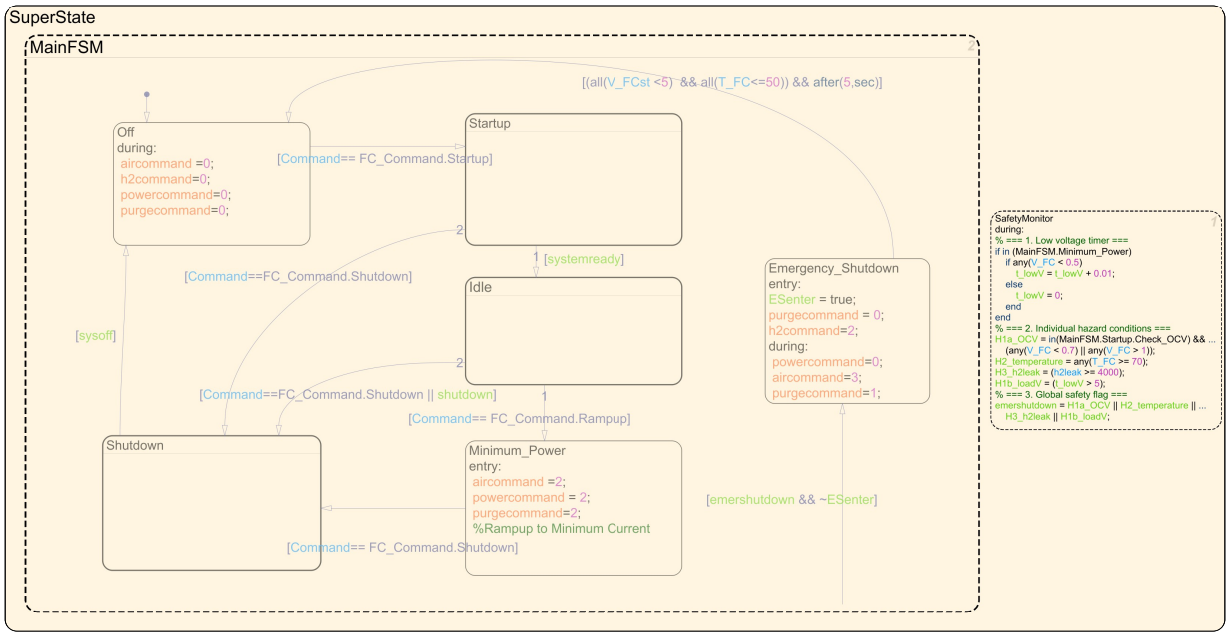

Figure 6.3: Finite State Machine Chart of the Imponator System

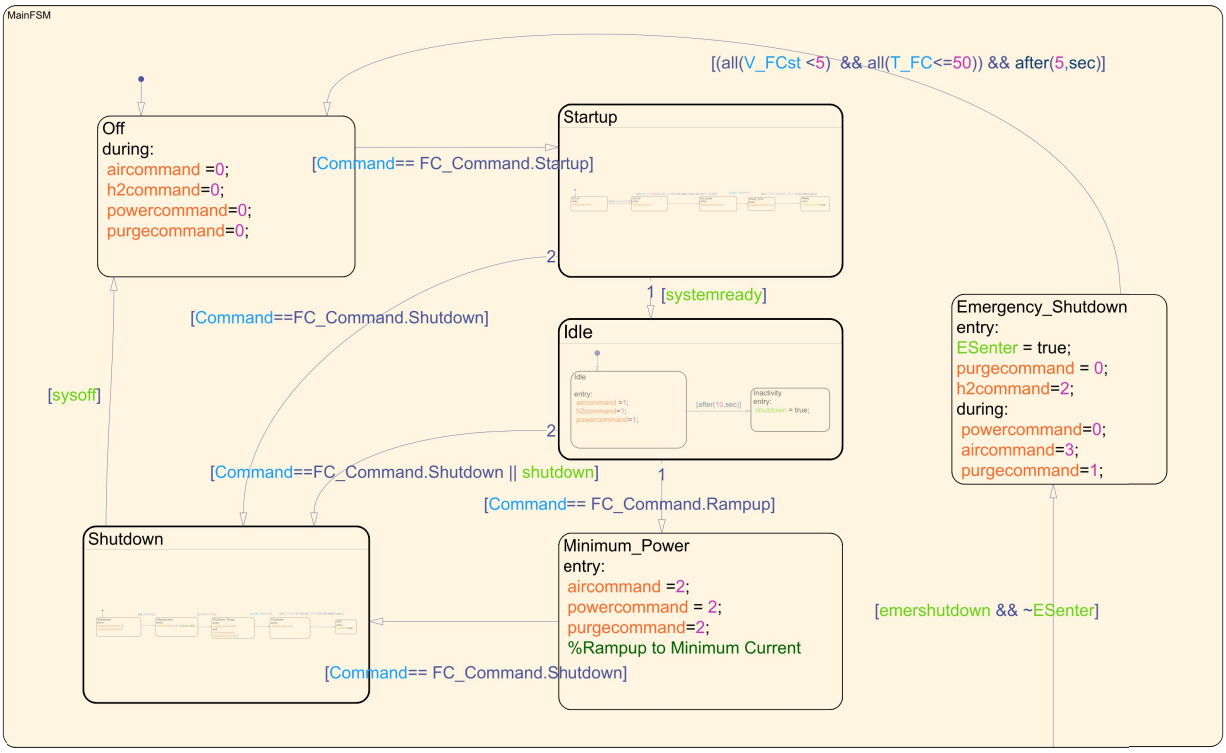

Figure 6.4: Main FSM Chart of the Imponator System

Table 6.2: Subsystem operation modes

Mode	Air Supply & Thermal Management Subsystem [aircommand]	Hydrogen Supply Subsystem [h2command]	Power Subsystem [powercommand]	Purging Subsystem [purgecommand]
0	Fans OFF	All H_2 valves CLOSED	Load switch OPEN	Purge valves CLOSED
1	Fans ON at fixed 10% for minimum OER	PRV ramp to STARTUP pressure	Load switch OPEN, OCV	Purge valves anode clean sequence
2	Fans regulated to also maintain T $\leq$50°C	Close main supply valve	Load switch CLOSED, rampup to 4A current	Periodic purge
3	Fans ON at MAX 100% for cooldown		Rampdown to 0A current, load switch OPENED	

Most notably, the FSM also has a Safety Monitor state running in parallel which detects all the 4 main hazards identified in MFM, which are formulated as control safety requirements in Table 6.3. The FSM here is responsible for meeting these requirements by design, as the Safety Monitor detects the hazards, and once detected it forces the system to enter Emergency Shutdown where system is turned Off as fast as safely possible. The results that verify these safety requirements can be seen in Section 5.5.1 for CS-S1 hydrogen leakage, Figure 6.6 for CS-S2 overheating, Figure 6.7 for CS-S3 OCV under voltage, and Figure 6.8 for CS-S4 loaded under voltage. Out of these the hydrogen detection for CS-S1 is not possible in the current real Imponator, but since its a hazard, it is given as an overall improvement for the real system.

Table 6.3: Safety requirements for the control system

ID	Requirement
CS-S1	The control system shall initiate emergency shutdown if the detected hydrogen leakage is ≥4000ppm [28].
CS-S2	The control system shall initiate emergency shutdown if stack core temperature ≥ 70°C.
CS-S3	The control system shall initiate emergency shutdown if unloaded OCV is <0.7V or >1V.
CS-S4	The control system shall initiate emergency shutdown if loaded cell voltage is <0.5V for >5s.

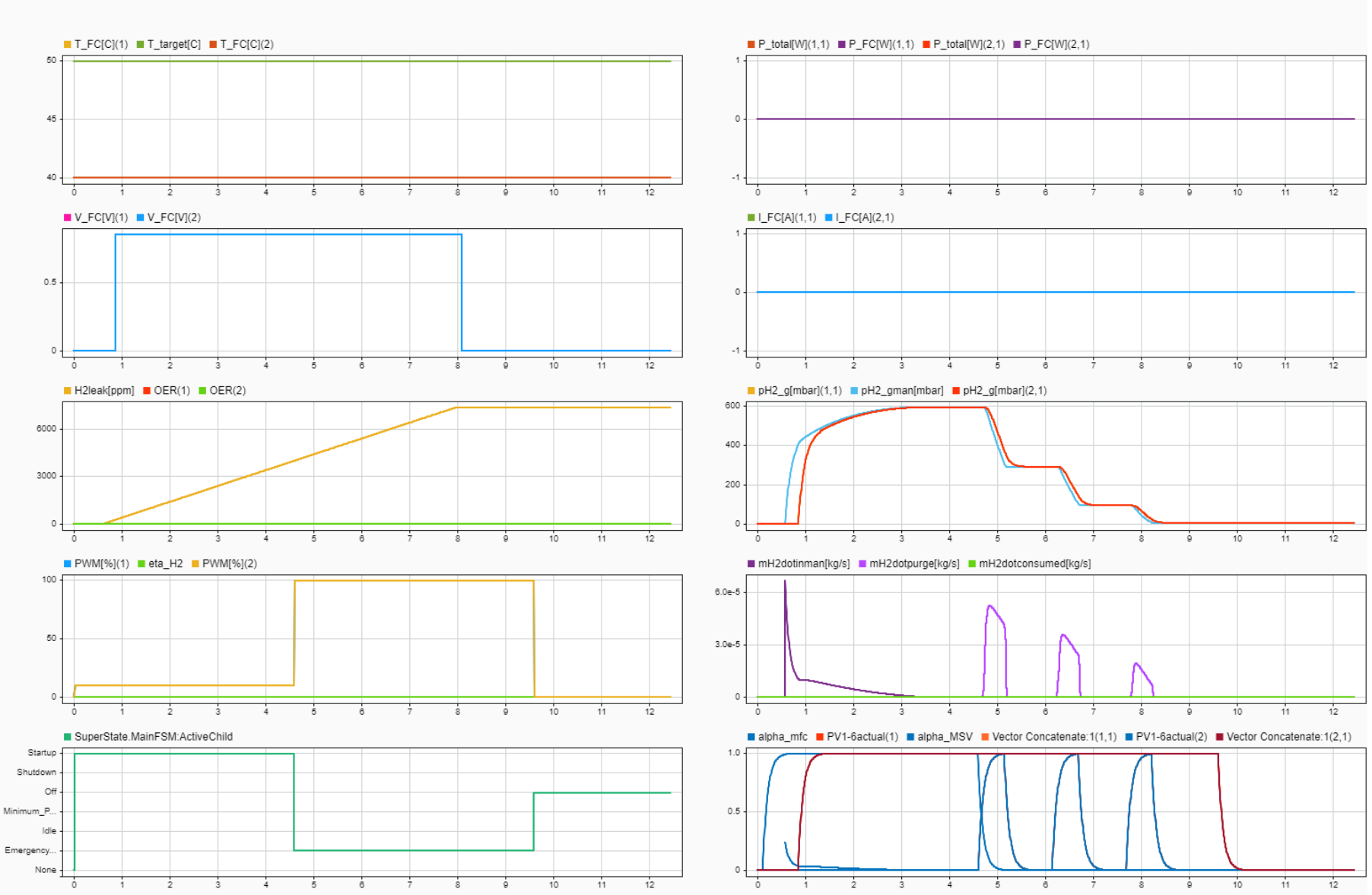

Figure 6.5: Response to ramping hydrogen leakage of 4000 ppm from model sensor

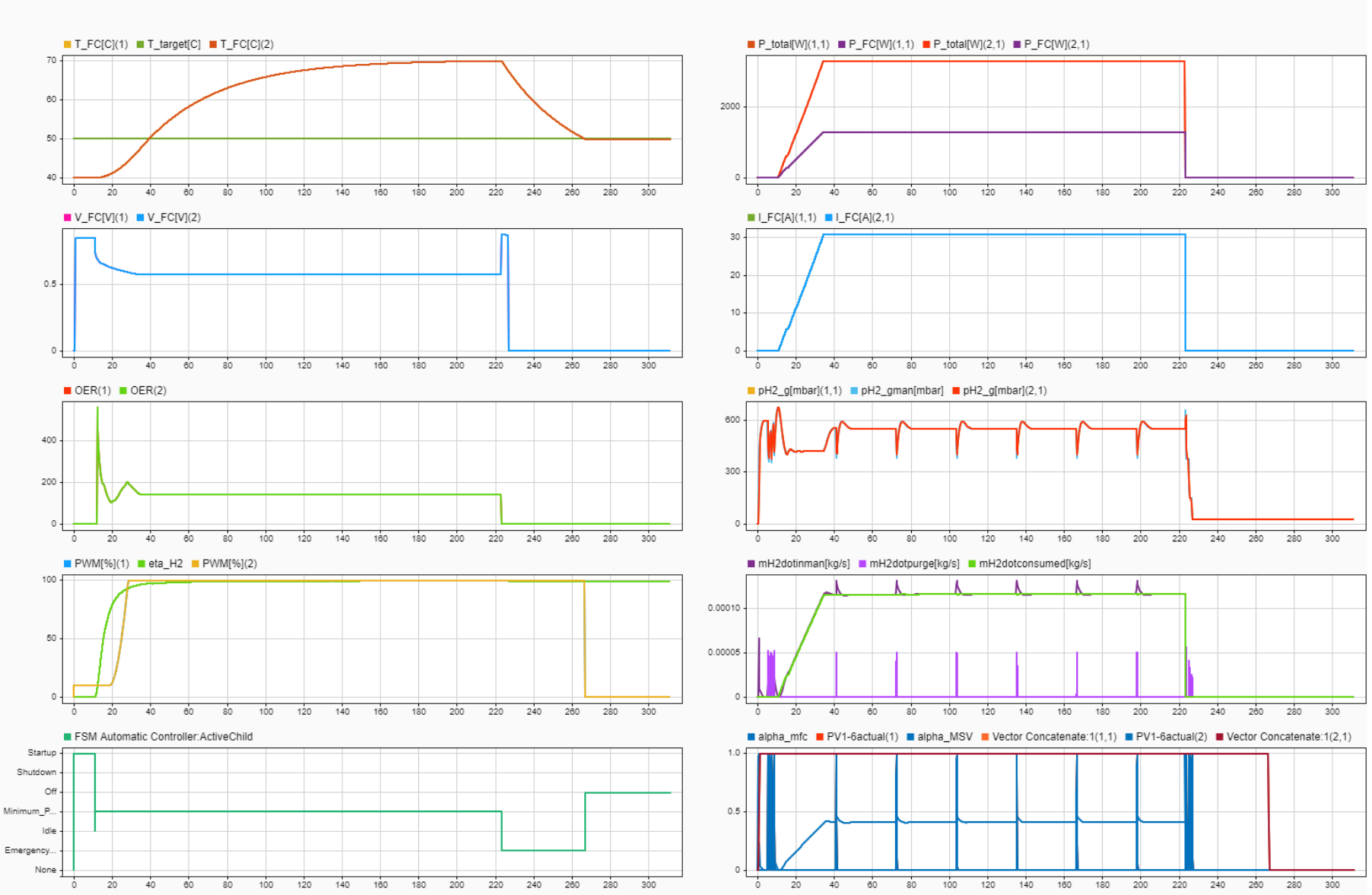

Figure 6.6: Response to stack temperature overheating to $70°$C

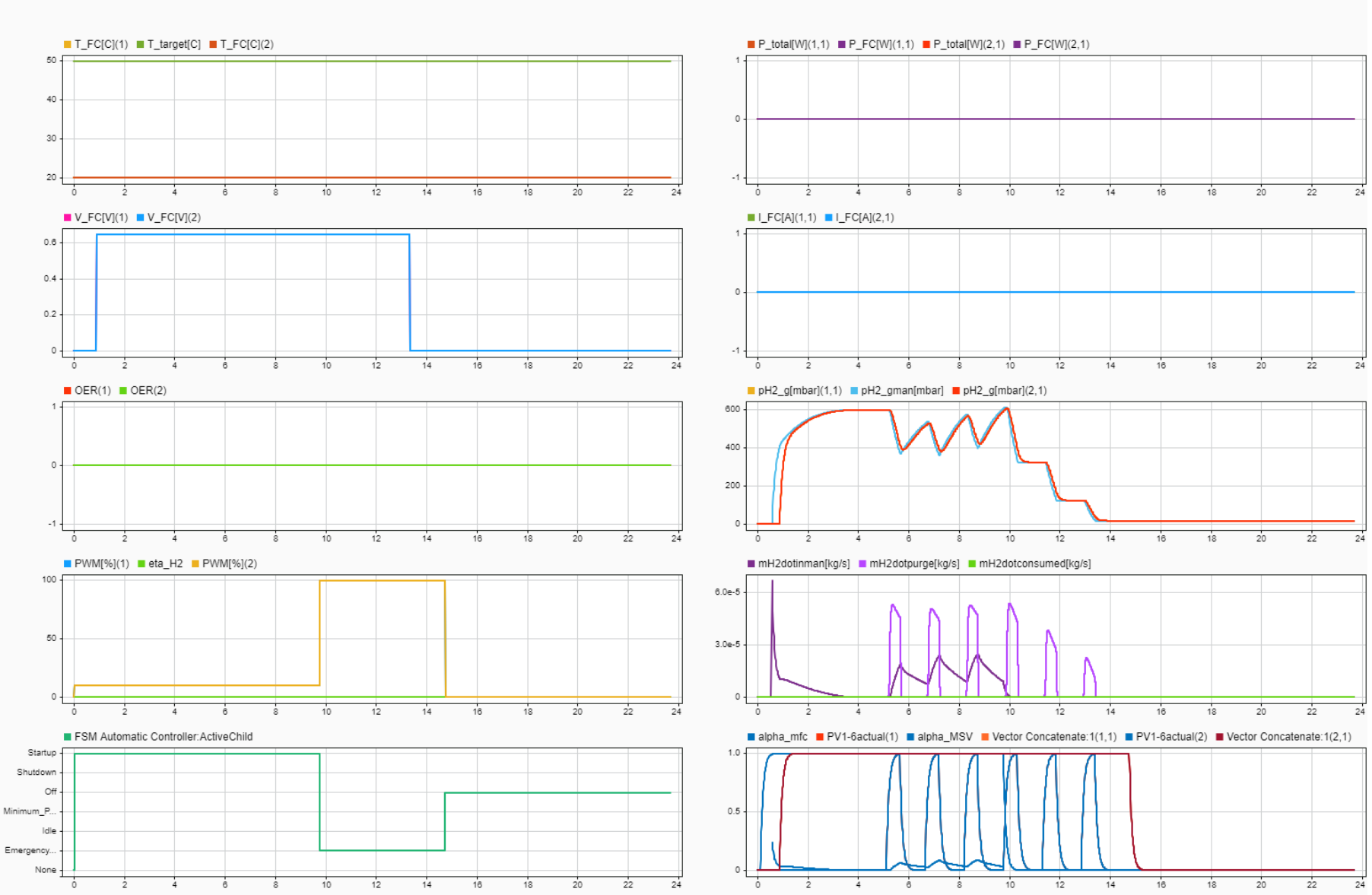

Figure 6.7: Response to OCV under voltage of 0.65V

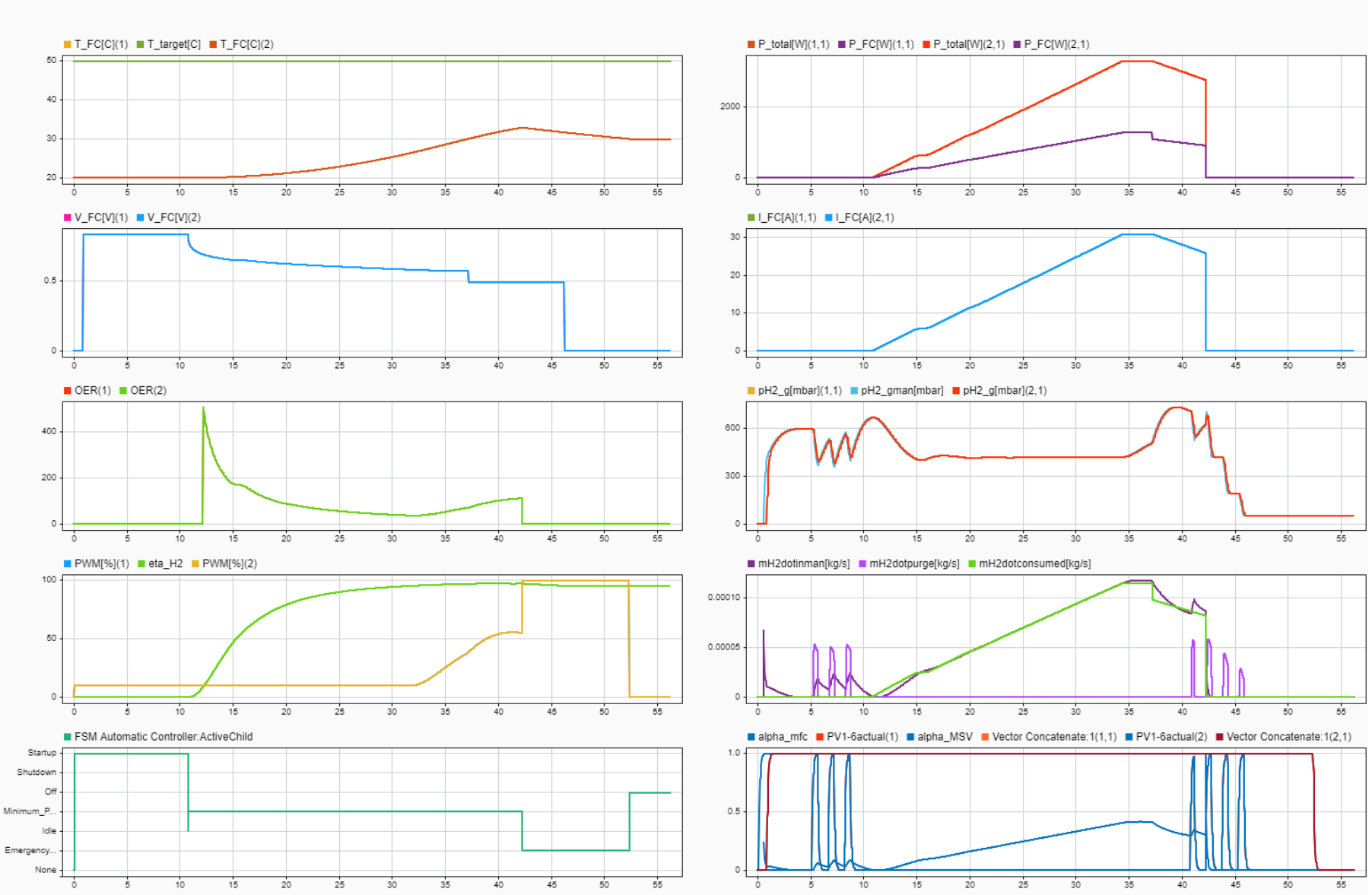

Figure 6.8: Response to loaded under-voltage of 0.49V for > 5s

6.2.2. Role of Subsystem Controllers

The FSM was responsible for determining the sequence of actions, however the subsystem controllers are responsible to carry out the action itself and report back to FSM. Mainly, they are responsible to achieve the control system design reliability requirements which can be seen in Table 6.4. These were formulated by understanding the existing Imponator system, reading literature on safe and reliable operation of fuel-cells and were iterative updated during modelling. Besides switching valves on and off, there were 3 main subsystem controllers that were developed based on the validated physical models. A temperature PID controller, current Nonlinear Reference Governor, and purging controller were designed and tuned. Out of these, the purging controller was twofold, with the Feedforward Scheduling of the purge interval, and Integral Threshold control of the purge duration. Therefore, the control reliability requirements are categorized by these 3 controllers that achieve them in Table 6.4.

Table 6.4: Reliability requirements categorized by control subsystems

ID	Requirement
Air & Thermal Regulation - Temperature PID Controller	
CS-R3	The control system shall maintain oxygen excess ratios of ≥2 during operation [26].
CS-R4	The control system shall keep the stack temperatures $\leq 50\,^{\circ}$C during operation.
CS-R5	The control system shall keep temperature within $\pm 1\,^{\circ}$C of desired value at maximum possible power.
Current Flow Regulation - Current NRG	
CS-R1	The control system shall maintain the stacks' hydrogen pressure between 400–700 mbar.g.
CS-R7	The control system at startup shall minimize the time in OCV [27].
CS-R8	The control system at startup shall ramp-up the fuel-cell system to the minimum power.
CS-R9	The control system shall maintain cell voltage between 0.5 V and 0.92 V when loaded.
CS-R10	The control system shall keep stack current within ± 1 A of demanded current.
Purging Optimization - Purging Controller	
CS-R6	The control system at startup shall purge anode before activating the load [27].
CS-R2	The control system shall optimize anode purging to remove impurities whilst maximizing hydrogen utilization.
CS-R1	The control system shall maintain the stacks' hydrogen pressure between 400–700 mbar.g.
CS-R11	The control system at shutdown shall purge anode after deactivating load [27].

The final control-model results of the entire automated startup and shutdown run can be seen in Figure 6.9 for 4A minimum current and Figure 6.10 for 31A maximum possible current, where hydrogen utilization was 97.4%. As before, results for stack 1 and 2 are plotted to avoid congestion, since all 6 stacks have the same responses due to homogeneity assumption. These results verify all the control reliability requirements, and the control safety requirements are also integrated in the controls if a hazard occurs.

Figure 6.9 shows the model results from a startup and ramp up to a minimum 4A current for each of the 6 stacks. After the first 10s, the startup is completed and the FSM determines that system is ready to start pulling load and enters Idle state. This system readiness means that fans have started, supply valves opened, stacks pressurized within 400-700mbar.g and startup anode clean sequence with 3 purges completed. Then the user has 10s to give a Rampup or Shutdown command, otherwise the FSM enters Shutdown automatically due to inactivity to minimize the time in OCV to prevent stack degradation. Here, a Rampup command is issued which makes the stack currents ramp up to 4A with the NRG while abiding voltage and pressure constraints. As the current is ramped up, purging controller begins to determine purging intervals and durations, and temperature PID controller is activated to keep stack temperatures $\leq 50\,^{\circ}$C. Here, the minimum power achieved by combining all 6 stacks is 1.2kW, and after some time shutdown is commenced which safely ramps down power, depressurizes anode, and decreases the stack

temperatures to below $\leq 30\,^{\circ}$C in normal operation.

More interestingly, the results of the maximum possible 31A current limited by overheating is seen in Figure 6.10. It is important to note, that this is for $20\,^{\circ}$C ambient temperature, which affects how much cooling the fans can provide and the initial stack temperatures, both affecting what the maximum possible current would be. In these results, more dynamics of the system and especially the subsystem controllers can be seen. The temperature PID is seen to control the fan PWM to achieve the temperature target, current NRG controlling the ramp rate limited by hydrogen pressure range, and purging controller purging more frequently due to the higher current demand.

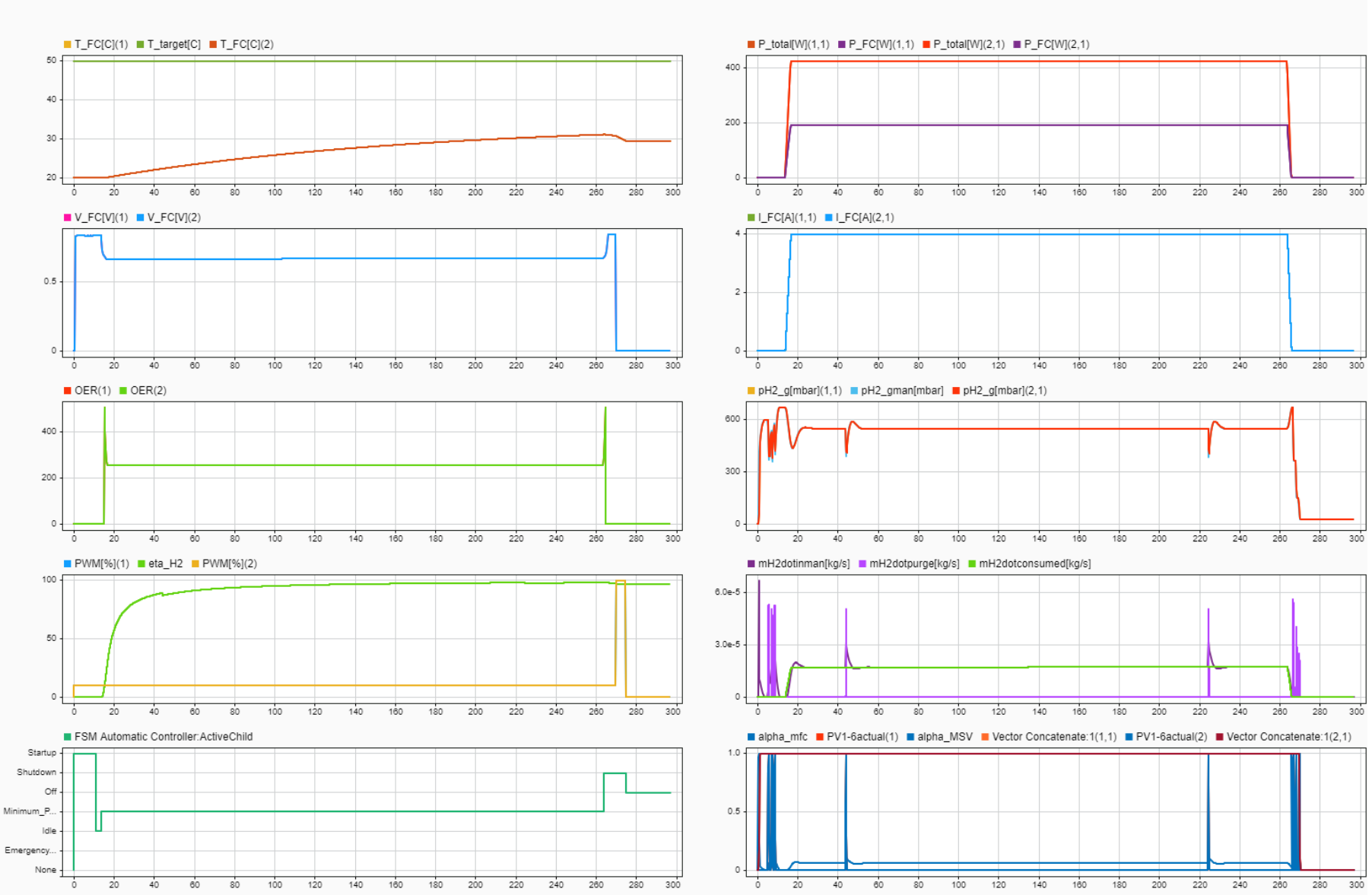

Figure 6.9: Final Imponator control-model results: 4A minimum current

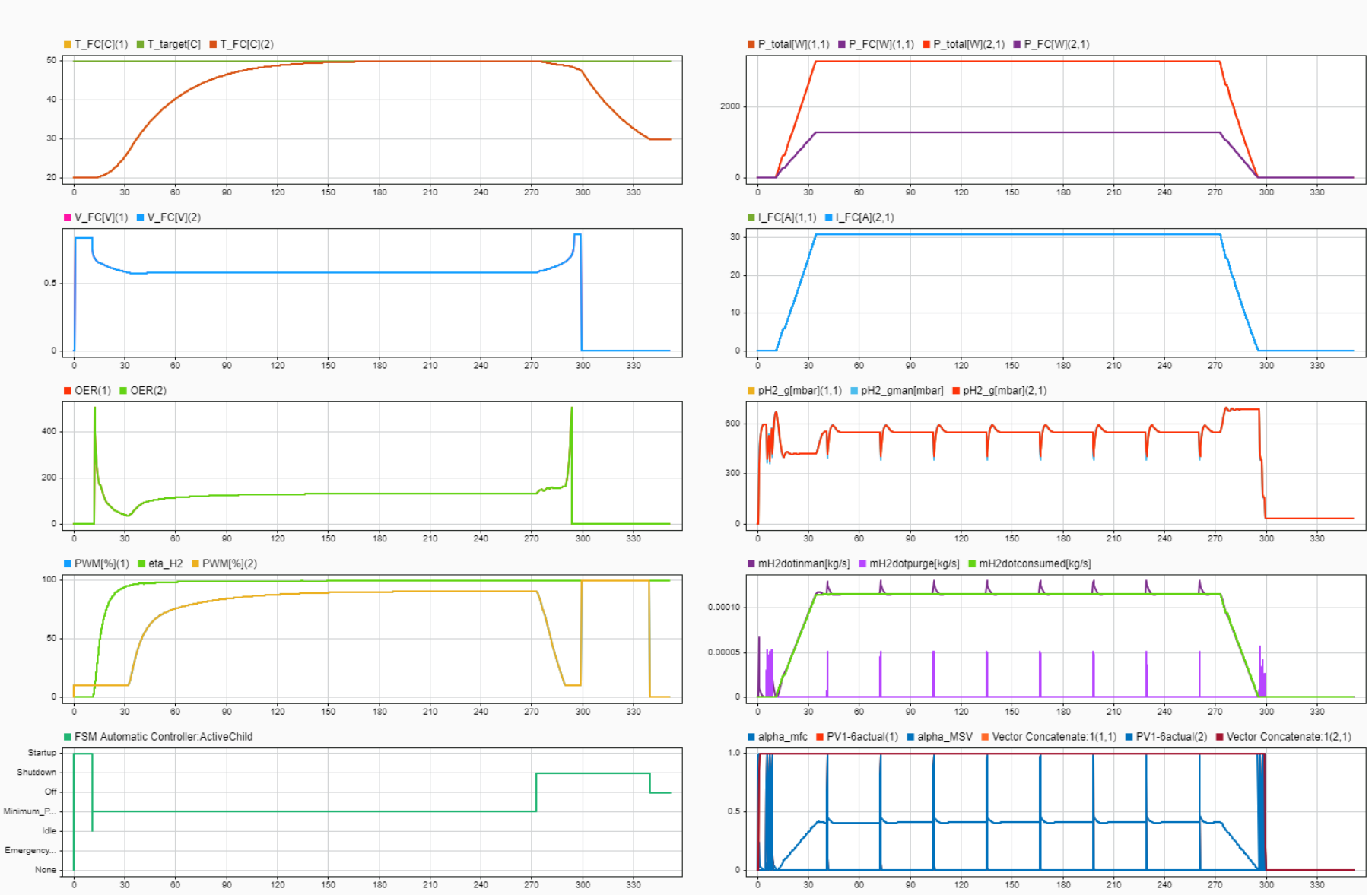

Figure 6.10: Final Imponator control-model results: 31A maximum possible current

7

Conclusion

The research objective RObj of this thesis was to automate the startup and shutdown of a multi-stack air-cooled open-cathode hydrogen fuel-cell propulsion system for aircraft, called the Imponator. The focus was to design the automation such that both startup and shutdown is safe and reliable, aimed to decrease the manual operation tasks and workload whilst testing with the experimental setup. This would transform the manual controls of the experimental setup to an automated supervisory control, closer to what would be expected in the control system of a hydrogen-electric aircraft.

Research Objective

To safely and reliably automate the startup and shutdown of a multi-stack air-cooled open-cathode hydrogen fuel-cell propulsion system for aircraft.

Firstly, a literature review was conducted in Chapter 2, through which the primary research and sub-research questions were iteratively developed, as seen in RQ. As a result of the literature review itself, the first two sub research questions were answered. From a control-theory approach, automation firstly requires designing a control-based model, and secondly automated control systems on this model. This is an efficient way to achieve RObj, by avoiding lab real-time control design.

Primary Research Question

How can startup and shutdown of a multi-stack air-cooled open-cathode hydrogen fuel-cell propulsion system for aircraft be automated in a safe and reliable way?
Sub research questions:

1. *How can the control system design requirements be defined to ensure safe and reliable start-up and shutdown procedures?*
2. *What are the most relevant control-oriented model types and controllers in automating the startup and shutdown?*
3. *How can the fuel-cell system be modelled, along with its startup and shutdown procedures?*
4. *How can the accuracy of the model to the real system be measured?*
5. *How can relevant model-based control systems be developed to automate the startup and shutdown?*

Relevant control-oriented model types and controllers were investigated , and it was determined to first design a high-level conceptual Multi-level Flow Model, to achieve a wholistic understanding of the safety and reliability needed for the system in Chapter 3. With the hazards and control functions from MFM, a supervisory Finite State Machine controller was designed to illustrate the required startup and shutdown sequences. The MFM also helped determine the physical subsystem models needed based on functional groupings, and determined the inputs and outputs needed from the physical models to keep them control-oriented. Thereafter, 6 subsystem physical models were built, namely Air Supply and Hydrogen Supply Subsystems as 2 inputs, Fuel Cell Subsystem as the center reaction model, and Power, Thermal

Management and Purging Subsystems as 3 outputs. In this way, the Imponator fuel-cell system was modelled specifically for the startup and shutdown sequencing answering the 3^{rd} sub-research question.

The operation of FSM with physical subsystems were verified to check appropriate subsystems mode commands and the switching of states within Chapter 4. Parameter estimation was conducted for TMS and FCS, and the entire system was validated in Chapter 4 to measure the accuracy of the model against real system. The validation metrics of R^2, RMSE, MBE showed that the voltage model performed quite well, temperature was acceptable but its MBE could be improved with better experimental data, and the hydrogen model (testing HSS, PS and PWS) had a high RMSE due to low MFC model fidelity, which could also be improved with MFC experimental data. These improvements were given as recommendations, but overall the model was deemed acceptable for subsystem controllers. This essentially answers the 4^{th} sub research question, as the accuracy was measured in terms of those 3 validation metrics.

Lastly, Chapter 5 develops the subsystem controllers needed to meet the control safety and reliability requirements, together with the supervisory FSM automatic controller to answer the 5^{th} sub research question. Here, a temperature PID controller, current NRG, and purging controller (Feedforward Interval Scheduler and Integral Threshold Duration controller) were developed. The combination of these subsystem controllers together with the FSM achieve the control safety and reliability requirements, giving the final control-model results of the entire thesis in Figure 7.1 for 4A minimum current and Figure 7.2 for 31A maximum possible current at $20\,^{\circ}$C ambient.

In conclusion, the results of this thesis answer all the research questions proposed in RQ and achieve the overall research objective RObj, safe and reliable automation of the startup and shutdown of the Imponator is achieved with the Simulink control-model. This is done by first building a control-model using MFM and physical models, validating it with experimental data, and building FSM supervisory and 3 subsystem controllers to achieve automation of the startup and shutdown of the Imponator.

This thesis has developed a methodology which is useful in transforming experimental hydrogen fuel-cell systems into operationally automated engine demonstrators and propulsion systems for aircraft. The impact of this work is that it defines a verified control-strategy with validated physical models, to achieve safe and reliable startup and shutdown automation, for the future of hydrogen-electric aircraft propulsion. This is a solution to the control challenge that is arising within hydrogen-electric aircraft, as it is an innovative research field, and requires a control-theory perspective and application. These control solutions are vital and are pioneering in bringing hydrogen fuel-cells to commercial aviation, which emerges as a strong energy-transition solution to achieve net-zero emissions in aviation. Lastly, with this framework, next steps are given as recommendations to improve the control-model and also implement it within the experimental setup using these results.

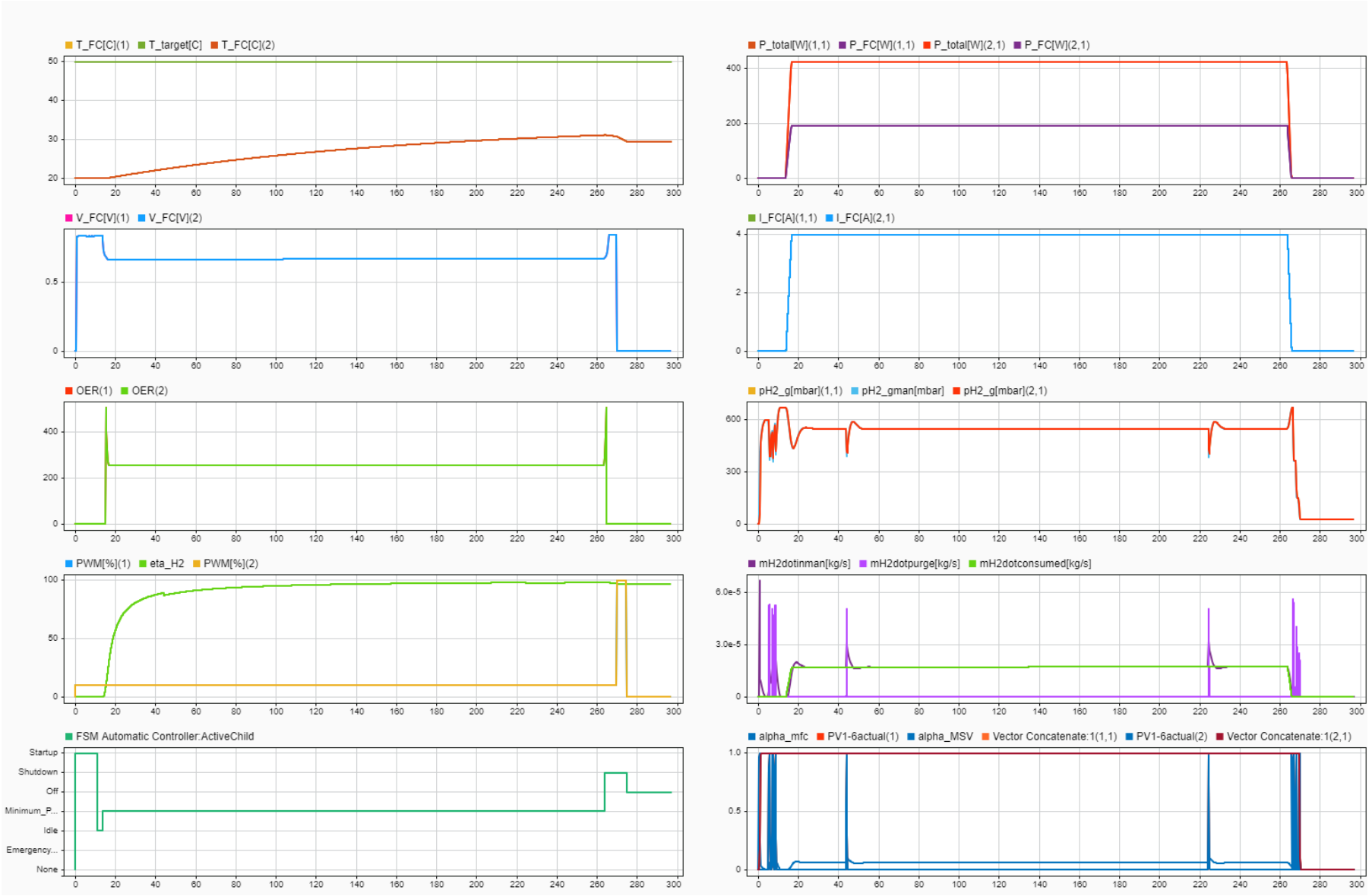

Figure 7.1: Final Imponator control-model results: 4A minimum current

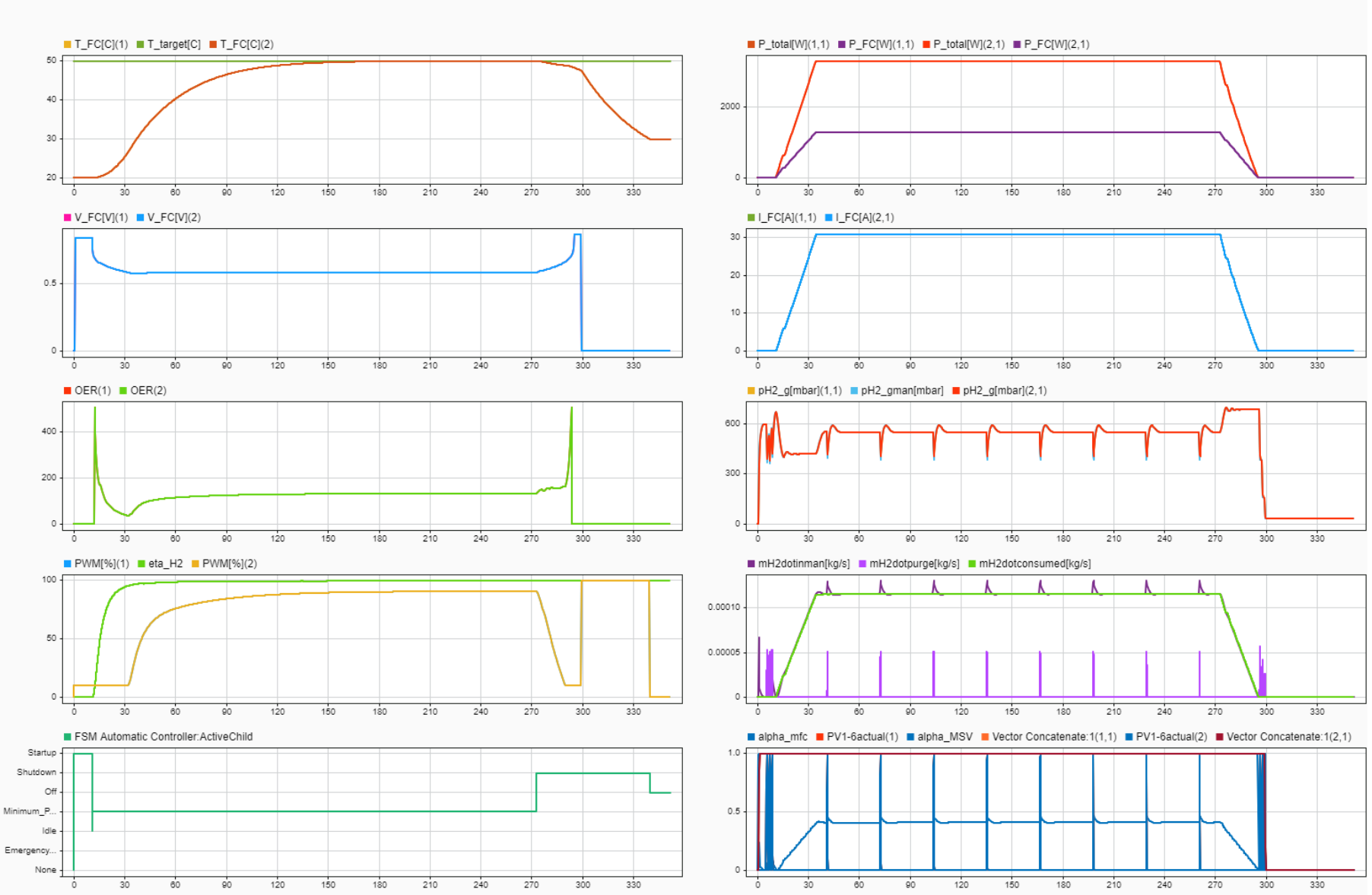

Figure 7.2: Final Imponator control-model results: 31A maximum possible current (with $T_{amb} = 20°C$)

8

Recommendations

This chapter provides a brief overview of the primary recommendations to take place after the thesis. The types of recommendations can be split into three sections, one for improvement of the existing Imponator control-model in Section 8.1, two is for exploring this control-model as a tool in Section 8.2, and three is for the integration of these control insights into the real system in Section 8.3.

8.1. Control-model Improvements

Here, 3 main improvements are given by priority. The first 2 are estimated to cause the largest improvement.

8.1.1. Mass Flow Controller Fidelity

The fidelity of the model MFC can also be increased, which shall allow for a more realistic pressure model. This starts with collecting experimental valve and mass flow data from the MFC, and pressure data from the pressure sensor located in the start of the anode manifold. With this data, the MFC can be modelled more accurately, and the mass flows can be validated directly. Then, the PID of the MFC can be tuned, and these gains can be directly put into the real PID controller of the real MFC, to improve the system's pressure response to purging and consumption. With a better pressure response to purging and consumption, the time required for ramp up and ramp down can be decreased, since currently the ramp rate is constrained by the pressure falling out of range.

8.1.2. Power Throttle

The focus of this thesis was to automate the startup and shutdown of the Imponator, therefore there is currently no 'Run' state occurring right after the startup. Within this run state, the idea would be to allow the user to continuously control the demanded throttle power or current, in the range from minimum 4A to maximum 31A. This requires an additional complexity of the current controller, to be able to handle current increasing and decreasing within the same state. Additionally, this wasn't implemented because practically it would also require modelling a highly detailed motor load, which has more dynamic interactions with the current and resistance. This wasn't necessary when automating the startup and shutdown sequences, however it becomes relevant when wishing to pursue implementing this recommendation.

8.1.3. Temperature Model Fidelity

The validation metrics of the temperature model can be improved, by gathering experimental data of the Imponator where outside wind does not play a role by keeping windows shut. This can allow better parameter estimation for the TMS parameters, and hence it would also perform better in validation. The other way around is also possible, to increase model complexity to take outside wind and temperature into account, but it would be too cumbersome for the scope of the Imponator, which is meant to be tested indoors. Hence, it is better to test within a closed room, where the ambient room temperature remains relatively stable.

8.2. Exploration as a Tool

The existing control-model has an important advantage, that can be explored further. Whilst the aim of the project was to investigate how to automate the Imponator, in the process, a validated control-model has

been developed. This control-model, can be used as a tool to explore different kinds of aspects of the Imponator, saving the time and resources needed for experimental testing. Some of these aspects are explored below, however many more are possible.

8.2.1. Mission Profile

A mission profile can be simulated by changing certain parameters such as altitude and temperature, to analyze what effects this has on the system performance. For example, with increasing altitude, the air density and air pressure will decrease, affecting the voltage that can be generated and hence the power. However, the temperature will also drop, which will help the fans cool the stacks, and therefore it may be possible to draw more current and hence higher power. For example, it was possible to draw higher current at lower ambient temperatures, such as in Figure B.1 and Figure B.2. These kind of interactions would be interesting to explore, to determine limiting factors of air-cooled open-cathode fuel-cells.

8.2.2. Failure Modes

Since there are 6 stacks in parallel, the failure of one of these stacks during a flight is safety critical. Therefore, it becomes relevant to develop control systems, that can handle a single stack failure, and preferably prevent a decrease in total power output. For these kinds of cases, it becomes vital to have independent control logic for each of the stacks. This would be needed when designing fail-safe or reduced-power modes. For example, a total system shutdown for a single stack overheating would not be acceptable whilst flying, and requires a fail-safe mode where other stacks still need to be operated sensibly. Investigations into these kinds of failure modes, and developing fail-safe control systems may be of interest for demonstrators, and this control-model serves as a good starting point.

8.3. Physical Imponator Integration

The FSM supervisory automatic controller, along with temperature PID, current NRG and purging controllers are the main outputs that can be mapped onto the real system. This mapping would be from the current Simulink model, to the real-time LabVIEW controls of the physical Imponator. Notably, due to the interactions present, several physical models such as the air supply, purging and power subsystems are required for the control, as they model useful parameters that the physical system cannot output. This relates to information such as purging mass flows or air mass flows, for which there are no existing sensors. Therefore, it may be easiest to map the entire Simulink model along with its controls onto LabVIEW, and only change the parameters that come from sensors.

Speaking of sensors, during the thesis a safety improvement has been recommended for the physical Imponator. An automated hydrogen leakage emergency shutdown has been designed in the model, however this requires a real hydrogen detection sensor on the Imponator, which currently does not exist. Thus this would be a strong recommendation, to implement a real hydrogen detection sensor onto the physical Imponator, to improve its safety in a critical hazard requiring immediate emergency shutdown.

All in all, physical integration is perhaps the most extensive recommendation, and would require significant amount of time. Since after the implementation, the automation deployment also needs to be tested with a demonstration, to determine whether it is meeting the control requirements. With this, the recommendations for post-thesis activities are concluded.

References

[1] Delft University of Technology. *TU Delft Corporate Identity and Logo Guidelines*. 2026. URL: https://www.tudelft.nl/huisstijl (visited on 04/21/2026).

[2] German Aerospace Center (DLR). *DLR Logos and Media Resources*. 2026. URL: https://www.dlr.de/de/vorschaubilder-logos-platzhalter/logos (visited on 04/21/2026).

[3] Airbus. *Airbus Logo - Brand Assets*. 2026. URL: https://www.brand.airbus.com/en/asset-library/airbus-logo (visited on 04/21/2026).

[4] ZAL GmbH. *ZAL Branding and Logo*. 2026. URL: https://brandfetch.com/zal.aero (visited on 04/21/2026).

[5] Helmut Schmidt University. *Helmut Schmidt University Website*. 2026. URL: https://www.hsu-hh.de/ (visited on 04/21/2026).

[6] German Aerospace Center (DLR). *D-LIGHT+ Project*. Accessed: 2026-04-21. 2026. URL: https://www.dlr.de/de/kf/forschung-transfer/projekte/d-light-plus.

[7] 3M Company. *Hydrogen Fuel Cells | 3M Hydrogen Technology*. Accessed: 29 October 2025. 2024. URL: https://www.3m.com.au/3M/en_AU/hydrogen-technology-au/applications/fuel-cells/.

[8] Ahmad Baroutaji et al. "Comprehensive investigation on hydrogen and fuel cell technology in the aviation and aerospace sectors". In: *Renewable and Sustainable Energy Reviews* 106 (2019), pp. 31–40. DOI: https://doi.org/10.1016/j.rser.2019.02.022. URL: https://www.sciencedirect.com/science/article/pii/S1364032119301157.

[9] Abubakar Unguwanrimi Yakubu et al. "A comprehensive review of primary cooling techniques and thermal management strategies for polymer electrolyte membrane fuel cells (PEMFCs)". In: *Heliyon* 10.19 (2024), e38556. DOI: 10.1016/j.heliyon.2024.e38556.

[10] Ohsub Kim et al. "Impact of fuel starvation–induced anode carbon corrosion in proton exchange membrane fuel cells on the structure of the membrane electrode assembly and exhaust gas emissions: A quantitative case study". In: *Journal of Power Sources* 615 (2024), p. 235032. DOI: 10.1016/j.jpowsour.2024.235032.

[11] Jixin Chen et al. "Optimization of purge cycle for dead-ended anode fuel cell operation". In: *International Journal of Hydrogen Energy* 38.12 (2013), pp. 5092–5105. DOI: 10.1016/j.ijhydene.2013.02.022.

[12] M. Chandesris et al. "Membrane degradation in PEM fuel cells: From experimental results to semi-empirical degradation laws". In: *International Journal of Hydrogen Energy* 42.12 (2017), pp. 8139–8149. DOI: 10.1016/j.ijhydene.2017.02.116.

[13] Yupeng Yang et al. "Overall and local effects of operating parameters on water management and performance of open-cathode PEM fuel cells". In: *Applied Energy* 315 (2022), p. 118978. DOI: 10.1016/j.apenergy.2022.118978.

[14] Francesco Mazzeo et al. "Assessing Open Circuit Voltage Losses in PEMFCs: A New Methodological Approach". In: *Energies* 17.11 (2024), p. 2785. DOI: 10.3390/en17112785.

[15] Morten Lind. *Functional Modelling of Technical Artefacts*. Cham: Springer, 2023. DOI: 10.1007/978-3-031-45918-4. URL: https://doi.org/10.1007/978-3-031-45918-4.

[16] *Petri Net Model*. ScienceDirect Topics. Accessed: 29 September 2025. 2025. URL: https://www.sciencedirect.com/topics/engineering/petri-net-model.

[17] Carl Adam Petri. *Communication with Automata*. New York: Springer. Originally published as “Kommunikation mit Automaten”, PhD Thesis, University of Bonn, 1962. 1996.

[18] Claudia Fecarotti et al. “A Petri net approach for performance modelling of polymer electrolyte membrane fuel cell systems”. In: *International Journal of Hydrogen Energy* 41.28 (2016), pp. 12242–12260. DOI: https://doi.org/10.1016/j.ijhydene.2016.05.138. URL: https://www.sciencedirect.com/science/article/pii/S0360319915304018.

[19] MathWorks. *What Is a State Machine?* https://nl.mathworks.com/discovery/state-machine.html. Accessed: 21 October 2025. 2024.

[20] Ali Molavi et al. “Design and Implementation of a Fuel Cell System Supervisory Controller for Automotive Applications Using Finite State Machines”. In: *2023 IEEE Transportation Electrification Conference and Expo (ITEC)*. 2023, pp. 1443–1450. DOI: 10.1109/ITEC55773.2023.10268183.

[21] Joseph Ishaku et al. “Control-oriented modeling for open-cathode fuel cell systems”. In: June 2014, pp. 268–273. DOI: 10.1109/ACC.2014.6859221.

[22] Mustafa Özbek et al. “Modeling and control of a PEM fuel cell system: A practical study based on experimental defined component behavior”. In: *Journal of Process Control* 23.3 (2013), pp. 282–293. DOI: 10.1016/j.jprocont.2012.11.009.

[23] Shanal S. Kumar et al. “A Simplified Control Oriented Model of an Open Cathode PEM Fuel Cell”. In: *2021 IEEE 12th Energy Conversion Congress & Exposition - Asia (ECCE-Asia)*. IEEE, 2021, pp. 2415–2420. DOI: 10.1109/ECCE-Asia49820.2021.9479098. URL: https://doi.org/10.1109/ECCE-Asia49820.2021.9479098.

[24] Bo Zhang et al. “Design and implementation of model predictive control for an open-cathode fuel cell thermal management system”. In: *Renewable Energy* 154 (2020), pp. 1014–1024. DOI: 10.1016/j.renene.2020.03.073.

[25] Yu-Fen Lin et al. “Experimental study on the optimal purge duration of a proton exchange membrane fuel cell with a dead-ended anode”. In: *Journal of Power Sources* 340 (2017), pp. 176–182. DOI: 10.1016/j.jpowsour.2016.11.039. URL: https://doi.org/10.1016/j.jpowsour.2016.11.039.

[26] Quentin Drouot et al. *Modeling and control of a PEM fuel cell system for an unmanned aerial vehicle during startup and shutdown*. Tech. rep. hal-04192279v1. HAL preprint, available online: https://hal.science/hal-04192279v1/document. Université Grenoble Alpes, 2023. URL: https://hal.science/hal-04192279v1.

[27] Mickael Soudan et al. “PEM fuel cell stack start-up and shutdown procedures: Issues and optimization”. In: *Journal of Power Sources* 196.16 (2011), pp. 6682–6689. DOI: 10.1016/j.jpowsour.2011.03.034.

[28] Heli Kalliomäki et al. *Hydrogen Fuel Cell Power System for Aranda*. Tech. rep. MARANDA Project Final Report. VTT Technical Research Centre of Finland, 2020. URL: https://cris.vtt.fi/ws/portalfiles/portal/33907180/MARANDA_TRA2020_HydrogenFuelCellPowerSystemForAranda_CLEAN_2019_10_18.pdf.

[29] Kervin Mora Pabón et al. “Optimal Control Algorithms of Air Supply Subsystem for Polymer Electrolyte Membrane Fuel Cell Systems”. In: *LAPSE:2023.1528* (2023).

[30] Morten Lind et al. “Enhanced reasoning with Multilevel Flow Modelling: Methodology and case study”. In: *Nuclear Engineering and Design* 289 (2015), pp. 230–244. DOI: 10.1016/j.nucengdes.2015.04.018.

[31] Morten Lind. *Functional Modelling of Control and Safety Functions*. Tech. rep. Available via DTU Orbit: https://backend.orbit.dtu.dk/ws/files/10427092/STSS_Lind_2012.pdf. Technical University of Denmark (DTU), 2012.

[32] Sanyo Denki Co., Ltd. *9SG1224P1G01 DC Fan Datasheet*. Manufacturer datasheet. n.d.

[33] Mouser Electronics. *9SG1224P1G01 DC Fan — Sanyo Denki*. Accessed: January 2026. 2024. URL: https://eu.mouser.com/ProductDetail/Sanyo-Denki/9SG1224P1G01.

[34] J. C. Amphlett et al. “Performance modeling of the Ballard Mark IV solid polymer electrolyte fuel cell”. In: *Journal of the Electrochemical Society* 142.1 (1995), pp. 1–8. DOI: 10.1149/1.2043959.

[35] Vögtlin Instruments AG. *Red-y Smart Series: Thermal Mass Flow Controllers and Meters for Gases*. Hydrogen mass flow controller specifications; full-scale flow ranges and operating conditions. Vögtlin Instruments AG. 2023. URL: https://www.voegtlin.com/en/mass-flow-meters-and-controllers-for-gases/red-y-smart-series/.

[36] Bürkert Fluid Control Systems. *Type 2861 – Direct Acting 2/2-Way Solenoid Valve*. Datasheet. Bürkert Fluid Control Systems. 2023. URL: https://www.burkert.com/en/Media/plm/DTS/DS/ds2861-standard-eu-en.pdf?id=DTS00000000000000001000173850ENQ (visited on 02/13/2026).

[37] Omar Ragb et al. “Multivariable Control for Fuel Cell Stacks”. In: May 2023.

A

Simulink Model

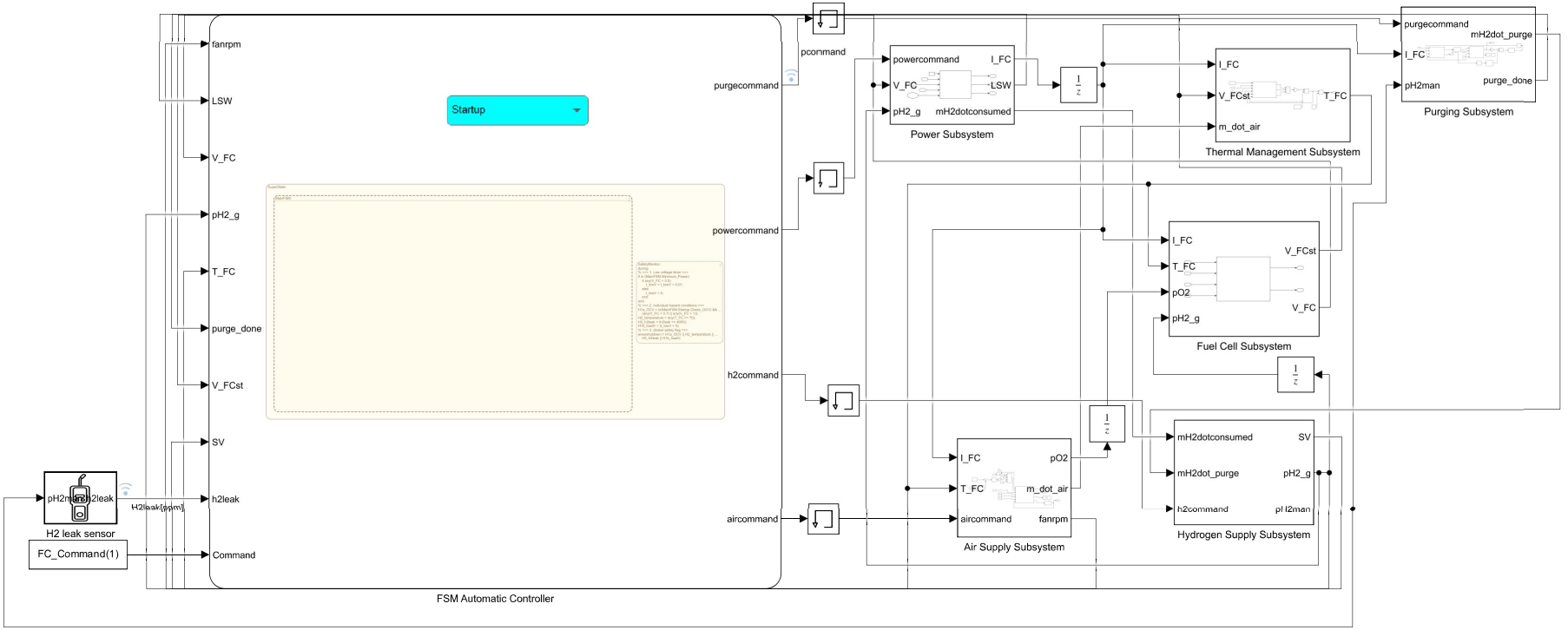

Figure A.1: Simulink model with integrated FSM chart and 6 physical subsystems (Report Figure 3.4)

B

Model Exploration

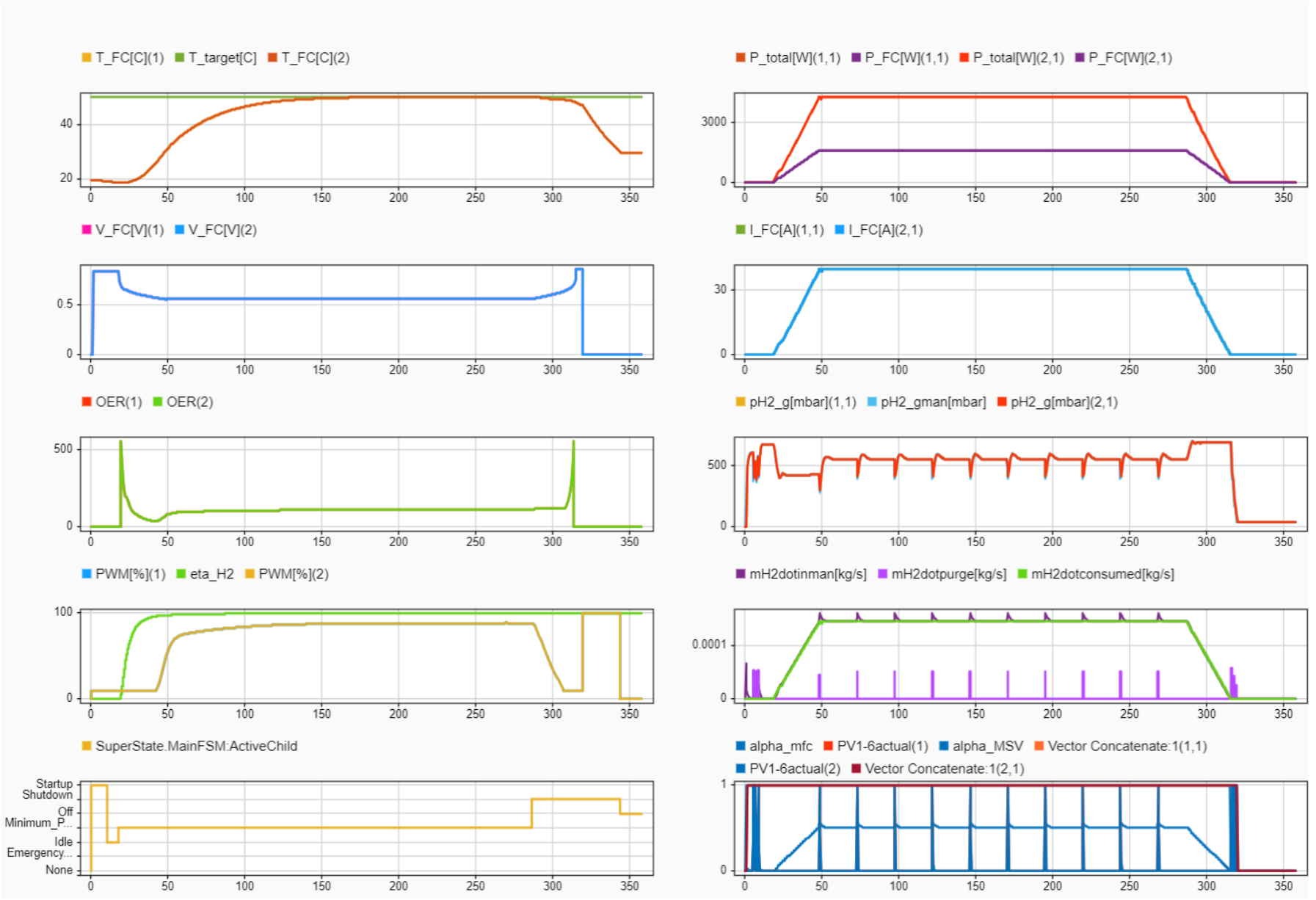

Figure B.1: Final Imponator control-model results: 40A at $T_{amb} = 10°C$

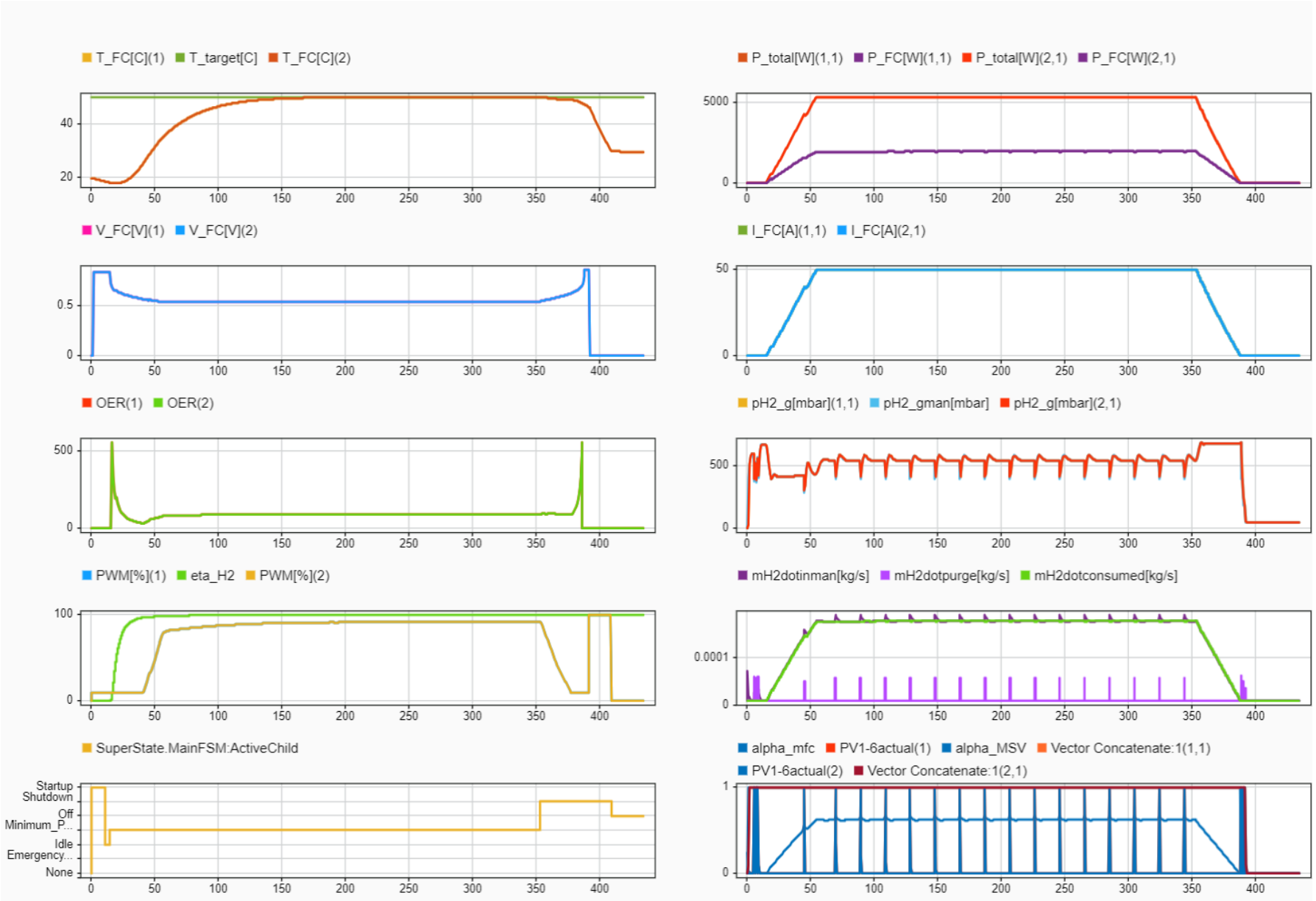

Figure B.2: Final Imponator control-model results: 50A at $T_{amb} = 0°C$